Development of a versatile microfluidic platform to study the ionic mechanisms of vesicular neurotransmitter transporters

Dissertation

for the award of the degree
Doctor rerum naturalium
(Dr. rer. nat.)
by the Georg-August-Universität Göttingen

within the doctoral program *IMPRS for Neuroscience*
of the Georg-August University School of Science (GAUSS)

submitted by
Helena M. Olsthoorn[1]

born in
Naaldwijk, the Netherlands

Göttingen 2021

[1] Answers to the name ‘Linda’

Members of the Thesis Advisory Committee

Prof. Dr. Reinhard Jahn (First referee)	Laboratory of Neurobiology, Max Planck Institute for Biophysical Chemistry, Göttingen
Prof. Dr. Tobias Moser (Second referee)	Institute for Auditory Neuroscience & InnerEarLab, University Medical Center, Göttingen
Dr. Ira Milosevic	Neuronal Physiology and Pathology Group, Wellcome Centre for Human Genetics, Nuffield Department of Medicine, University of Oxford

Members of the examination board

Prof. Dr. Silvio O. Rizzoli	Dept. of Neuro- and Sensory Physiology, University Medical Center, Göttingen
Prof. Dr. Nils Brose	Dept. of Molecular Neurobiology, Max Planck Institute of Experimental Medicine, Göttingen
Prof. Dr. Ralf Heinrich	Dept. of Cellular Neurobiology, Georg-August Universität, Göttingen

Date of oral examination: October 12th, 2021

“Anything that can go wrong, will go wrong.”

Murphy’s Law

“Nevertheless, she persisted.”

Mitch McConnel, Congress.gov. February 7, 2017. p. S855,
soon after it became an expression adopted by the feminist movement

I hereby declare that I have written the thesis independently and with no other sources and aids than quoted.

Helena M. Olsthoorn
Göttingen, August 30th , 2021

Table of content

Acknowledgments

This page is dedicated to all the people in the last four years who, at one point or another, had more faith in me or my project than I did and helped me believe in that again, even if I have failed to mention your name here.

In the first place, I would like to thank my supervisor Prof. Reinhard Jahn for this opportunity. Your unlimited optimism and belief in my capabilities and the project were a great motivator. I am thankful that I had the chance over the years to listen to your stories and experiences. I have learned from you what it means to be a great scientist.

I would like to express my gratitude to Prof. Tobias Moser and Dr. Ira Milosevic for agreeing to join my thesis advisory committee. Beyond the regular scientific discussion, I am thankful for your support and understanding in every project phase. I want to thank Dr. Eleonora Perego for being a delight to collaborate with and Prof. Marcella Chiari for her support.

To my lab – I know we always joke that all students want to stay because we are so friendly and so much fun, but you know what, it is true. I was one of those students, and I could not have wished for better colleagues (past and present). Brigitte, Sigrid, Dieter, Heike, Dagmar, Peter, and Elisa, my time would have been a lot more chaotic without your technical, organizational and bureaucratic support. You are the silent power behind the lab. Marcello, thank you for your valuable scientific feedback and support and for being the happy and wise spirit of this lab. Rashi and Sonja, thank you for sharing this adventure with me from the beginning until the end through the good and the bad times. Jenni and Delane, thank you for the everyday, from light chit-chat to life questions.

I would not have been in Göttingen if it were not for the IMPRS Neuroscience team. Thank you, Michael Hörner, Sandra Drube, Jonas Barth, and Franziska Kühne, for making moving to a new country much easier than it should be, removing bureaucratic hurdles every step of the way. You changed my life by accepting me into this program and choosing the great people I shared this class with.

I would like to take a moment to appreciate the unsung heroes of academia, all the members working in our facilities. Particularly, the workers of the *feinmechanik* who can produce anything for you, the carpenters, who literally removed doors to open the way for me, the animal care workers (especially Sascha Krause, Simone Brauer, and Dr. Ulrike Teichmann) who always have the animal's best interest at heart. Behind every great scientist, there is a great support system.

Speaking of a great support system, Ronja, Tal, Myrto, thank you for being unapologetically yourselves and often wiser than me. Your friendship means the world to me. I am thankful for all the undisputable amazing people I have met and the friends I have made in the last four years through (beach)volleyball, Happy Hours, and the Göttingen community. Last but not least, I want to thank the people I left behind to come to Göttingen; my parents, Wouter, Marian, Judith, Carline, Steven, and Maud. Thank you for dragging me out of my bubble from time to time and thereby helping me to keep both feet on the ground.

Abstract

This thesis described the development of a novel, versatile microfluidic platform for studying the ionic mechanisms of vesicular neurotransmitter transporters in rodent synaptic vesicles (SVs). The level of filling of an SV with neurotransmitters is relevant as it is an influential factor in neuronal communication. The quantal load of a single SV does not saturate postsynaptic receptors (Barberis et al., 2004; Ishikawa et al., 2002). Changes in the expression of the proteins responsible for neurotransmitter uptake (vesicular neurotransmitter transporters, e.g. VGLUT, VGAT, VNUT) changed the amount of neurotransmitter that was stored and released and thereby changed the behavior of the animal (Fon et al., 1997; Takahashi et al., 1997).

Neurotransmitter filling in SVs has two main components; the vacuolar ATP-driven proton pump (V-ATPase) and the uptake of neurotransmitters. The role of the V-ATPase is the generation of the electrochemical gradient ($\Delta\mu H^+$) across the vesicle membrane, which the vesicular neurotransmitter transporters use to load neurotransmitters into the vesicular lumen (Forgac, 2007). These two processes are intricately connected and co-occur in SVs in physiological conditions. Each of the currently available approaches to study these mechanisms is limited in their way: neuronal cell culture or brain slices based methods have limited control of the environment to decipher the details of the ionic mechanism, whereas isolated SVs or proteoliposomes in spectrofluorometers and the single vesicle assay (Farsi et al., 2016; Upmanyu et al., 2021) only allow for the addition of compounds, with no option of removal of a compound once added. Many of these approaches have a static nature in common; once a compound is added to the experiments, it cannot be removed. The microfluidic platform developed during my PhD addresses this limitation.

An assay capable of dynamically and repetitively changing the environment of SVs has to fulfill specific requirements. First of all, antibody immobilization is required in a manner that can sustain the shear rate in the microfluidic device. Secondly, these antibodies have to be able to stably immunocapture SVs. For accurate quantification, antibodies and SVs have to be immobilized at a sufficiently high density. Lastly, the microfluidic device has to be capable of solution changes faster than 1 second. This new assay can then be used to study the unanswered questions on the loading and maintenance of neurotransmitter filling in synaptic vesicles.

In this thesis, three different surfaces (2D epoxy, siPEG/siPEG-biotin, copoly(DMA-NAS-MAPS)) were used to functionalize the glass surface. First antibody immobilization in static conditions was established on each surface, followed by immunocapture of SVs in static conditions. All three surfaces performed well. A microfluidic device was developed in collaboration with Dr. Eleonora Perego (Sarah Köster group, X-ray laboratory), which fulfilled the requirements. Together with a home-built pressure clamping holder (compatible with the biological material on the surface), these parts finalized the microfluidic platform.

Immunocaptured SVs on each surface were subjected to the flow in the microfluidic channel, resulting in the wash off of the previously immobilized SVs on the 2D epoxy and siPEG/siPEG-biotin coverslips. Only SVs immobilized on the copoly(DMA-NAS-MAPS) coverslips showed stable immunocapture under 30 minutes of 3mm/s flow conditions. The copoly(DMA-NAS-MAPS) surface was therefore chosen as the final surface for the assay. Preliminary experiments were executed to test the ability of the assay to measure acidification in SVs and the de-acidification upon removal of ATP from the buffer, which was successful.

This assay combines the following advantages compared to other existing methods; no need for highly pure SV preparations, possible capture of a wide range of targets, simple analysis of micrometer-sized spots containing concentrated vesicles, possible SV capture from small samples, and fast and repetitive exchange of solutions. Overall, the system allows for a high degree of experimental flexibility. The ability to change solutions with a high temporal resolution allows us to address the long-standing questions on, for example, glutamate efflux and clarify how neurotransmitter concentration in the SV is maintained.

1 Introduction

1.1 Neuronal communication

Electrical activity inside neurons and chemical communication between neurons are the basis for information processing of the nervous system. Chemical communication between neurons takes place through specialized contact sites, named chemical **synapses**. These small structures, usually 1-2 µm in diameter, allow transmission of signals between two neurons. A narrow gap is found between the specialized contact sites of the pre- and postsynaptic neuron, also known as the **synaptic cleft**. Synaptic transmission is arbitrated by small molecules, termed **neurotransmitters**, released from the presynaptic neuron. Neurotransmitters in synapses are stored in small spherical organelles called **synaptic vesicles** (SVs).

The release of neurotransmitters at the presynaptic neuron is initiated by the arrival of an action potential, resulting in the depolarization of the plasma membrane. This depolarization results in an influx of Ca^{2+}-ions through voltage-sensitive Ca^{2+} channels. Synaptic vesicles are triggered to fuse with the presynaptic membrane, releasing their content into the synaptic cleft, a process called **exocytosis**. Diffusion allows the neurotransmitter to move across the cleft to the postsynapse. The postsynaptic neurons contain receptors that recognize the neurotransmitters and change the electrical properties of the postsynaptic cell, either through **ionotropic** receptors (ligand-activated ion channels) or through **metabotropic** receptors (receptors associated with G-protein mediated second messenger cascades). At the presynapse, SVs undergo a reversal process called **endocytosis** to be recycled for the arrival of a new signal.

1.1.1 Synaptic vesicle cycle

The merging and re-emerging of membranes at the synapse was first described by Heuser and Reese (Heuser and Reese, 1973) and coined **synaptic vesicle recycling**. The synaptic vesicle cycle has been reviewed many times, focusing on different aspects (Haucke et al., 2011; Rizzoli, 2014; Südhof, 2004) and can be described by six significant steps (Figure 1). SVs arrive at the synapse after transportation along microtubules in the axon by kinesin-mediated transport from the Golgi apparatus. The first step is the filling of these (new) SVs with neurotransmitters (1). SVs that are filled and ready for release preferentially reside within the **active zone**[2]. This clustering and docking of SVs at the release sites is the second step (2). A fusion-competent state is achieved by priming, in which the SNARE[3] complexes are partially assembled (3). The above-mentioned influx of Ca^{2+} ions results in rapid fusion of the primed SVs (4)(Katz and Miledi, 1969).

[2] An area on the presynaptic membrane, opposite of the post-synaptic receptors, observed in electron microcopy images due to its high density.
[3] SNARE stands for SNAP receptor, SNAP stands for soluble NSF attachment proteins, NSF stands for N-ethylmaleimide-sensitive fusion protein.

The SNARE assembly is thought to provide the energy to mediate and drive this fusion event. The changes in calcium concentration are sensed by the calcium-binding synaptic vesicle protein synaptotagmin, triggering the fusion event (Brose et al., 1992). It has been debated whether synaptic vesicles fuse entirely with the plasma membrane or whether a fusion pore is formed briefly to allow neurotransmitters to leave without completely fusing the membranes, termed kiss-and-run. Incomplete fusion with the membrane could explain the observations of fast endocytosis. Despite early indications of the possibility of incomplete fusion (Aravanis et al., 2003), later work revealed that kiss-and-run, as defined, does not exist. Instead, the fast endocytosis observation can be explained by “ultrafast endocytosis” as a retrieval process after complete fusion (5). The retrieval of proteins and lipids in ultrafast endocytosis (<1 sec) is clathrin-independent and results in large endocytic vesicles through quick bulk membrane retrieval (Watanabe et al., 2013, 2014). The other pathway of endocytosis after complete fusion is clathrin-mediated endocytosis (CME) (5), which is slower (15 sec) (Granseth et al., 2006). Following the clathrin-mediated endocytosis, the vesicles could potentially be recycled directly and filled with neurotransmitters. However, as this requires high specificity of protein and membrane selection during endocytosis, the vesicles are likely traveling through an endosomal compartment after clathrin uncoating (6). In this endosomal compartment, vesicle proteins and membranes are rearranged to generate fusion-competent SVs again (Südhof, 2004). After the rearrangement at the early endosomal compartment, they bud off, and the whole cycle starts over with neurotransmitter filling (Jahn and Boyken, 2013). Budding off from the early endosomal compartments or from the large endocytic vesicles formed in the ultrafast endocytosis hypothesis is also clathrin-mediated (Watanabe et al., 2014).

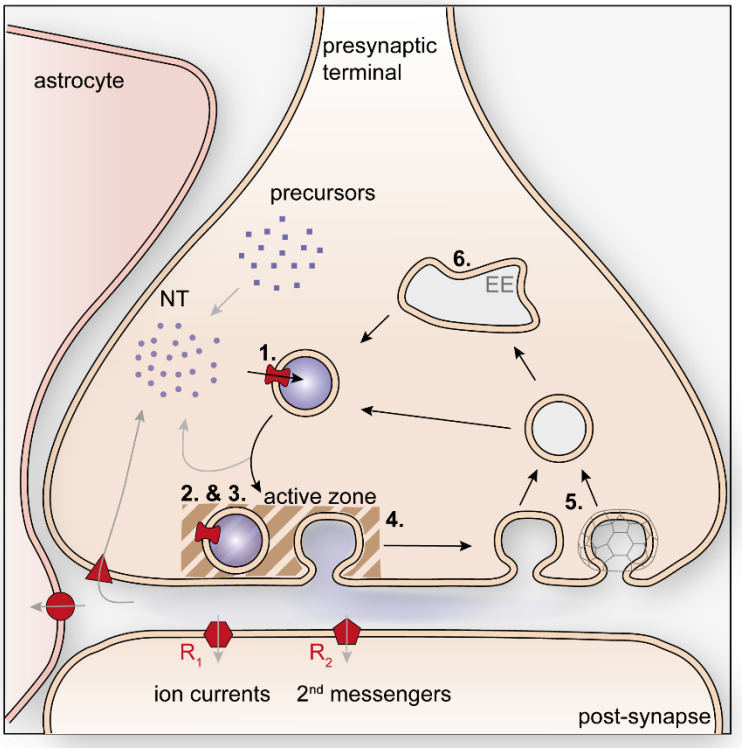

Figure 1. Synaptic vesicle cycle at the presynaptic terminal. SVs are filled with neurotransmitters (NT) through the NT transporter proteins (red hourglass shape) (1), the SVs are docked and primed in the active zone (brown striped area) (2&3), and NT is released through exocytosis (4), this is followed by ultrafast or clathrin based endocytosis (5), and after potential resorting in early endosomes (6), the cycle restarts.

1.1.2 Synaptic vesicles

The small spherical trafficking organelle called SV was visually observed for the first time between 1954 to 1956 by analyzing electron microscopy images, and it was proposed to be the source of the miniature pulses observed at synapses at that time (Palay, 1956; De Robertis and Bennett, 1955). It was postulated to be the structural component of neurotransmitter release and estimated initially to be 200 to 500 Å in diameter. With improved electron microscopes, SVs were determined to have a diameter of approximately 40 nm (Takamori et al., 2006). They are uniform in size and highly abundant; based on the assumptions that the human central nervous system has 10^{11} neurons, each neuron 10^3 synapses (Kandel et al., 2012), each synapse on average 300-500 SVs (Wilhelm et al., 2014), we have an estimated range of 10^{16}-10^{17} number of SVs in our brain (Jahn and Boyken, 2013). Due to its high abundance, the ability to purify SVs from the brain, and its essential role in neuronal communication, the composition of SVs is better understood than most other trafficking organelles (Takamori et al., 2006; Taoufiq et al., 2021). After early identification of many of the trafficking proteins present on SVs (Jahn and Südhof, 1993, 1994), Takamori et al. (2006) used mass spectrometry (MS) analysis to specify the lipid and protein composition of SVs (Figure 2), providing a more quantitative model of the average SV. The majority of proteins on SVs are shared even by SVs storing different neurotransmitters (Grønborg et al., 2010). The most abundant proteins were synaptophysin (syp) and synaptobrevin/VAMP2 (syb2), 31.5 and 69.8 copies, respectively (Takamori et al., 2006; Wilhelm et al., 2014). The vacuolar ATP-driven proton pump (V-ATPase) responsible for the generation of the electrochemical gradient ($\Delta\mu H^+$) across the vesicle membrane was determined to only have an average copy number between 1 and 2, surprisingly little considering its significant role in vesicle acidification and filling (see 1.2.1).

Improved MS methodologies detected three times more proteins (approximately 1500) than previously possible, especially many low-abundance proteins that previously escaped detection. This improved approach largely confirmed the copy numbers mentioned above. However, the previously ‘hidden’ population of proteins hint that the heterogeneity in of SVs is higher than initially thought, as the copy numbers found for most of these SV proteins was less than one per SV (Taoufiq et al., 2021). This result suggests that these proteins are either only present on subpopulations of SVs or only ephemerally interacting with SVs. The high complexity of these organelles is further increased by the possibility that they may not have a fixed stoichiometric composition and are constantly influenced by cytoplasmic factors. Quantification at a single vesicle level has provided a first glance at inter-vesicle variability of specific SV proteins (eg. synaptophysin and synaptobrevin/VAMP2), while others showed minimal variation (eg. V-ATPase) (Mutch et al., 2011).

Vesicular neurotransmitter transporters are one of the main protein classes essential for the SV filling with neurotransmitters. Different vesicular neurotransmitter transporters transport specific types of neurotransmitters. Takamori et al. (2006) calculated that the transporters for the excitatory neurotransmitter glutamate VGLUT1 and VGLUT2 have approximately ten copies per vesicle (9.0 and 14.4, respectively) based on quantitative dot blotting and MS data. This copy number has recently been corroborated in our laboratory using quantitative MS, finding per vesicle on average 8.3 copies for VGLUT1, 12.9 copies of VGLUT2, 16.2 copies of VGAT (inhibitory neurotransmitter transporter for γ-amino butyric acid (GABA) and glycine), and 4.7 copies of ZnT3 (vesicular transporter for Zink ions) (Upmanyu et al., 2021).

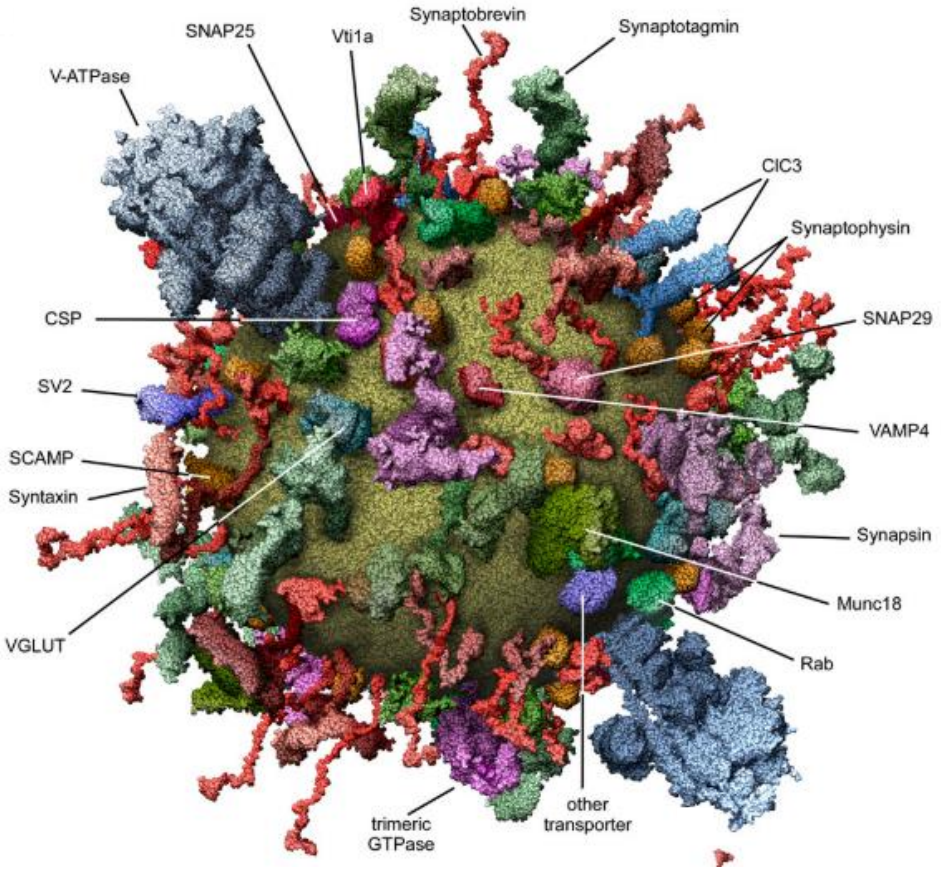

Figure 2. Molecular model of composition of an average synaptic vesicle from the rat brain, seen from the outside (Takamori et al., 2006)

However, these numbers still represent an averaged image of SVs, neglecting the diversity found in SVs. Even though SVs share a basic set of proteins, variation in copy numbers between neurons or single vesicles is highly likely. This variation becomes apparent when the neurotransmitter transporters are investigated. The phenotype of SVs is determined by the presence of specific neurotransmitter transporters as no other SV protein is exclusively found on only one subpopulation of vesicles (Grønborg et al., 2010; Takamori et al., 2000b, 2000a). 27 subpopulations of SVs can be identified using super-resolution microscopy based on which neurotransmitter transporter(s) is/are present on the vesicle, indicative of the complexity of this trafficking organelle (Upmanyu et al., 2021).

The individual SV approach used by Upmanyu et al. (2021) revealed high variability of copy numbers between vesicles, which was obscured in the earlier executed bulk assays. Therefore, it has to be kept in mind while studying SVs that these small organelles are highly complex and variable.

1.2 Neurotransmitter filling

The composition of SVs is an important factor in determining the neurotransmitter filling mechanism. Neurotransmitter filling is an influential factor in neuronal communication. Even before the SV was identified as the structural unit, spontaneous, miniature postsynaptic responses were observed, leading to the hypothesis that an elementary base unit is responsible for this response, which was named the quantum (del Castillo and Katz, 1954; Fatt and Katz, 1952). A short time later, the SV was identified as the structural equivalent of this base unit, resulting in the vesicular hypothesis for neurotransmitter release; a single vesicle is equivalent to the quantum, and variations in responses are either mediated through the release of multiple vesicles or postsynaptic modulations (Katz, 1971). It was not until 15-20 years later that it was considered that the filling of SVs could influence quantal size. The proteins responsible for neurotransmitter uptake into the SVs were identified, and the manipulation of their expression changed the amount of neurotransmitter that was stored and released and changed the animal's behavior (Fon et al., 1997; Takahashi et al., 1997). The possibility of variability in the concentration of neurotransmitters stored in the SV has been shown in synaptosomes (isolated pinched off nerve endings) and at the neuromuscular junction. Prolonged depolarization of the synaptosomes, increased the quantal size of glutamatergic SVs (Bole et al., 2002). High-frequency stimulation of the neuromuscular junction decreased the acetylcholine content in SVs (Naves and Van Der Kloot, 2001). These changes in neurotransmitter filling can potentially influence the associated postsynaptic current greatly as the postsynaptic receptors are not saturated by a single SV (Barberis et al., 2004; Ishikawa et al., 2002). So besides postsynaptic modifications, synaptic cleft clearing, and variability in exocytic ability, the level of filling of an SV with neurotransmitter is an influential factor in neuronal communication.

1.2.1 Electrochemical gradient

The precise concentration of the neurotransmitters in SVs remains a topic for debate. Nonetheless, conservative estimates of glutamate concentration in SVs is in the 60-210 mM range, about a ten-fold higher than cytoplasmic glutamate concentration (Burger et al., 1989; Riveros et al., 1986). Therefore, the mechanism of SVs filling with neurotransmitters requires a form of active transport. The mechanism has two main components, the vacuolar ATP-driven proton pump (V-ATPase), and the vesicular neurotransmitter transporters. The role of the V-ATPase is the generation of the electrochemical gradient ($\Delta\mu H^+$) across the vesicle membrane by pumping protons into the vesicular lumen. The vesicular neurotransmitter transporters use this gradient to load neurotransmitters into the vesicular lumen (Forgac, 2007). These two processes are intricately connected and co-occur in SVs under physiological conditions.

The electrochemical gradient ($\Delta\mu H^+$) is composed of the membrane potential ($\Delta\Psi$) and the pH gradient (ΔpH). It is formed by the activity of the electrogenic V-ATPase, which converts cytosolic ATP into ADP, Pi, and H^+. The mammalian V-ATPase is a complex multi-subunit protein (approximately 910 kDa in total) build-up of two main domains, V_1 and V_0, with each multiple subunits, eight (A-H) and six (*a*, *c*, *c'*, *c''*, *d*, *e*), respectively. Some of these subunits exist in multiple isoforms. For example, the V-ATPase found on synaptic vesicles is formed with the a_1 isoform, while the a_3 isoform is found on late endosomes and lysosomes. The peripheral V_1 domain hydrolyzes ATP, while the V_0 domain, located in the membrane, translocates the protons across the membrane bilayer into the lumen (Abbas et al., 2020; Mazhab-Jafari et al., 2016; Wang et al., 2020). The pumping activity of the V-ATPase of protons into the lumen of the SV affects not only the ΔpH by decreasing the luminal pH but also the $\Delta\Psi$, as the V-ATPase only translocates the positively charged protons (Blakely and Edwards, 2012; Farsi et al., 2017; Forgac, 2007).

The electrochemical gradient (Eq. 3 and 4) is the energy of the proton concentration gradient provided by the V-ATPase. It is a combination of the electrical ($\Delta\Psi$) (Eq. 1) and the chemical (ΔpH) energy contribution (Eq. 2).

$$\Delta G_{electrical} = zF\Delta\psi \qquad \textit{Eq. 1}$$

$$\Delta G_{chemical} = 2.303RT\log\frac{[H^+{}_{in}]}{[H^+{}_{out}]} \qquad \textit{Eq. 2}$$

$$\Delta\mu H^+ = \Delta\psi + 2.303\frac{RT}{zF}log\frac{[H^+{}_{in}]}{[H^+{}_{out}]} \;\; or, simplified \qquad \textit{Eq. 3}$$

$$\Delta\mu H^+ = \Delta\psi + 2.303\frac{RT}{zF}\Delta pH \qquad \textit{Eq. 4}$$

in which $\Delta G_{electrical}$ = electrical energy, z = ion valence (for H^+=1), F = Faraday constant, $\Delta G_{chemical}$ = chemical energy , R = gas constant, T = temperature in Kelvin, $\Delta\mu H+$ = electrochemical gradient, $\Delta\Psi$ = membrane potential, ΔpH = pH gradient across membrane

The balance between the $\Delta\Psi$ and the ΔpH in the electrochemical gradient depends on the permeability of the membrane to counter ions, the buffering capacity inside the lumen of the SV, the activity of the proton pump (Sun-Wada et al., 2003), and the proton efflux. Due to the small volume of an SV ($19.86 * 10^{-21}$ L) (Takamori et al., 2006), even a single proton would drastically acidify the lumen if the lumen did not have any buffering capacity. Recent studies have estimated the pH in the lumen of different vesicles, finding a slightly lower pH in glutamatergic SVs (pH 5.80) compared to GABAergic SVs (pH 6.44) (Egashira et al., 2016). Studying the $\Delta\Psi$ reveals variation in $\Delta\Psi$ from ~60-90 mV with on average an 11.99 (± 5.2) mV larger membrane potential for glutamatergic SVs compared to GABAergic SVs (Farsi et al., 2016). Additionally, the $\Delta\Psi$ does not only depend on the concentration of free protons but also the concentrations of other cations, anions, buffered protons, and any other particles/proteins carrying a charge.

1.2.1.1 Other contributors to the overall ion balance

As already mentioned, the increase of protons into the lumen of the SV by the pumping activity of the V-ATPase affects both the ΔpH and the ΔΨ resulting in the electrochemical gradient. Further pumping of the V-ATPase requires a reduction of the overall electrochemical gradient, either by reducing the ΔΨ, the ΔpH, or both. For example, an influx of charge balancing anions dissipates the ΔΨ, resulting in an overall decrease of the electrochemical gradient. This in turn allows the V-ATPase to pump in more protons affecting both ΔΨ and ΔpH.

A prime candidate for this charge balancing ion is chloride (Edwards, 2007; Hell et al., 1990). The chloride channel (ClC) protein family includes chloride channels and transporters. Even though some studies could not confirm the presence of ClC3 on SVs (Takamori et al., 2006) or only at very low abundance (Taoufiq et al., 2021), this is probably due to technical difficulties in detecting the alpha-helical chloride channel proteins. As other experimental approaches found ClC3 (Stobrawa et al., 2001) and ClC7 on SVs (Grønborg et al., 2010).The intracellular isoforms ClC3 to ClC7 are postulated to function as transporters, exchanging chloride for protons (Jentsch, 2007). The suggested stoichiometry for ClC3 is the exchange of one luminal proton for two Cl^- ions, as has been determined for ClC7 (Graves et al., 2008; Scheel et al., 2005). A knockout model of ClC3 showed impaired acidification of the SVs (Stobrawa et al., 2001) and decreased inhibitory transmission (Riazanski et al., 2011), indicating that ClC3 might contribute to the SV electrochemical gradient as a possible electrical shunt dissipating the ΔΨ, increasing the proton pumping ability of the V-ATPase, promoting ΔpH. However, mice in which ClC3 is converted to a Cl^- channel showed normal SV acidification and miniature excitatory postsynaptic currents (mEPSCs) were not affected either, questioning the role of ClC3 in SVs (Weinert et al., 2020). Another potential candidate for chloride permeability is the vesicular glutamate transporter (VGLUT) itself as discussed in more detail in 1.2.3.1

Another way to affect the balance between ΔΨ and ΔpH is cation permeability. Exchange of cations with luminal protons affects the ΔpH while maintaining the ΔΨ (in case of a 1:1 exchange). Studying SV filling of glutamate has revealed a cation/H^+ exchanger on the vesicle membrane (Goh et al., 2011). Na^+/H^+ exchanger (NHE) proteins are membrane proteins that exchange H^+ for Na^+ across the membrane with a stoichiometry of 1:1 (Bianchini and Pouyssegur, 1994). The isoforms NHE6-NHE9 are all found on distinct intracellular compartments, with NHE6 located on early recycling endosomes (Nakamura et al., 2005). All isoforms were shown to play a role in regulating the pH in their distinct intracellular compartment through the exchange of protons for sodium or potassium. The presence of NHE6 on SVs specifically was determined by western blotting of purified SVs (Preobraschenski et al., 2014). Using the NHE inhibitor ethyl-isopropyl amiloride (EIPA), only the alkalinization through sodium was affected, potassium alkalinization remained unchanged (Farsi et al., 2016), indicating that the NHE6 exchanger on SVs exchanges sodium but not potassium as was similarly found for NHE7 (Milosavljevic et al., 2014).

Lastly, the actual neurotransmitter molecules differentially impact the ΔΨ (Chaudhry et al., 2008). When the negatively charged glutamate is transported into the SVs, it functions comparable to the above-described chloride ions. The negative charges dissipate the ΔΨ, allowing for an increase of ΔpH or ΔΨ. Cationic neurotransmitters, such as acetylcholine and monoamines, have the opposite effect and increase the contribution of ΔΨ (when not exchanged with another positive charge), therefore requiring a decrease of ΔpH. As discussed in later sections, this difference in the impact of different neurotransmitters is also reflected in their uptake mechanisms and dependence on different electrochemical gradient components.

1.2.2 Vesicular neurotransmitter transporters

The vesicular neurotransmitter transporters are integral membrane proteins that utilize the above-mentioned electrochemical gradient to accumulate neurotransmitters in the lumen of the vesicles. The neurotransmitter transporter proteins are found in three different solute carrier (SLC) families: SLC17, SLC18, and SLC32 based on their amino acid sequence, substrate specificity, energetics, and inhibitors (Masson et al., 1999; Omote and Moriyama, 2013). The uptake of anionic neurotransmitters (glutamate, aspartate, and nucleotides) is mediated by the first family SLC17. Besides four plasma membrane type 1 phosphate transporters, the SLC17 family consists of the three vesicular glutamate transporters (VGLUT1–3), the lysosomal excitatory amino acid transporter (VEAT) (also known as H^+/sialic acid transporter Sialin), and the vesicular nucleotide transporter (VNUT). The second family, SLC18, accumulates the cationic neurotransmitters; acetylcholine and the monoamines dopamine, norepinephrin, and serotonin. The monoamines are transported by the vesicular monoamine transporters (VMAT1 and VMAT2) and acetylcholine is transported by the vesicular acetylcholine transporter (VAChT). Recently the newest member of the SLC18 family has been identified transporting polyamines, named vesicular polyamine transporter (VPAT) (Hiasa et al., 2014). The last family (SLC32) has just one member, the vesicular GABA transporter (VGAT), also called vesicular inhibitory amino acid transporter (VIAAT), as it transports the inhibitory neurotransmitters GABA and glycine. New, less abundant, vesicular transporters are still being discovered by studying SVs in detail (Taoufiq et al., 2021).

Overall, SLC17 and 18 both belong to the major facilitator superfamily (MFS). VGAT shows no homology to the vesicular transporters from the SLC17 or 18 families (Bevensee, 2014) and belongs to the acid/polyamine/organocation (APC) superfamily.

1.2.2.1 SLC17 family (VGLUT1-3 and VNUT)

VGLUT1 was the first vesicular transporter identified of the SLC17 family (Ni et al., 1994). It was specifically found on synaptic vesicles (Bellocchio et al., 1998). Simultaneously another group found that the *eat*-4 gene, the *C. elegans* equivalent of VGLUT1, is important for glutamatergic signaling (Lee et al., 1999). Studying isolated vesicles revealed glutamate transport activity and the protein was named VGLUT1 (Bellocchio et al., 2000; Takamori et al., 2000b). cDNA of the two other isoforms of VGLUT1 was identified and named VGLUT2 (Aihara et al., 2000; Takamori et al., 2001) and VGLUT3 (Fremeau et al., 2002).

Each cDNA predicted proteins of a length of 560-600 amino acids with 12 putative transmembrane domains, as usual for MFS family proteins (Law et al., 2008). VGLUTs have a longer cytoplasmic C-terminal than the plasma membrane residing members of the SLC17 family, which helps the protein localize to SVs (Voglmaier et al., 2006). Despite their structural similarities, the VGLUT isoforms are expressed in different brain regions, with VGLUT3 being co-expressed in cholinergic and serotoninergic neurons instead of glutamatergic neurons (Fremeau et al., 2002; Gras et al., 2002; Schäfer et al., 2002). VLGUT2 is expressed predominantly in early development (Miyazaki et al., 2003), while VGLUT1 is predominantly responsible for glutamatergic signaling in adult neurons (Fremeau et al., 2004; Wojcik et al., 2004).

In mammals, all three VGLUT isoforms are closely related with 75% of sequence identity overlap, with the main divergence on the N- and C- termini (Li et al., 2020). 3D homology models of VGLUTs based on MFS family members have been postulated and used to examine the biochemical characteristics of VGLUTs (Pietrancosta et al., 2020). However, this is no longer necessary for VGLUT2 as Li et al. (2020) were the first to provide a cryo-EM structure for a vesicular neurotransmitter transporter. This new structure provides valuable structural information about the specific functioning of VGLUT2, for example showing that the R322 cluster in the C-terminal includes a histidine– glutamate pair not observed in the MFS family member homologs of VGLUTs, suggesting that this pair might play a role in the specificity to bind glutamate (Li et al., 2020).

ATP is essential as an energy source to create the abovementioned electrochemical gradient. However, the significance of nucleotides as neurotransmitters should not be forgotten. Although early evidence hinted at a vesicular ATP transporter (Gualix et al., 1999; Luqmani, 1981), it was not until 2008 that the protein responsible for the nucleotide transport was identified (Sawada et al., 2008). The SLC17A9 protein was found through gene mining and identified to be the VNUT using reconstitution in liposomes. It was shown that besides ATP, it could transport ADP and GTP.

1.2.2.2 SLC18 family (VMAT1,2 and VAChT)

VMAT1 and 2 were first identified in rats. cDNA was cloned and overexpressed in CHO cells, which showed ATP-dependent dopamine uptake. This cDNA encoded for a protein belonging to the MFS family but did not look like the known plasma membrane transporters, so VMAT1 was discovered (Erickson et al., 1992; Liu et al., 1992). The human cDNAs for VMAT1 and 2 were quickly identified, resembling two proteins of 514 and 525 amino acids long, respectively (Erickson et al., 1995, 1996). VMAT1 is primarily found in the central nervous system (CNS), while VMAT2 is mainly found on neuroendocrine cells of the peripheral nervous system (PNS). VMATs both transport various monoamines such as serotonin, epinephrine, norepinephrine, and dopamine (Erickson et al., 1996). Besides the different locations, the kinetic differences between them indicate distinct functions, even though the amino acid sequence overlap is about 60%. For example, VMAT2 transports histamine, while VMAT1 does not (Erickson et al., 1995). They also vary in their inhibitor sensitivity (Erickson et al., 1996).

VAChT was identified by modifying the *C. elegans*' *unc*-17 gene (Alfonso et al., 1993). Shortly after, the human and rodent homologs were isolated, revealing a 532-amino acid protein with 12 possible transmembrane domains (Erickson et al., 1994, 1995).

Even though no crystal or cryo-EM structures are available for VMAT1 and 2 or VAChT, almost all MFS proteins have 12 trans-membrane domains with the C- and N-terminals facing the cytoplasm (Law et al., 2008). Due to the highly conserved amino acid sequences of the vesicular transporters in the MFS family, structural models have been developed using bacterial homologs of VMAT2 (Yaffe et al., 2014) to study the mechanisms and stoichiometry of these transporters.

1.2.2.3 SLC32 family (VGAT)

The sole member of the SLC32 family, VGAT, was first identified studying the nematode *C. elegans.* They found that the *unc*-47 gene was responsible for the failed GABAergic signal transmission (McIntire et al., 1993). It was isolated as a possible GABA transporter, followed shortly after by identifying the rodent equivalents (McIntire et al., 1997; Sagné et al., 1997). The isolated cDNA revealed a 495 or 525-amino acid-long protein for mice and rats, respectively. VGAT is predominantly found in GABAergic and glycinergic neurons of the CNS (neocortex, hippocampus, cerebellum, striatum, septal nuclei, and reticular nucleus of the thalamus). Some limited expression is also found in the PNS (Gasnier, 2004).

Early on, it was clear that VGAT transports both GABA and glycine (Chaudhry et al., 1998). VGAT has an uptake affinity for GABA of Km ~ 5 mM, and glycine was shown to inhibit GABA transport (IC_{50} ~ 25 mM) (McIntire et al., 1997). Additional evidence for the uptake of glycine by VGAT was found using knock-out mice. The disruption of VGAT reduced the release of GABA and glycine (Wojcik et al., 2006). Moreover, it has now been shown that besides glycine and GABA, VGAT can also translocate β-alanine (Juge et al., 2013). The ability to transport more than one neurotransmitter complicates the phenotype and subpopulation determination of SVs even further. Usually, the phenotype of a neuron or an SV is determined by the type of vesicular neurotransmitter transporter present. The phenotype of inhibitory neurons and SVs cannot be determined in that manner as it depends on which neurotransmitter has been taken up into the SV. The 'decision' of the transporter to take up either GABA or glycine was initially thought to be directly proportional to the presynaptic cytosolic transmitter content. However, a detailed analysis of the data implies that the uptake of GABA/glycine is more carefully regulated by the proximity and expression levels of proteins responsible for GABA and glycine supply (Aubrey, 2016). For example, L-glutamic acid decarboxylase(GAD)65 synthesizes GABA from glutamate and is also suggested to form a complex with VGAT to promote efficient GABA synthesis and increase the GABA uptake into SVs (Buddhala et al., 2009).

No crystal or cryo-EM structure is available for VGAT yet, allowing for an ongoing debate on the actual structure. Based on computer predictions when first discovered, it was suggested that both the N- and C-terminus face the cytosol with an estimated 10 transmembrane domains (McIntire et al., 1997). Mass spectrometry combined with epitope-specific antibodies disputes this and proposes that instead, VGAT possesses an uneven number of transmembrane domains, now estimated to be nine. In this case, the N-terminus is located towards the cytoplasm, while the C-terminus faces the SV lumen (Martens et al., 2008). Hopefully, with the recent victory to obtain the cryo-EM structure for VGLUT2, similar approaches will be used to shed more light on the structure of VGAT.

1.2.3 Uptake of neurotransmitters

Besides the structural differences between the transporters described above, the charge differences between the neurotransmitters (negative for glutamate and ATP, positive for monoamines and acetylcholine, neutral for GABA and glycine) are a second indicator that there must be distinct transport mechanisms for each protein. The transport of each of them is coupled to the electrochemical gradient. However, they rely differently on the two aspects of the electrochemical gradient (ΔpH and ΔΨ) (Chaudhry et al., 2008). Especially the mechanisms of the negatively and neutrally charged neurotransmitters are not fully established, as explained in more detail in the following paragraphs (Figure 3).

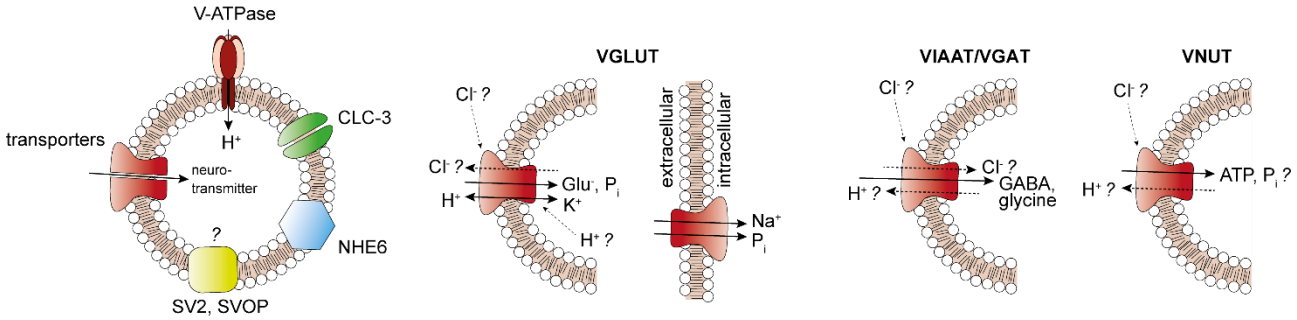

Figure 3. Current overview of neurotransmitter synaptic filling ionic mechanisms. Depicted from left to right; an SV with the main protein groups postulated to play a role in SV filling, suggested ionic mechanisms for VGLUT in SV membrane and VGLUT on plasma membrane (inverted orientation when compared to SV), suggested ionic mechanism for VGAT/VIAAT, suggested ionic mechanism of VNUT.

1.2.3.1 VGLUT

Studies on the ionic filling mechanism of glutamate by VGLUT1 and 2 in the last two decades have led to contradicting results and contesting theories. Originally before its role in glutamate uptake was discovered, VGLUT1 was thought to be a brain-specific Na+-dependent inorganic phosphate (P_i) co-transporter (BNPI) on the plasma membrane (Aihara et al., 2000; Ni et al., 1994). The discovery of its new role prompted an investigation into its mechanism with these main conclusions (summarized in Figure 3) (recently reviewed elaborately by (Pietrancosta et al., 2020)).

i. Glutamate uptake is influenced by both ΔpH and ΔΨ, to a different extent

As a negatively charged neurotransmitter, the inside positive ΔΨ of approximately 80 mV is theoretically sufficient to transport glutamate into the SV at the expected concentrations. Experimentally, ΔΨ was supported to be the main driving force for glutamate transport (Maycox et al., 1988; Moriyama and Yamamoto, 1995). However, using nigericin, a K+/H+ exchanging ionophore that can dissipate the ΔpH reveals a supporting role of the ΔpH in glutamate uptake (Bellocchio et al., 2000; Tabb et al., 1992).

ii. Chloride has a significant impact on glutamate uptake in multiple ways

A biphasic dependence of VGLUT on chloride has been shown. Low cytosolic concentrations (4-6 mM Cl^-) of chloride increase the glutamate uptake, while a further increase of chloride inhibits glutamate uptake. This effect was initially attributed to two possible interpretations; 1. Chloride binds allosterically to VGLUT to increase its activity, 2. Chloride influx into the SV allowed for an increase in ΔpH (Naito and Ueda, 1985; Wolosker et al., 1996). However, later findings revealed a possibly even more complex role of chloride. Besides an allosteric binding site for chloride, chloride was also shown to compete with the substrate-binding site (Bellocchio et al., 2000). The reconstitution of purified VGLUT in liposomes, allowed for controlled luminal and cytosolic environments and supported the possibility of the two possible binding sites. It further revealed that VGLUT might work as either a chloride/glutamate exchanger or 'leak' channel for chloride (Preobraschenski et al., 2014; Schenck et al., 2009). Initially, no permeability for chloride was observed (Juge et al., 2010). However, follow-up studies reported both permeation and allosteric activation of chloride (Chang et al., 2018; Eriksen et al., 2016) are reported. Structural evidence from the cryo-structure of VGLUT2 identifies R184 as the allosteric chloride binding site (Li et al., 2020), and it reports a possible Cl^- channel that intersects with the glutamate binding site.

iii. Cations might have the ability to transport or bind to VGLUT too

The ability of VGLUT to transport cations such as Na^+, K^+, and H^+ has received contradicting evidence as well. Where one study finds that Na^+, K^+, and H^+ cannot permeate through VGLUT, but H^+ allosterically activates glutamate uptake (Eriksen et al., 2016), others indirectly find that VGLUT functions as a proton-glutamate exchanger (Tabb et al., 1992; Wolosker et al., 1996) or as a proton- K^+ (Preobraschenski et al., 2014) or even a proton- Na^+ exchanger (Rossano et al., 2017). H128 on VGLUT2 could be the initial H^+ binding site for allosteric activation (Li et al., 2020)

iv. VGLUT can transport P_i

In line with VLGUTs original discovery, they can transport phosphate as well. Whether two distinct binding sites for phosphate and glutamate exist, as initially reported (Juge et al., 2006) or they bind to the same substrate-binding site remains debated. The latest evidence suggests competition for the same binding site with phosphate transport either energized by the electrochemical gradient or an outward sodium gradient (Cheret et al., 2021; Preobraschenski et al., 2018). When on SVs, VGLUT faces the cytosol transporting both glutamate and phosphate by the electrochemical gradient with a preference for glutamate based on the concentrations in the cytosol. When on the plasma membrane, VGLUT faces the extracellular space, phosphate is transported coupled with sodium, with low affinity competition of glutamate.

It turns out that VGLUT does not have an exact single mechanism stoichiometry. The partial knowledge available to us today indicates that this complex ionic mechanism of neurotransmitter filling changes depending on the environment (Preobraschenski et al., 2014); the membrane VLGUT is in (plasma membrane or SV) and the thereby associated difference in ion and neurotransmitter concentrations, further influenced by the possible allosteric effects of chloride and protons.

1.2.3.2 <u>VGAT</u>

GABA and glycine are neutral at physiological pH and, based on those biochemical properties, are suggested to rely on both components of the electrical chemical gradient equally. However, experimentally there is no consensus on this. Using purified VGAT in proteoliposomes, GABA uptake was observed when a positive ΔΨ was formed but not when a ΔpH was formed (Juge et al., 2009). However, another group attributed equally important roles to ΔpH and ΔΨ in GABA uptake. Studying proteoliposomes and rat SVs they found that GABA uptake was similar at chloride concentrations of 0 (domination of ΔΨ) and 150 mM (domination of ΔpH). Additionally, the reduction of either the ΔpH or the ΔΨ resulted in a decrease in GABA uptake (Hell et al., 1990). Mechanistically, two possibilities have been proposed (Ahnert-Hilger and Jahn, 2011).

1. *VGAT functions as a chloride-GABA co-transporter*.

   With VGAT as a chloride-GABA co-transporter, the protein provides the necessary chloride conductance for continued proton pumping, further stimulating chloride and GABA co-transport. Juge et al. (2009) showed that VGAT couples the transport of chloride with GABA; for every GABA molecule, two chloride ions were co-transported into the SV. The possibility that GABA-proton exchange takes place was excluded through their experiments.

2. *VGAT functions as a proton-GABA exchanger*.

Though not observed by Juge et al. (2009), increased support for VGAT as a proton-GABA exchanger is accumulating. In this case, a neutralizing current is required for which CLC-3 is the most likely candidate, as discussed in 1.2.1.1. The pH and electrical gradients could be monitored using single-vesicle imaging, and it revealed that exclusive exchange of GABA and protons took place, with no involvement of other ions (Farsi et al., 2016). This model also fits with early findings in which the luminal proton concentration strongly influenced GABA uptake (Hell et al., 1990). Recently Egashira et al. (2016) confirmed this model using cultured hippocampal neurons, monitoring luminal pH of GABAergic SVs. GABAergic vesicles have a higher resting pH (~6.4) than glutamatergic vesicles (~5.8), and the luminal pH dynamics with and without VGAT support the theory that VGAT is a proton-GABA exchanger (Egashira et al., 2016).

Even though the most recent evidence seems to support VGAT as a proton-GABA exchanger, the exact stoichiometry is undetermined. Preliminary data from my master thesis (Olsthoorn, 2017) shows that the purified VGAT reconstituted in proteoliposomes exhibits a substrate-independent proton leak. Additionally, the role of other ions has not been studied extensively for VGAT.

1.2.4 Maintaining neurotransmitter gradient

Once SVs are filled with neurotransmitters against their concentration gradient, the vesicular content has to remain stable until the arrival of the action potential and the resulting exocytosis. When isolated SVs are filled with glutamate, followed by dissipation of the ΔμH+, glutamate quickly leaks out of the SVs (Burger et al., 1989, 1991; Hartinger and Jahn, 1993). A more in-depth look at the observed efflux in isolated SVs revealed that this efflux could be minimized by reducing the temperature or blocking with DIDS[4] (Burger et al., 1989, 1991; Hartinger and Jahn, 1993), indicating that a protein on the SV membrane is most likely responsible for the efflux, potentially the neurotransmitter transporter itself. In the nerve terminal, however, the vesicular glutamate seems to be retained. Removal of either the presynaptic glutamate or inhibiting the V-ATPase, resulted in a substantial decrease of evoked EPSCs, but only a minor reduction in mEPSCs (Ishikawa et al., 2002; Takami et al., 2017; Wu et al., 2007). The limited reduction in mEPSCs indicates that glutamate storage in SVs in the nerve terminal is relatively stable, with possibly only a minor influence of neurotransmitter leakage on synaptic transmission. The substantial decrease in evoked EPSCs is explained by endocytosed vesicles not being refilled, resulting in an accumulation of empty SVs reducing the evoked EPSCs over time. It remains unclear why glutamate storage in SVs is more stable in brain slices than in isolated SVs and how glutamate storage is mediated.

[4] 4,4'-diisothiocyanatostilbene-2,2'-disulfonic acid (DIDS), an inhibitor of anion transport

The possible mechanism of neurotransmitter efflux and the thereby associated information about maintaining glutamate storage levels is one more important step in our overall understanding of neurotransmitters, SVs, and synaptic transmission in general. Is SV content determined by the balance between uptake and efflux (also known as steady-state-model), or is it determined by a preset maximum equilibrium (also known as the set-point model)(Williams, 1997)? In the set-point model, the number of transporter proteins only affects the speed of filling, not the level of filling, while in the steady-state model, more transporter proteins result in increased SV filling. A single VGLUT transporter is sufficient to fill an SV in *Drosophila* (Daniels et al., 2006), supporting the set-point model. On the contrary, another study found that the neurotransmitter content is, at least to some extent, determined by the copy number of VGLUT1 (Wojcik et al., 2004) or VMAT2 (Pothos et al., 2000) which is supportive of the steady-state-model.

Just as for the glutamate filling, the two components of the ΔμH+ affect glutamate efflux/retention. When isolating SVs from rat brain, if the ΔμH+ is maintained, vesicular glutamate is retained (Burger et al., 1989), in line with another study that shows that the presence of the ΔμH+ is necessary to retain glutamate in SVs (Carlson and Ueda, 1990). Early radioactive uptake assays indicated a possible role for chloride. Dissipation of the ΔpH (and not ΔΨ) combined with the presence of 20 mM chloride resulted in rapid efflux of glutamate, even while the V-ATPase was still functioning, resulting in a new lower equilibrium glutamate concentration (Wolosker et al., 1996). More detailed kinetics of glutamate efflux are unavailable at the moment, with the specific role for VLGUT in efflux remaining undetermined.

1.3 Aim of this study

As explained in the previous sections, neurotransmitter filling in SVs has two main components; formation of the ΔμH+ and uptake of neurotransmitters. For measuring neurotransmitter uptake, two direct measuring methods have been used so far; either radiolabeled assays for uptake of neurotransmitters (Burger et al., 1989; Carlson and Ueda, 1990; Maycox et al., 1988) or electrophysiology for indirect measurements of loaded neurotransmitters (Goh et al., 2011; Riazanski et al., 2011). New fluorescent probes measuring the concentration of GABA or glutamate content have recently become available (Hires et al., 2008; Masharina et al., 2012), motivating the development of a new uptake assay (by Dr. Julia Preobraschenki and Dr. Iman Kattan, to be published). This uptake assay uses a fluorescent intensity-based glutamate sensor iGluSnFR (Marvin et al., 2013) for direct measurements of glutamate content in SVs.

Investigation of the formation and changes in ΔμH+ have relied mostly on fluorescent-based approaches, relying on the availability of pH-sensitive and potentiometric probes. ΔpH measurements in isolated SVs and proteoliposomes initially relied heavily on the probe acridine orange (Bellocchio et al., 2000; Schenck et al., 2009), which due to its nonlinear response to ΔpH is difficult to use for quantitative measurements (Rottenberg and Moreno-Sanchez, 1993).

pH-sensitive proteins such as *pHluorin* (Farsi et al., 2016) and *mOrange2* (Egashira et al., 2015) and other probes (see (Farsi, 2015) for an overview) have been used to collect valuable quantitative data on SV acidification within their pH response range. Compared to pH sensitive probes, only limited potentiometric probes to study ΔΨ have been available. Oxonol dyes have been used most extensively until recently (Goh et al., 2011; Preobraschenski et al., 2014; Wolosker et al., 1996). However, estimates of the ΔΨ are not the most accurate due to the low precision of these dyes (Shapiro, 2000). Significant improvements are taking place to improve ΔΨ dyes with more accurate ΔΨ measurements being achieved using the VF2.1.Cl[5] probe (Farsi et al., 2016; Miller et al., 2012).

The continued development of these new probes contributes greatly to our knowledge of neurotransmitter uptake. Nonetheless, the currently available assays have their limitations when trying to answer some of the questions that remain. Experiments relying on neuronal cell culture or brain slices for fluorescent imaging or electrophysiology provide valuable *in vivo* information on the neurotransmitter uptake mechanisms. However, these experiments do not provide the controlled environment necessary to decipher the details of the ionic mechanisms. Bulk experiments using isolated SVs or proteoliposomes in spectrofluorometers, using the abovementioned fluorescent probes, allow for this controlled environment to study the ionic mechanisms. However, the nature of these experiments only allows the addition of compounds, with no removal option once added. Additionally, they always represent an average of a batch of SVs or proteoliposomes. The single vesicle assay developed in this lab addressed that limitation allowing for more detailed information of subpopulations of SVs (Farsi et al., 2016; Upmanyu et al., 2021). Many of these approaches have their static nature in common; once a compound is added to the experiments, it cannot be removed.

To decipher how glutamate or GABA uptake in SVs is coupled to the energy gradient a detailed study of the on- and off-kinetics of the ΔΨ and ΔpH is required. Precisely timing the addition of components such as varying concentrations of ATP, Cl-, and neurotransmitter allows for detailed study of the on-kinetics. This requires a system with fast solution changes. Studying the off-kinetics of these components requires the removal of components from the environment of the SVs with a high temporal resolution. Through the removal of components such as ATP, the efflux mechanism of glutamate can be studied by influencing the electrochemical gradient in a flexible manner.

During my PhD, I aimed to develop a new dynamic assay capable of dynamically changing the environment of SVs repetitively by immunocapturing SVs on a glass surface and attaching a microfluidic device. This new assay can then be used to study the unanswered questions on the loading and maintenance of neurotransmitter filling in synaptic vesicles.

[5] a photo-induced electron transfer-based voltage-sensitive dye

The system to be developed should have the following properties:

i. Stable immunocapture of SVs
   The single vesicle assay developed by Zohreh Farsi already revealed that SVs immobilized through adsorption do not survive fast superfusion of solutions. Therefore, instead of adsorptive approaches, more stable capturing approaches are necessary. Stable capturing of the complex organelle SVs is far more complex and could potentially affect the health of the SVs. Instead, antibodies will have to be immobilized stably to ensure stable immunocapture of the SVs.
ii. Sufficiently high density to allow for accurate quantification
   Quantification of single SVs requires the averaging of thousands of SVs to acquire a decent signal-to-noise ratio. To circumvent this problem, the SVs must be immobilized at a sufficiently high density to result in a small area containing thousands of SVs, resulting in a sufficient signal-to-noise ratio immediately without averaging. The area has to be small enough to capture the background signal in the same image to obtain this signal-to-noise area and allow the solution changes to occur more or less simultaneously to the whole area.
iii. Fast solution changes
   From Zohreh Farsi's work, we also learned that the kinetics of the transporter mechanisms reside in the seconds range (Farsi et al., 2016), therefore the system requires the ability to change solutions within at least the seconds range, preferably faster to measure the kinetics. This can be achieved by the development of a microfluidic platform. Additionally, using a microfluidic platform allows for the addition and (especially interesting) the removal of any substance quickly in a controlled manner, providing a solution for the limitation of the static nature of currently available methods.
iv. Stability during flow
   During the necessary fast solution changes, the SVs have to remain in place. This stability during flow requires high stability of the antibody binding to the glass surface. The antibodies must be covalently bound to the surface to prevent the risk of antibody detachment under flow and fulfill the requirement of SVs stability during flow.

In this thesis, three different surfaces are prepared and tested for their ability to provide stable immunocapture of the SVs. A microfluidic device was developed in collaboration with Dr. Eleonora Perego (Sarah Köster group, X-ray laboratory), which fulfills these requirements together with a pressure clamping device compatible with the biological material on the surface. Preliminary experiments were executed to test the ability of the assay to measure acidification in SVs and the de-acidification upon removal of ATP from the buffer. This assay now allows us to address the long-standing questions on, for example, glutamate efflux and clarify how neurotransmitter concentrations in SVs are maintained.

2 Materials and Methods

2.1 Materials

2.1.1 Buffers and solutions

Table 1. List of buffers and solutions used in the methods described in this section. All solutions were prepared with ultrapure water (Milli-Q).

Buffer/solution	**Composition**
Homogenization buffer	320 mM sucrose, 5 mM Hepes, pH 7.4 (NaOH)
CPG column buffer	300 mM glycine, 5 mM Hepes, pH 7.3 (KOH)
PBS (1x)	2.7 mM KCl, 1.5 mM KH2PO4, 137 mM NaCl, 8 mM Na2HPO4, pH 7.35
TBS (T) (1x)	15 mM Tris-HCl, pH 7.4, 150 mM NaCl (0.5 % (v/v) Tween 20)
SSC (1x)	150mM NaCl, 15mM sodium citrate, pH7
Lysis buffer	200 mM NaCl, 100mM Tris-HCl, 5 mM EDTA, 0.2% (v/v) SDS, pH 8.5
TAE (1x)	Tris 20 mM, Acetic acid 10 mM, EDTA 1 mM, pH 8.5
Phosphate free column solution	150 mM NaCl, 10 mM MOPS, pH 6.5
Upper gel buffer for SDS-PAGE	0.5 M Tris-HCl, pH 6.8
Lower gel buffer for SDS-PAGE	1.5 M Tris-HCl, pH 8.8
SDS-PAGE Running buffer	25 mM Tris-HCl, 192 mM Glycine, 0.1 % SDS
1x TransBlot Turbo buffer	20% (v/v) 5x TransBlot Turbo Buffer, 20% (v/v) pure ethanol
Blocking solution 1	100 mM ethanolamine, 100 mM Tris pH9
Blocking solution 2	50 mM ethanolamine, 100 mM Tris, pH9
Activity buffer	300 mM glycine, 2 mM MOPS, 2 mM MgCl, 30 mM KCl_2

2.1.2 Antibodies

Table 2. List of used antibodies

Antibodies	Species	Application (dilution)	Company	Category number
IRDye 800CW Anti-Rabbit IgG	Goat polyclonal	WB (1:10.000)	Licor	926-32211
IRDye 680CW Anti-Mouse IgG	Goat polyclonal	WB (1:10.000)	Licor	926-68070
Synaptophysin 1 IgG	Mouse monoclonal	Immobilization	Synaptic Systems	101 011
Synaptobrevin 2 IgG	Mouse monoclonal	Immobilization	Synaptic Systems	104 211
Biotin IgG	Polyclonal rabbit antiserum	Immobilization	Synaptic Systems	291 002
VGAT IgG	Rabbit monoclonal	Immunoisolation of SVs	Synaptic Systems	131008
Synaptophysin 1 – Oyster 488	Mouse monoclonal	Detection of immobilized SVs (1:1000)	Synaptic Systems	n.a.
Synaptobrevin 2 – Oyster 550	Mouse monoclonal	Detection of immobilized SVs (1:1000)	Synaptic Systems	n.a.
Alexa Fluor 488 antimouse IgG	Goat polyclonal	Detection of immobilized antibody (1:1000)	Invitrogen	A32723

2.2 Methods

2.2.1 Genotyping of transgenic mice

Transgenic mice were genotyped with the support of Brigitte Barg-Kues (Laboratory of Neurobiology, MPIbpc, Göttingen, Germany) based on the protocol provided by Dr. Zohreh Farsi (Farsi, 2015). The animal care workers provided ear samples of the spH-21 transgenic mice and stored them at -20 ºC until processing. To extract the genomic DNA, they were incubated overnight on a thermoshaker (maximum 400 rpm at 60°C) with 300 µL per ear sample of 100 µs/ml protein kinase K (Roche) in lysis buffer. The next day the samples were centrifuged for 2 min at 18.800 x *g*.150 µL of 6M (saturated) NaCl solution was added to each sample and quickly vortexed, followed by centrifugation at 18.800 x *g* for 5-10 min at room temperature. The resulting supernatant was transferred to a new Eppendorf and inverted six times with 0.75 volumes of isopropanol. This mixture was centrifuged for 5-10 min at 18.800 x *g* at 4 ºC. The supernatant was discarded carefully, and 500 µL of 70% ethanol was added to the pellet and centrifuged for 10 minutes at 18.800 x *g* at 4 ºC. Immediately after centrifugation, the supernatant was discarded, and the Eppendorfs were inverted to dry for 20-30 min before resuspension with 30 µL water for 30 min to 1 h at room temperature stored at 4 °C until use.

Three primers (Table 3) for amplifying synaptobrevin, pHluorin, and synaptopHluorin were designed using the primers designed by Li et al. (2005) as a guideline, improving their GC content and melting temperature for more successful DNA amplification based on the advice of Dr. Ulrike Teichmann. Primer for the control (IL_21) were obtained from Dr. Zohreh Farsi.

Table 3. List of primers. All primers were obtained from Eurofins Scientific.

Gene	Forward primer	Reverse primer
synaptobrevin	5'- tgc acc tcc tcc aaa cct ta	5'- gct agt gct gaa gta aac gat g
pHluorin	5'- gag ttg tcc caa ttc ttg ttg	5'- agc agc tgt tac aaa ctc aag
synaptopHluorin	5'- tgc acc tcc tcc aaa cct ta	5'- agc agc tgt tac aaa ctc aag
IL_21	5'- cta ggc cac aga att gaa aga tct	5'- gta ggt gga aat tct agc atc atc c

Table 4. PCR for each genomic DNA sample.

PCR reaction mixture	**PCR program**
- 5 µL 10x PCR reaction buffer containing MgCl2 (Sigma) - 38.5 µL of water - 1 µL Forward primer (10 µM) - 1 µL Reverse primer (10 µM) - 1 µL dNTP (10 mM, ThermoFisher Scientific) - 2.5 µL REDTaq Genomic DNA polymerase (Sigma, 1u/µl) - 1 µL Genomic DNA	Step 1: 95 °C 2 min Step 2: 95 °C 45 s Step 3: 56 °C 45 s Step 4: 72 °C 2 min 30 x cycles of steps 2-4 Step 5: 72 °C 5 min Step 6: maintain at 4°C

Polymeric chain reaction (PCR) was performed for each genomic DNA sample as described in Table 4, adapted from (Farsi, 2015). 20 µL of the PCR samples were mixed with 5µL loading dye (Gel loading dye Purple 6X, New England BioLabs). A 2% agarose gel was prepared in 1x TAE buffer with 3:100 dilution of GelGreen Acid Stain (Biotum) on which the PCR samples and 10 µL of 0.1 mg/ml 1kb DNA ladder (GeneRuler, Thermo Scientific) were loaded. The gel was run at 100 V for 30 min in 1x TAE buffer. The gel was imaged under UV light (Figure 4). Only animals that tested positive for all four genes were used in SV purification protocols.

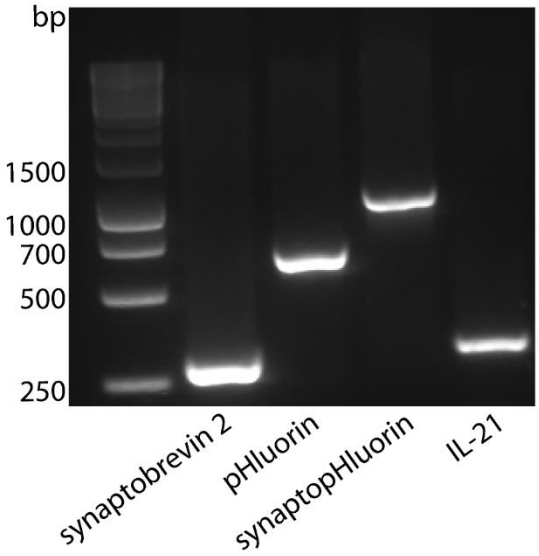

Figure 4. Example of genotyping results for a spH-21 positive animal.

2.2.2 Isolation of synaptic vesicles

For the preparation of lysate supernatant containing SVs (LS1) from the spH-21 mouse brains, the original protocol was developed by (Ahmed et al., 2013), followed by modifications to the protocol by Dr. Zohreh Farsi (Farsi et al., 2016) and Dr. Marcelo Ganzella (Ganzella et al., 2021). In this thesis, the protocol kindly provided by Dr. Marcelo Ganzella was followed (Figure 5a), modified for the purification of six animals at a time, and other minor modifications marked in bold here. Briefly, six mice were decapitated, and the excess white matter was dissected and removed. The rest of their brains were homogenized in **5 mL** ice-cold homogenization buffer per brain with 200 µM PMSF and 1 µg/ml Pepstatin A followed by two steps of differential centrifugations (first centrifugation: 2700 rpm, 10 min, SS34, supernatant for second centrifugation: 11.000 rpm, 15 min, SS34). The pellet was resuspended using **0.5 mL** ice-cold homogenization buffer per brain. The obtained synaptosomes were hypo-osmotically disrupted and centrifuged (20.000 rpm, **35 min,** SS34), resulting in the lysate supernatant (LS1) used in the spH-21 SV immobilization approaches. To store the LS1, 10x PBS and a protease inhibitor cocktail tablet (cOmplete, EDTA/-free, Roche) were added before snap freezing the aliquots with liquid Nitrogen and storage at -80 ºC.

The preparation of rat LS1 and purified SVs from Wistar rat brains (Huttner et al., 1983; Nagy et al., 1976) largely follows similar steps as for the LS1 from mouse brains described above with just one additional washing step for the synaptosomes before lysis (Figure 5b). A detailed protocol can be found in Huttner et al. (1983).

Here I briefly describe the steps after LS1 to obtain purified SVs. The LS1 was centrifuged to concentrate the SVs through pelleting. The SVs were resuspended and loaded onto a continuous sucrose gradient. After centrifugation, SVs were collected from the 200-400 mM region in the gradient and loaded onto a CPG-3000 column. Fractions from the second peak were collected and concentrated as they were shown to contain SVs. SVs were resuspended in sucrose buffer and SV aliquots were snap-frozen with liquid Nitrogen and stored at -80 ºC.

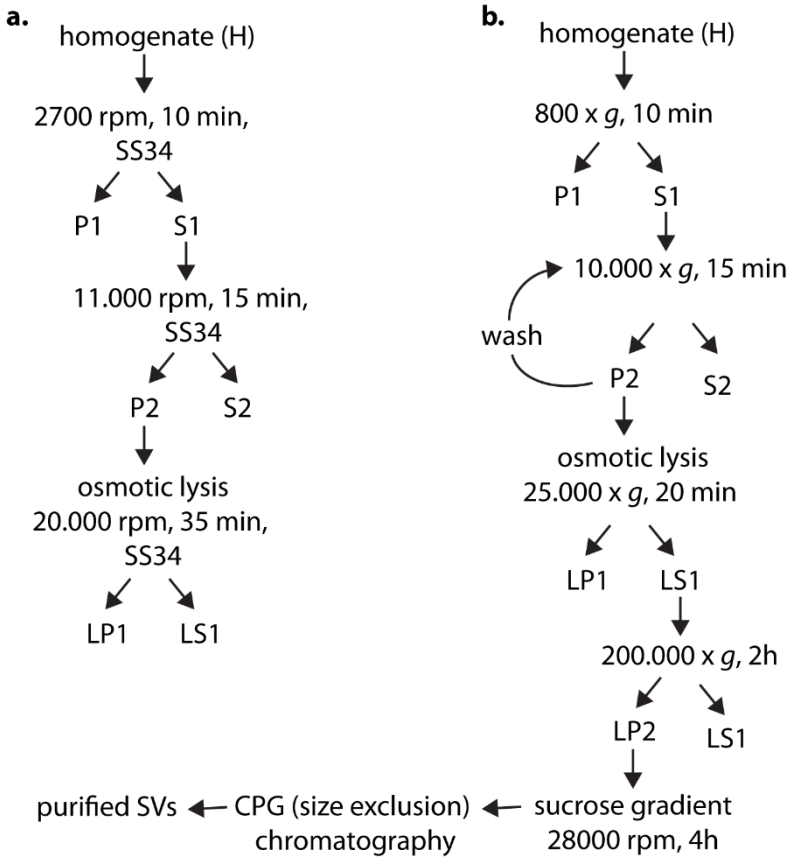

Figure 5. Subcellular centrifugation protocols for synaptic vesicles. a) Protocol to prepare LS1 from spH-mouse brains (based on Marcelo Ganzella and Ahmed et al. (2013). b) Protocol to prepare LS1 and purified SVs from rat brains (based on Hutnner et al. (1983)).

2.2.3 Purification of antibodies

Affinity purification of synaptophysin (syp) clone 7.2 antibody (cat no. 101011) was purified in two different ways using affinity purification based on two different elution methods; Gentle Ag/Ab elution buffer (Thermo Cat. No. 21027) or low pH elution. The low pH elution protocol using buffers with amines, which can interfere with the coupling chemistries used in later steps if not completely removed from the buffer. The gentle Ag/Ab elution buffer does not contain amines, however its high salt concentration results in diluted antibodies once dialyzed. Both protocols are based on the original protocol from Henrik Martens at Synaptic Systems (Göttingen) and in case of the low pH elution Henrik Martens developed the protocol in collaboration with Dagmar Diezman. The supernatant of the syp clone 7.2 antibody was prepared and provided by Synaptic Systems. First, the columns were prepared by taking apart a 2.5 mL syringe and putting a filter (35 µM Pores MoBiTec #S1235) at the bottom. 1 mL of protein-G-sepharose slurry (4 FastFlow Amershau – GE healthcare) was loaded onto the filter.

For the low pH elution approach, the column was then equilibrated with 20 to 30 mL of 1x PBS, pH7.4. Then 5 mL of supernatant was diluted with PBS in a 1:1 manner, and this volume was loaded onto the pre-equilibrated column. The flow-through was collected and stored at -20 degrees to be reused in future purification sessions. The column was then washed with 15-20 mL until the OD_{280} did not change anymore. In the meantime, 7 Eppendorfs were prepared with the first one containing 20 µL of 1.5M Tris, pH8.8, and the other six containing 40 µL. When the washing was completed, elution of the antibody with 0.1M glycine, pH 3.0 took place by adding 250 µL (first Eppendorf) or 500 µL (following Eppendorfs) to the column and collecting the flow-through in the prepared Epppendorfs. Immediately after collections, the Eppendorf was vortexed. The concentration of the collected antibody was measured on the Nanodrop followed by dialysis at 4 ºC to PBS in a Slide-A-Lyzer dialysis Cassette (ThermoScientific, 2000 MWCO) over three days, changing the dialysis buffer twice a day. If necessary, the antibody was concentrated using Amicon centrifugal filters (100k NMWL, Merck Millipore) after the dialysis process. The purified antibodies' affinity was tested using a dilution scheme to detect syp in LS1 Western blots.

The Gentle Ag/AB elution buffer protocol follows the same steps as the above-mentioned low pH elution with the following modifications. Instead of PBS, a phosphate-free column solution was used. Instead of using the low pH glycine solution for the elution, the gentle Ag/Ab elution buffer was used for elution, which did not require preparing the Eppendorfs with Tris buffer. Instead, 500 µL (first Eppendorf) and 1 mL (following Eppendorfs) of the elution buffer were applied to the column, collected, and vortexed.

2.2.4 Western blotting

SDS-PAGE gels and Western blotting (Yang and Mahmood, 2012) were performed to check antibodies' purification and the SV purification. Protein samples were prepared using 4x NuPAGE LDS Sample Buffer (Thermo Fisher Scientific, NP0008) and (in case of antibody purification) boiled at 95 °C for 5 min. Samples were run on 10% SDS-PAGE gels with 3.75% stacking gels, 60 V for stacking, 120 V for resolving.

The proteins were then transferred to a nitrocellulose membrane using the Trans-Blot Turbo Transfer System (Bio-Rad). Before incubating the primary antibodies, the membranes were blocked in 5% non-fat dry milk in TBST for 1 h at room temperature. Incubation with primary antibodies varied from 1 h to overnight depending on the antibody, followed by three five-minute washes with TBST before incubation with the secondary antibody (1:10.000, IRDye 800CW secondary antibodies, Licor) for 1 h at room temperature. After final washes (three times five minutes TBS), visualization was achieved using the Odyssey CLx Infrared Imaging System (Licor).

2.2.5 Protein concentration determination

To determine the concentration of LS1 or purified SV samples, Pierce 660nm Protein Assay Reagent was used according to manufacturer instructions. Pre-diluted protein Assay Standards from Bovine Serum Albumin (BSA) set (Thermo Scientific) were used for the calibration curve. The Tecan Genios Pro plate reader was used to determine the absorbance at 650 nm in a 96-well plate to calculate the protein concentrations. The NanoDrop™ ND-1000 UV-Vis Spectrophotometer (Thermo Scientific) was used to determine the protein concentration of the purified antibody.

2.3 Development of the microfluidic assay

2.3.1 Glass surface modifications

2.3.1.1 2D Epoxy coverslip

2D epoxy coverslips were obtained from PolyAn in the standard dimension of 25 x 60 mm, thickness 1.5H. The glass is coated with a thin layer of silane with available epoxy coverslips.

The antibody attachment protocol was based on the operation manual provided by PolyAn and adapted through experimental optimization. High signal-to-noise ratios for antibody and SVs immobilization were obtained with the following protocol.

Antibody immobilization: Antibody solutions of 0.5mg/mL were prepared in 1x PBS buffer pH7.4 and centrifuged for 10 min at 18.800 x *g* at 4 ºC to remove any aggregates. 15 µL of the antibody solution was deposited on the 2D epoxy coverslip and incubated for 1 h in the incubator (28 ºC, 10% CO_2, 90% humidity) in a humidity chamber with wet towels. Multiple washes with reducing salt concentration followed this incubation (twice 2x SSC pH 7, once 0.1 SSC pH 7, twice Milli-Q water, each wash 5 min). Deactivation of the residual active epoxy groups on the surface was performed using blocking solution 1 for 1 h in the incubator (28 ºC, 10% CO_2, 90% humidity) in a humidity chamber with wet towels, followed by the same washing steps as before and an additional 5 min 1x PBS pH 7.4 wash.

Detection of immobilized antibody: In case of detecting immobilized antibodies on the glass surface, coverslips were labeled in 60 min using secondary goat-anti-mouse antibody Alexa Fluor 488 in a 1:1000 dilution in 0.1M Tris pH 8. After the above-mentioned washing steps, the coverslips were dried with Nitrogen gas before imaging.

SV immobilization: In the case of SV immobilization, after the immobilization of the primary antibody, the coverslips were blocked with 2mg/mL BSA in PBS for 30 minutes at room temperature on the shaker instead of labeling with secondary antibody. This step helped prevent unspecific binding of the SVs in the next step. The SVs were attached using 600 µg/mL LS1 solution obtained from rat brains mixed with 2 mg/mL BSA to further reduced unspecific binding. After an incubation of 30 min at 4 ºC the coverslips were rinsed thrice for 5 minutes with 1x PBS pH 7.4 with 2 mg/mL BSA. The coverslips were incubated with Oyster 550 labeled syb2 antibody or Oyster 488 labeled syp antibody using a 1:1000 ratio in 1x PBS pH 7.4 with 2 mg/mL BSA to detect the SVs at 4 ºC, followed by one 5 min wash with 1x PBS pH 7.4 with 2 mg/mL BSA and two washes with 1x PBS before imaging with the epi-fluorescent microscope.

2.3.1.2 siPEG/PEG-biotin coverslip

In this thesis, I modified a one-step PEG-silane (siPEG) modification approach (Schaedel et al., 2019). At first, high precision microscope coverslips (1.5H, 24 * 60 mm, Carl Roth GmbH+Co) were thoroughly cleaned by 30 min immersion in acetone, followed by 15 min of immersion in ethanol 96%, both while agitated (on shaker). After rinsing extensively with MilliQ water, the coverslips were immersed in 2% Hellmanex III for 2 hours while shaking, followed by extensive rinsing with water and drying with Nitrogen.

As a functional group we used biotin, by mixing 1 mg/mL siPEG (10 kDa, Nanosoft Polymers) with 1 mg/mL siPEG-biotin (10kDa, Nanosoft Polymers) in 96% ethanol with 0.1% HCl (for controls only 2.5 mg/mL siPEG was used). The coverslips were immersed in the siPEG/siPEG-biotin solution for three days at room temperature and kept on the shaker, followed by two 15 min washes (ethanol 96% and water). After they were dried with Nitrogen gas and used immediately.

Antibody immobilization: The antibodies to be immobilized on the siPEG/siPEG-biotin surface were streptavidin labeled before immobilization using the LYNX Rapid Streptavidin Antibody Conjugation Kit (Bio-Rad, USA) according to the manufacturer's instructions. 100 µg of antibody was modified using the LYNX^{TM} modifier reagent and then reacted with 100 µg of streptavidin mix.

The immobilization of antibodies on the siPEG/siPEG-biotin surface follows almost the same steps as described for the 2D epoxy coverslips with some minor surface-specific modifications. Antibody solutions of 0.5 mg/mL were prepared in 1x PBS buffer pH 7.4 and centrifuged for 10 min at 18.800 x g at 4 ºC to remove any aggregates. 15 µL of the antibody solution was deposited on the siPEG/siPEG-biotin coverslip and incubated for 15 min at room temperature in a humidity chamber with wet towels. After a quick dip in 4x SSC pH 7, multiple washes followed with reducing salt concentration (once 4x SSC, twice 2x SSC, once 0.1 SSC pH 7, thrice Milli-Q water, each wash 10 min).

Detection of immobilized antibody: In case of detecting immobilized antibodies on the glass surface, coverslips were labeled in 30 min using secondary goat-anti-mouse antibody Alexa Fluor 488 in a 1:1000 dilution in PBS. After two washes with PBS and two with Milli-Q water, the coverslips were dried with Nitrogen gas before imaging.

SV immobilization: After immobilization of the primary antibody, the coverslips were blocked with 2mg/mL BSA in PBS for 30 min at room temperature on the shaker. The SVs were attached using 600 µg/mL LS1 solution obtained from rat brains mixed with 2 mg/mL BSA. After an incubation of 30 min at 4 ºC the coverslips were rinsed thrice for 5 minutes with 1x PBS pH 7.4 with 2 mg/mL BSA. The coverslips were incubated with Oyster 550 labeled syb2 antibody or Oyster 488 labeled syp antibody using a 1:1000 ratio in 1x PBS pH 7.4 with 2 mg/mL BSA to detect the SVs at 4 ºC, followed by one 5 min wash with 1x PBS pH 7.4 with 2 mg/mL BSA and two washes with 1x PBS before imaging with the epi-fluorescent microscope.

2.3.1.3 Copoly(DMA-NAS-MAPS) coverslip

A substrate that has shown to bind proteins at a high density is the copolymer DMA-NAS-MAPS developed by Marcella Chiari's laboratory (Istituto di Chimica del Riconoscimento Molecolare (ICRM), Milan) (Cretich et al., 2004; Pirri et al., 2004). The protocol used in this thesis is based on these publications and the advice and experience of Dr. Marina Cretich and Prof. Marcella Chiari. The DMA-NAS-MAPS was purchased from Lucidant Polymer under the name MCP-2.

Firstly, high precision microscope coverslips (1.5H, 24 * 60 mm, Carl Roth GmbH+Co) were cleaned using O_2 plasma for 10 min (Diener Plasma System type 'Zepto'). In that time, the copolymer coating solution was prepared by vortexing 100 µL of 50X MCP-2 solution with 4.9 mL of 20% ammonium sulfate solution. After cleaning, the coverslips were submerged in the freshly prepared copolymer coating solution for 30 min at room temperature, followed by carefully dipping and swirling them in Milli-Q water. The coverslips were dried first using Nitrogen gas, followed by further drying at 80 ºC in the oven for 15 min.

Antibody immobilization: Antibody solutions of 1mg/mL were prepared in 1x PBS buffer pH7.4 and centrifuged for 10 min at 18.800 x g at 4 ºC to remove any aggregates. The coverslips were then moved to an automated piezo driven, non-contact dispensing system of ultra-low volumes (S3 sciFLEXARRAYER), and a rectangular pattern of 400pL droplets of antibody solution was spotted on the coverslips. The coverslips were then incubated overnight at room temperature in a humidity chamber with saturated NaCl solution. Deactivation of the residual active groups on the surface was performed directly without washing steps using a blocking solution 2 for 1 h at room temperature, followed by dipping and swirling them in Milli-Q water.

Detection of immobilized antibody and SV immobilization: The detection of immobilized antibodies and the capture of SVs and their detection followed the same steps as described for the siPEG/PEG-biotin coverslips.

2.3.2 Microfluidic device

The field of microfluidics deals with the technology involved in manipulating and controlling small amounts of fluids in the range of 10^{-6} to 10^{-18} liter through channels sized in the micrometers range (Lichtenberg et al., 2019; Whitesides, 2006). A microfluidic system is typically a few centimeters in size and consists of a microchannel network, inlet(s), and outlet(s) for fluid control. Due to its miniaturized nature, microfluidics requires only small amounts of (expensive or limited) reagents and are easily portable. The small volumes of liquid used also result in fast reaction times. Additionally, many versatile designs are possible, allowing for optimal designs for each circumstance and potentially detecting multiple samples in parallel (Sackmann et al., 2014).

Manipulation and control of the fluids require an understanding of fluid dynamics. Fluids in microscopic environments behave slightly differently in microfluidic systems compared to macroscopic scale systems. How a fluid behaves depends on the forces acting on this fluid and is represented by the dimensionless Reynolds' number Re. Re is the ratio between inertial forces to viscous forces (Eq. 5). The inertial forces are defined by the velocity of the fluid and the length of the system, the viscous forces are impacted by the fluid viscosity (Klein and Dietzel, 2020).

$$Re = \frac{inertial\ forces}{viscous\ forces} = \frac{\rho * v * L}{\mu} \qquad \textit{Eq. 5}$$

in which ρ is the fluid density, v is the characteristic fluid velocity, L is the relevant length scale of the system, and μ is the viscosity

The same physical forces govern fluids in the micro- and macro world, but the impact of the different forces is changed due to the different ratio of surface over volume. A Reynolds' number >2000 represents fluids that would mix stochastically and result in a turbulent flow. Below 2000, a system has a laminar flow, which means the flow velocities along the whole channel are constant in time. The Reynolds's number for microfluidic channels is usually below 1 (Song et al., 2018). Therefore microfluidic systems usually deal with a laminar flow profile, which allows for predictable fluid dynamics and diffusion kinetics and overall a great deal of control (Perego, 2019).

2.3.2.1 Polydimethylsiloxane (PDMS) device

The microfluidic device was designed by Dr. Eleonora Perego (Sarah Köster's group, X-ray facility) as described in more detail in her PhD thesis (Perego, 2019). A three-inlet device (channel length 2.3 cm, width 1 mm, and height 100 µm) (Figure 6a) was designed to allow fast solution changes. The switching of these solution changes was experimentally tested using fluorescein solution by Sebastian Smyk (Sebastian Smyk, 2017).

Briefly, the master wafers were created following standard photo-lithography methods (Duffy et al., 1998; McDonald and Whitesides, 2002). The negative photo-resist (SU8-3050) was spin-coated on a silicon wafer. The alignment of the photomasks followed the soft

baking of these wafers (95 ºC for 45 min). After exposure to UV light through this mask, the wafers were baked and developed for 15 min at 95ºC. They were coated with (heptafluropropyl)- trimethylsilane overnight. To create the polydimethylsiloxane (PDMS) device, liquid PDMS was mixed with the cross-linker (10:1 ratio) and poured onto the wafers. They were then cured for 1 h at 65 ºC. The PDMS device was cut out, cleaned with isopropanol, dried with Nitrogen, and stored until further use.

2.3.2.2 Plasma attachment

Assembly of the 2D epoxy modified glass coverslip with the PDMS device was first tested using air plasma for attachment. This attachment method would require both the PDMS device and the glass coverslip with immobilized antibodies to be exposed to air plasma for 12 sec at 40 W (Diener Plasma System type 'Zepto') (Perego, 2019). They would then be then pressed together to form a covalent bond. To test if the immobilized antibodies would be damaged by the air plasma treatment, antibodies were immobilized on the 2D epoxy coverslip as described above. They then received air plasma treatment. To test the protective abilities of PDMS and aluminium, the area of the immobilized antibody was covered with either a 1 cm x 1 cm piece of PDMS or aluminium during the air plasma treatment. This piece was removed immediately after the treatment. Plasma treatment was followed by the usual detection of immobilized antibodies by labeling with goat-anti-mouse IgG Alexa Fluor 488 as described above for 2D epoxy coverslips. Attachment by only treating the PDMS device to plasma treatment was tested as well. In this case, the PDMS device was plasma treated and subsequently placed on the 2D epoxy coverslip. Combined they were placed at 37 ºC for 3 hours to complete the attachment. The coverslips was then labeled and analyzed as described above.

2.3.2.3 Pressure clamping attachment

The modified glass coverslip was assembled with the PDMS device in a homemade device holder inspired by (Chen et al., 2014) as biological materials do not survive the conventional plasma treatment attachment approach (Huang et al., 2013). The device holder has a based metal plate with a cutout for the modified glass coverslip. The PDMS device is carefully placed on the glass coverslip and covered by a 1 mm glass plate. A second metal plate closes the device, and pressure is applied by tightening eight bolt screws. Windows are available in both metal plates to allow for fluorescent imaging and holes are present in the PDMS, the glass plate and the top metal plate to allow tubing to be attached. A sketch and image of the microfluidic device in the device holders can be found in Figure 6b. The glass plate uniformly distributed the applied pressure for secure closing of the full device, preventing any leakage from heterogeneously distributed pressure.

2.3.2.4 Solution exchange

Solution exchange in the microfluidic device was driven by 3 neMESYS Low Pressure module 290N pumps controlled by the QmixElements software. The pumps followed a preprogrammed switching pattern that resulted in a continuous flow of 3 mm/s overall in the main channel of the microfluidic device.

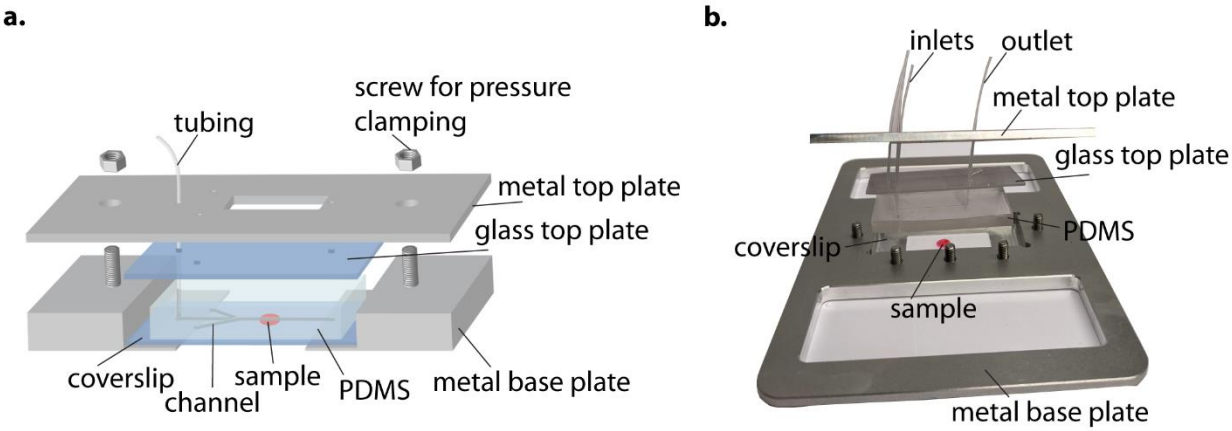

Figure 6. Microfluidic device inside the pressure clamping device holder. a) sketch of the three-inlet, one outlet microfluidic PDMS device inside a pressure holder. b) the actual microfluidic device in holder set-up.

2.4 Preliminary characterization of SVs

2.4.1 Flow experiments

Surfaces were prepared, and antibodies and SVs were immobilized as described in 2.3.1. All coverslips for flow experiments were kept in PBS at 4 ºC until the beginning of the experiments. The microfluidic device was prepared as explained in 2.3.2. The device was assembled within 1 min to prevent drying out of the coverslips, and PBS or other buffering solution was injected manually at first to confirm that the device did not leak and to prevent drying out of the antibodies/SVs. The tubing was then connected to the 3 neMESYS Low Pressure module 290N pumps, and a continuous flow of 3 mm/s was applied to the inlets of the system for 30 min, collecting the flow-through at the outlet. Images were taken before the pumps were turned on and after 30 min of continuous flow for 2D epoxy coverslips and siPEG/PEG-biotin coverslips to analyze the binding stability of the antibodies/SVs. For copoly(DMA-MAPS-NAS) coverslips images were taken every minute during the flow.

2.4.2 SV activity using pH measurements

Studying the pH changes in the SVs, spH-LS1 was used in the immobilization process on the copoly(DMA-MAPS-NAS) coverslips. The coverslips then followed the same assembly process as described for the flow experiment. Instead of PBS, an activity buffer was used. Two out of three inlets contained this buffer. The third inlet was filled with activity buffer to which MgATP was added in different concentrations (0-4 mM). The pumps were programmed to increase and decrease two of the inlets asynchronously (timing of the pattern is varied from experiment to experiment), resulting in a continuous flow inside the channel, adding and removing MgATP's availability to the SVs. Images were acquired every 200 ms to monitor the changes in fluorescence continuously.

2.4.3 Subpopulation specific immobilization

GABAergic SVs were immunoisolated according to the protocol developed by Evi Zhuleku in her master thesis under the supervision of Dr. Marcelo Ganzella and I (Zhuleku, 2020). A detailed protocol is available in the thesis. Briefly, Protein G Dynabeads (Thermo Fischer) were incubated with VGAT antibody (Synaptic Systems). After washing off unbound antibodies, the beads were incubated overnight with spH-LS1, followed by washing. SVs were then eluted from the beads using the complementary peptide for the antibody. This elution then contained a highly enriched GABAergic SV sample used for immobilization on a copoly(DMA-MAPS-NAS) coverslip as previously described.

2.4.4 Image acquisition and analysis

The images were either acquired using an epifluorescence microscope (Axioverter 200M, ZEISS) or the home-built TIRF set-up optimized and improved by Lasse Oberstrass under my supervision. Details of the TIRF set-up are available in his master thesis (Oberstrass, 2018). Intensity analysis of the obtained images was performed using ImageJ, statistical analyses of the intensities were performed using GraphPad Prism.

3 Results

In this section, I describe the development and testing of the properties required for a microfluidic SV capture assay. Covalent binding of the antibodies was required to achieve efficient immunocapture of SVs and stability during flow. Three different glass surface modification methods were tested for their ability to immobilize antibodies stably and evaluate stable immunocapture of SVs by these antibodies.

3.1 Glass surface modification approaches

Covalent binding of antibodies or other proteins to a glass surface requires the presence of functional groups. Borosilicate glass naturally does not have functional groups that can react with proteins. Therefore, to have antibodies or other proteins covalently bound to the surface, it has to be derivatized with protein-compatible functional groups. One of the classic ways of functionalizing glass or silica surfaces is through silylation/silanization. The hydroxyl groups on the glass surface attack and displace the alkoxy groups on the silane forming a covalent -Si-O-Si- bond (Van Der Voort and Vansant, 1996), allowing the addition of reactive groups to glass by using organofunctional silanes (Halliwell and Cass, 2001). In an ideal situation, these silanes form a monolayer on the surface (Van Der Voort and Vansant, 1996).

The first modified surface tested was the functionalized 2D epoxy coverslip from the company PolyAn. The glass surface is functionalized with epoxy groups through the coating with a thin silane layer. These epoxy groups can directly be used to covalently couple the antibody to the surface by the nucleophilic addition reaction of the primary amines of lysines and arginines of the antibody with the epoxy groups on the surface. The primary amines attack a carbon atom of the three-membered epoxide ring on the glass surface, leading to an opened ring with an amine group and hydroxyl group, resulting in covalent binding of the antibody (Figure 7a). In favor of this approach is its relative simplicity, as the coverslips are delivered functionalized and do not require any further modification of the surface or the antibody. Additionally, previously successful coupling of antibodies to epoxy group coated Eupergit C1Y methacrylate microbeads (Burger et al., 1989; Takamori et al., 2000a) is a good indicator that the antibodies remain active after the coupling.

For the second surface modification tested, I functionalized the coverslips myself using PEGylation, allowing for modifications and flexibility in the capturing approach not available when functionalized coverslips are acquired commercially. PEGylation is the process of modifying a surface or substrate with poly(ethylene glycol) (PEG). PEG is a neutral, non-toxic, water-soluble polymer that forms an inert coating resisting non-specific protein adsorption (Ostuni et al., 2001; Zalipsky and Harris, 1997) and is a prime candidate for the passivation of surfaces. PEG cannot react directly with glass, and therefore a two-step reaction is needed in which the glass first has to be functionalized through silanization, followed by a chemical reaction to bind the PEG to the silane-modified surface (Wolter et al., 2007).

However, one-step PEGylation protocols have been developed to reduce the number of steps and the variability of the final product (Gidi et al., 2018), using a monofunctional mPEG-silane (siPEG). In this thesis, I used such a one-step siPEG protocol (Schaedel et al., 2019), in which the siPEG is bound to the glass surface through the reaction of the PEG-attached-silane with the hydroxyl groups on the glass surface (Figure 7b). The antibodies were captured on this surface using a biotin-streptavidin bridge. The biotin was presented on the surface by using a 1:1 mixture of siPEG and the heterobifunctional siPEG-biotin. The antibody was directly coupled to streptavidin (a tetramer with four biotin binding sites) using the primary amines available on the antibody. This streptavidin labeled antibody was deposited on the biotin containing functionalized glass surface, allowing immobilization of the antibody through the binding of biotin and streptavidin.

The third surface modification approach was chosen based on its ability to control the density of active groups on the surface. Functionalizing free hydroxyl groups (silanols) on a glass surface is not a highly efficient reaction, and therefore it is difficult to reach a high density of covalently bound molecules by only relying on the free hydroxyl groups and binding points. A previously developed copolymer from the laboratory of Dr. Marina Cretich and Prof. Marcella Chiari (Istituto di Chimica del Riconoscimento Molecolare (ICRM), Milan) (Cretich et al., 2004; Pirri et al., 2004) circumvent this limitation by combining the features of the monomers N,N-dimethylacrylamide (DMA), N,N-acryloyloxysuccinimide (NAS), and [3-(methacryloyl-oxy)propyl]trimethoxysilyl (MAPS), together forming copoly(DMA-NAS-MAPS). MAPS reacts covalently with the free silanols to stabilize the whole coating (Figure 7c). NAS is the reactive group that reacts with primary amines on the antibody to bind it to the copolymer covalently. DMA facilitates the adsorption of the copolymer on the glass surface, preventing non-specific binding on the glass surface. Copolymerization allows for flexible modification of the number of the reactive groups in the system, thereby influencing and determining the density of reactive groups on the surface, allowing for a higher density of reactive groups than otherwise possible based on the free silanols. This polymer has a 2 nm thin layer in dry conditions, which swells up to a hydrophilic hydrated layer with optimal antifouling properties of 18-22 nm in wet conditions.

All three surfaces theoretically had the potential to fulfill the properties required for the development of this method. Whether these surfaces fulfill the pre-determined features in practice is analyzed by establishing the following points: antibody binding to the glass surface, effective immunocapture of SVs after antibody immobilization, development of the microfluidic system allowing for fast solution changes, and stability of the binding during flow. Each of these will be addressed in the following sections.

In antibody microarrays, non-specific adsorption of proteins to the surface is one of the most commonly seen problems caused by physical adsorption (physisorption). Physisorption is caused by the hydrophobic forces, ionic interaction, van der Waals forces, and hydrogen bonding (Bee et al., 2006; Hoehne et al., 2011; Norde, 2008). Non-specific adsorption is a reoccurring theme throughout the results presented here and can present problems at three different levels of these experiments.

i. Labeled secondary and primary antibodies are used to detect the immobilized antibodies and SVs on the surface, respectively. However, if these labeled detection antibodies non-specifically adsorb to the surface, they can lead to false-positive results and higher background signals, both unwanted complications.
ii. SVs could be adsorbed onto the respective surfaces instead of immunocaptured by the covalently bound antibodies. We aim for specific immunocapture of SVs by the immobilized antibodies, as SVs attached through adsorption cannot survive the fast solution changes required in the microfluidic device. Additionally, non-specific adsorption of SVs increases the background signal.
iii. The primary antibody used for covalent coupling to the glass surface could adsorb to the surface instead or in addition to the intended covalent coupling. This adsorption could result in initial positive results in the static experimental conditions. However, it turns into detrimental results when flow is applied to the system as there is a high likelihood that adsorbed antibodies with immunocaptured SVs attached to them will wash off when flow is applied.

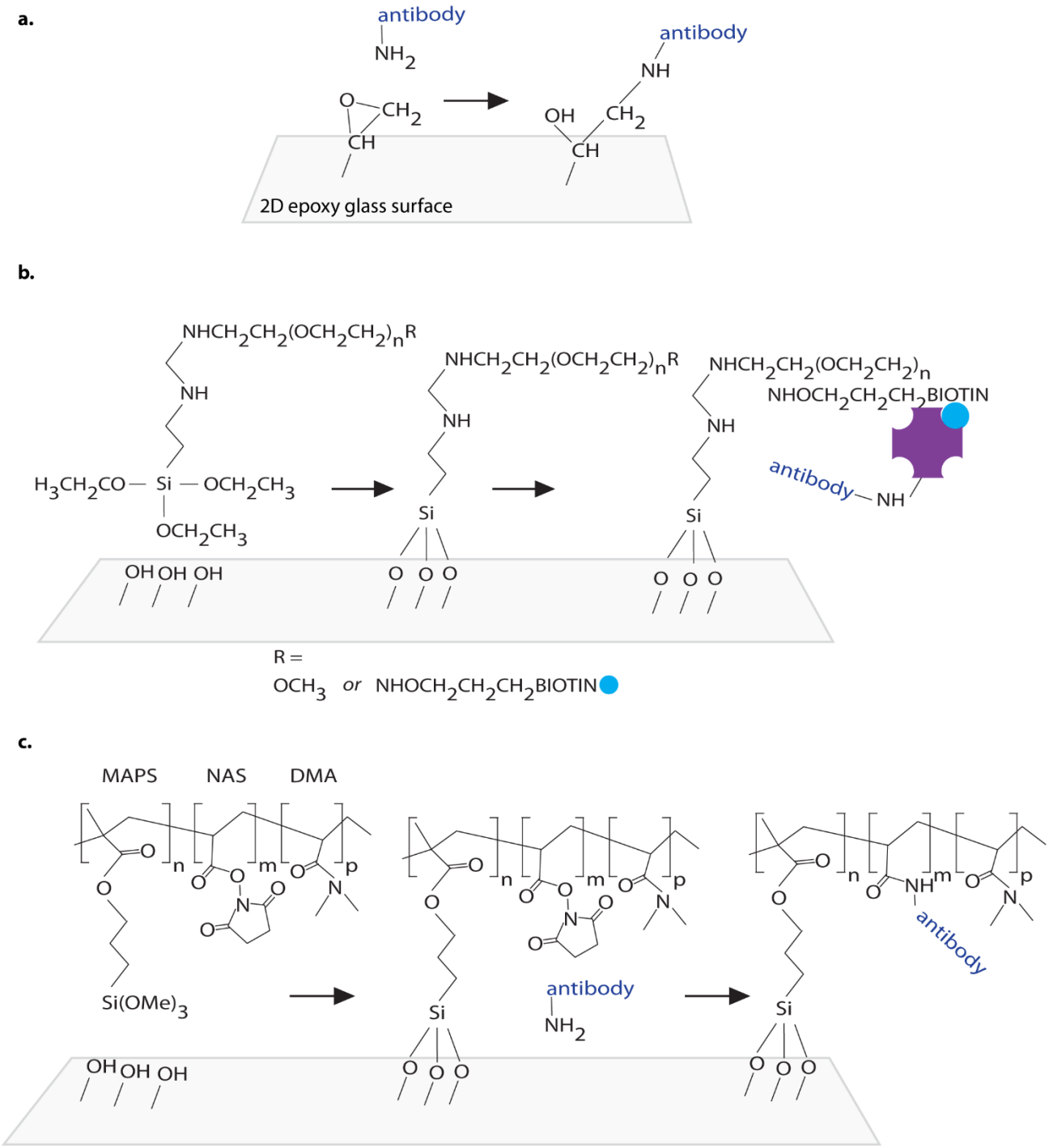

Figure 7. The three surface chemistries used to functionalize the glass slides. a) 2D epoxy coverslips from PolyAn. b) siPEG/siPEG-biotin coverslips with the attachment of streptavidin labeled antibodies. c) Copoly(DMA-MAPS-NAS) coverslips.

3.2 Antibody binding to the glass surface

Antibodies were immobilized to the glass surface using the previously described chemistries. The results for each surface (2D epoxy, siPEG/siPEG-biotin, and copoly(DMA-MAPS-NAS)) are reported here.

3.2.1 2D epoxy coverslip

Unfortunately, the commercially acquired 2D Epoxy coverslips (PolyAn) do not divulge details on how the surfaces are chemically modified to attain the chemical groups required, and the density of these chemical groups is not publicized. I tested and optimized the incubation time, incubation buffer, and washing steps to improve direct covalent coupling of the primary antibody and reduce background signals. Antibodies were deposited on the coverslip using a Gilson pipette. A 15 µL droplet of 0.5 mg/ml antibodies resulted in a circular dot formation on the coverslip. Mouse monoclonal antibodies for syp and syb2 were used as they are the most abundant proteins on SVs (Takamori et al., 2006; Wilhelm et al., 2014). Incubation of the antibodies with the surface was followed by deactivation of all the non-reacted epoxy groups (experimental details available in Methods 2.3.1.1), and binding of the deposited antibodies with the surface was determined by labeling with secondary goat-anti-mouse Alexa Fluor 488 labeled antibodies. The fluorescent signal of these detection antibodies was imaged using an epifluorescence microscope. Where primary antibodies were deposited, a high signal was observed. A clear border of this signal with their immediate environment where no primary antibodies were deposited was visible, indicating localized binding of the antibody to the surface (Figure 8b). Additionally, in the absence of the primary syp or syb2 antibodies, the secondary goat-anti-mouse Alexa Fluor 488 labeled antibodies created a limited background signal. Syp and syb2 antibodies were successfully detected on the 2D epoxy coverslips (Figure 8c), with more consistent results for syp compared to syb2.

3.2.2 siPEG/siPEG-biotin coverslip

For the siPEG/siPEG-biotin coverslips, the coverslips were functionalized using a one-step PEGylation procedure using a 1:1 mixture of siPEG and siPEG-biotin. Instead of attaching streptavidin and the syp antibody in a two-step process, I chose to covalently couple streptavidin and the syp antibody before immobilizing the antibody on the surface. In this way the streptavidin labeled antibody could be directly applied to the PEGylated coverslip, eliminating the need for two consecutive labeling steps of streptavidin and the antibody on the surface.

The availability of biotin on the siPEG/siPEG-biotin coverslip is essential to immobilize the streptavidin labeled syp antibodies. Therefore, I tested the availability of biotin on the surface using anti-biotin antibodies. The anti-biotin antibodies were deposited using the same droplet placement as used for the 2D epoxy coverslip and detected by the secondary goat-anti-mouse Alexa Fluor 488 labeled antibodies. Biotin was clearly detected on the siPEG/siPEG-biotin coverslip while absent in the negative control with only siPEG (Figure 9a and b).

With the confirmation of the presence of biotin on the siPEG/siPEG-biotin surface, the same droplet placement as for the 2D epoxy coverslip was used to deposit the streptavidin labeled antibodies on the prepared siPEG/siPEG-biotin surface detected by the secondary goat-anti-mouse Alexa Fluor 488 labeled antibodies. After optimizing incubation times and washing steps, the streptavidin labeled syp antibody was detected on the siPEG/siPEG-biotin surface but not on the siPEG-only surface. This binding of the streptavidin labeled antibodies is specific to the biotin groups, as antibodies not labeled with streptavidin were not able to bind to the surface (Figure 9c and d). As evident from Figure 9, streptavidin labeled syp antibodies were successfully immobilized on the siPEG/siPEG-biotin surface coverslips with limited unspecific binding.

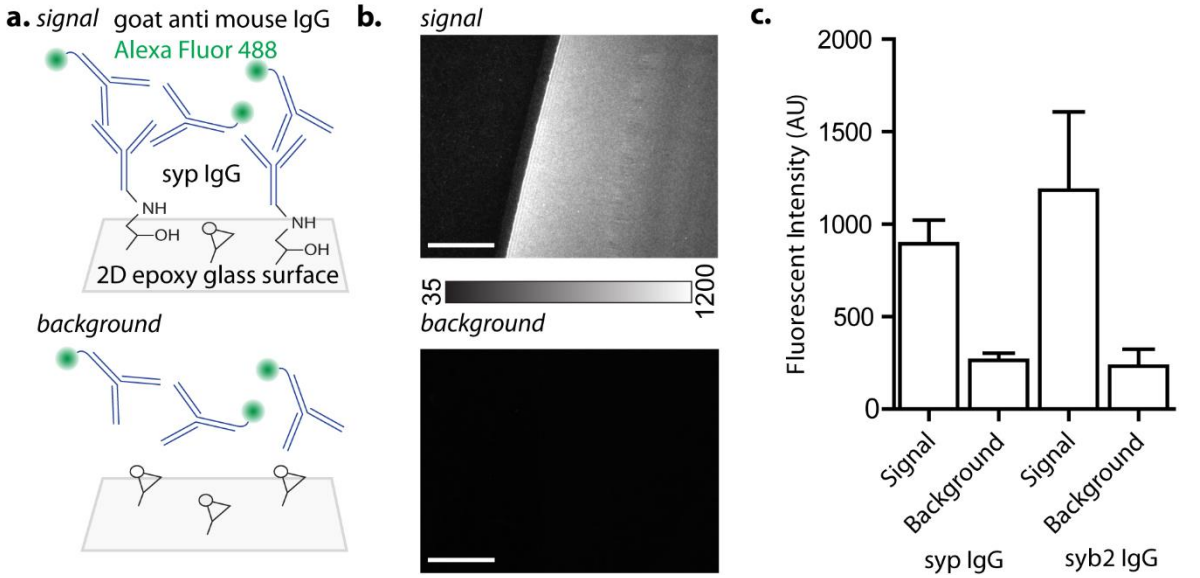

Figure 8. Attachment of synaptic vesicle protein antibodies (syp and syb2) on 2D epoxy coverslips. a) Sketch of experimental conditions in signal vs background conditions. b) Epi-fluorescence images of the circular pattern of the syp antibody (magnification: 100x, scale bar: 20 µm). c) Average fluorescent intensity of syp and syb2 antibodies compared to the presence of only goat-anti-mouse Alexa Fluor 488 IgGs (background), (syp IgG, n = 5, syb2 IgG, n =2).

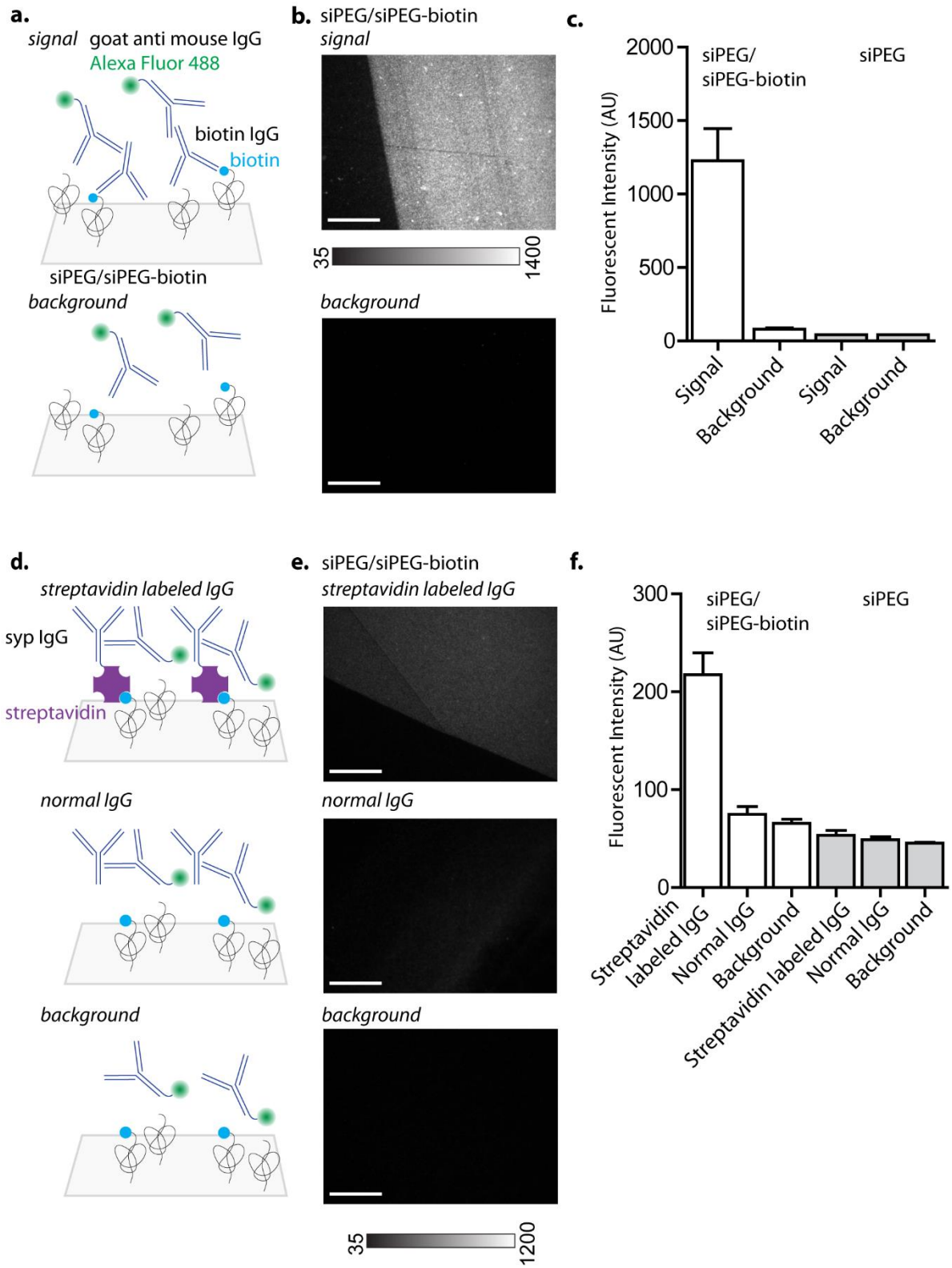

Figure 9. Attachment of syp antibody on PEGylated glass coverslips. a and d) Sketch of experimental conditions. b) Epi-fluorescent images of the circular pattern of anti-biotin antibody to reveal the presence of biotin after PEGylation of siPEG/siPEG-biotin (magnification: 100x, scale bar: 20 µm). Background is the measurement of only goat-anti-mouse Alexa Fluor 488 IgGs. c) Average fluorescent intensity in the presence and absence of anti-biotin antibody, as well as the presence and absence of siPEG-biotin during PEGylation (n = 2). e) Epi-fluorescent images of the circular pattern of streptavidin labeled and non-labeled syp antibody on siPEG/siPEG-biotin coverslips. f) Average fluorescent signal detected in the presence/absence of streptavidin labelled/normal/no syp antibody on either siPEG/siPEG-biotin or siPEG-only coverslips (n=4).

3.2.3 copoly(DMA-NAS-MAPS) coverslip

The third surface modification tested here is the copolymer (DMA-NAS-MAPS). Its design combined each component's favorable characteristics, resulting in a surface resistant to protein adsorption, with a high density of available active groups (Cretich et al., 2004; Pirri et al., 2004). After the coating process was finished, the coverslips with copoly(DMA-NAS-MAPS) were transferred to the sciFLEXARRAYER S3, where droplets of syp antibody of approximately 400 pL were deposited on the coverslip surface without disturbing the surface. A rectangular pattern of 10 x 6 syp antibody droplets was printed on the copoly(DMA-NAS-MAPS) coverslip, and after incubation and washing, subsequently labelled with the goat-anti-mouse Alexa Fluor 488 antibody. Syp antibody binding results in a strong localized signal with almost no background in a clear circular pattern (Figure 10).

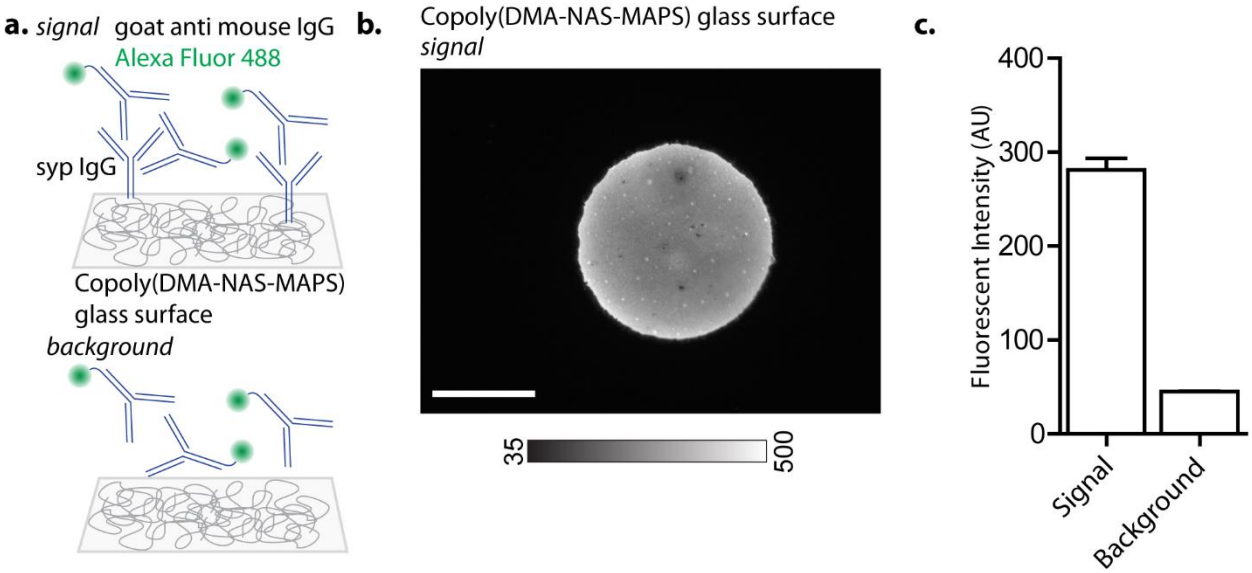

Figure 10. Attachment of syp antibody on copoly(DMA-NAS-MAPS) coverslips. a) Sketch of experimental conditions. b) Representative epi-fluorescent image of syp antibody detected by goat-anti-mouse Alea Fluor 488 antibody (magnification: 20x, scale bar: 100 µm). c) Average fluorescent intensity measured in epi-fluorescent images (n = 3).

3.3 Antibody activity and SV immunocapture

All three of the surfaces resulted in immobilized syp antibodies. Therefore, I chose to test the antibody activity and SV binding for each surface. Due to the difference in chemical modifications of each surface, it is possible that they could result in a different orientation/modification and density of the bound antibodies. For each surface, it was analyzed whether the following two requirements could be fulfilled; 1. the bound antibodies have to retain their activity and ability to bind SVs, 2. SVs have to be specifically captured by the antibody, not through unspecific adsorption of SVs on the surface.

3.3.1 2D epoxy coverslip

Initial tests of the antibody activity and SV binding were performed using highly purified SVs. The 2D epoxy coverslips then showed high background levels outside of where the localized primary antibody was immobilized (data not shown). These background levels indicate SVs attachment to the surface instead of immunocapture by the immobilized antibodies. To reduce this non-specific background, I used rat LS1 mixed with 2 mg/ml bovine serum albumin (BSA) instead of purified SVs. Binding of BSA and other soluble proteins in the LS1 mixture to the surface can reduce the non-specific binding of the SVs to the surface. The SVs were successfully captured using these modifications by the surface-attached syp antibodies and detected using Oyster 550 labelled syb2 antibodies (Figure 11). As negative controls, different components of the sandwich were left out. Only minimal background signals were detected in the absence of the surface-attached syp antibodies or the SVs themselves. Low background signal indicates that the SVs detected are not adsorbed to the glass surface but actually captured by the syp antibodies as intended. It also reveals that immobilization of the syp antibodies on the 2D epoxy surface did not render all antibodies inactive.

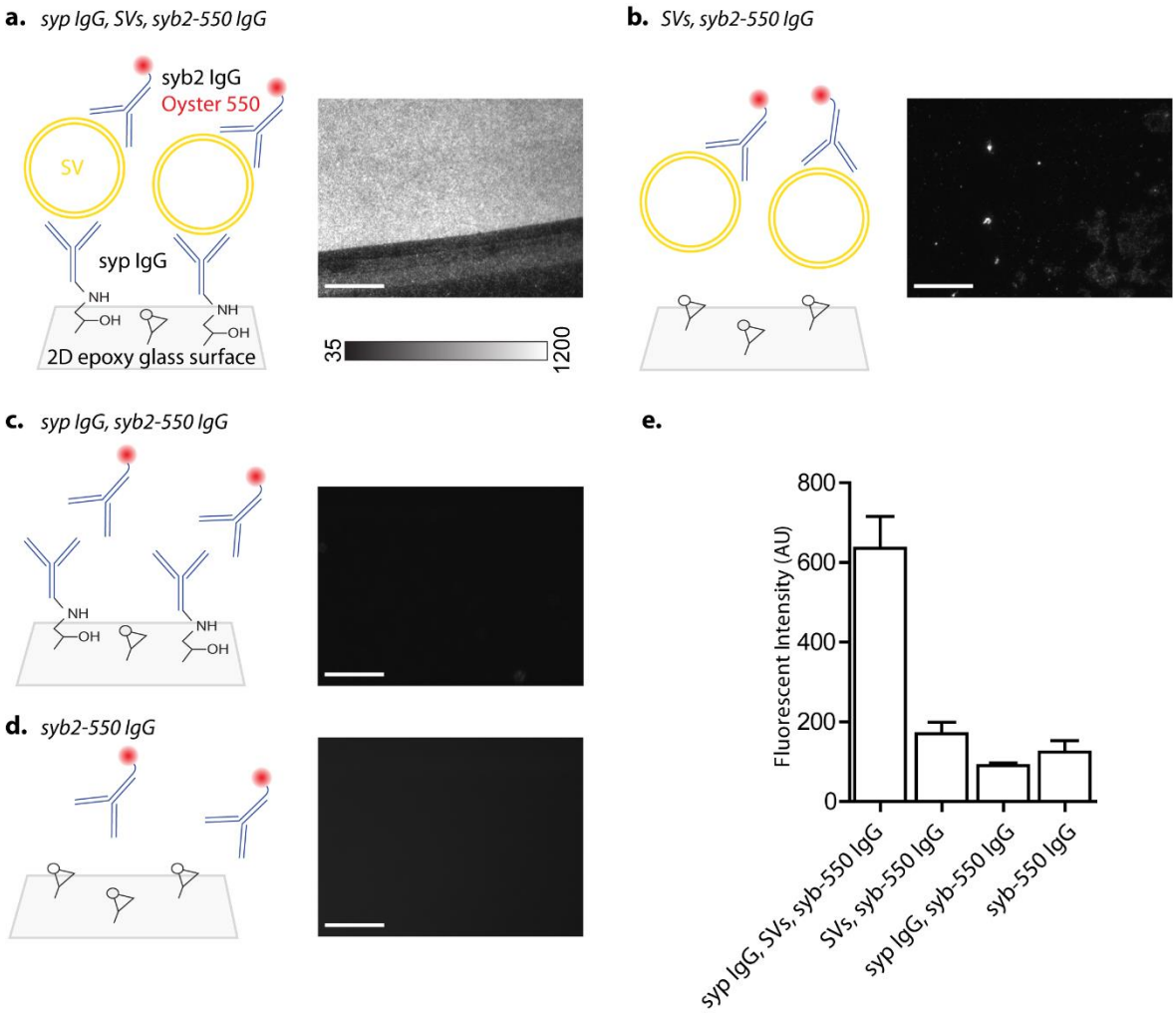

Figure 11. Attachment of SVs from LS1 in the presence of 2 mg/ml BSA on 2D epoxy coverslips. a-d) a sketch of each experimental condition and a corresponding representative epi-fluorescent image reveals the specific capture of SVs by immobilized syp antibodies (magnification: 100x, scale bar: 20 µm). e) Averaged fluorescent intensity for all conditions (n=3).

3.3.2 siPEG/siPEG-biotin coverslip

Using the acquired knowledge that LS1 with 2 mg/ml BSA reduces unspecific binding of SV, similar experiments were executed on siPEG/siPEG-biotin and siPEG-only coverslips. I successfully detected SVs bound on siPEG/siPEG-biotin coverslips only when streptavidin labeled syp antibodies were used for immobilization. In the absence of antibodies altogether and in the presence of antibodies not labeled with streptavidin, little to no SV presence was observed. Similarly, when only siPEG was used, little to no SV presence could be observed. These results show not only that SVs do not bind unspecifically to the modified surface, but also that the antibody retained its ability to bind SVs, despite the modification necessary to label it with streptavidin, as well as the ability of streptavidin to bind to biotin (Figure 12).

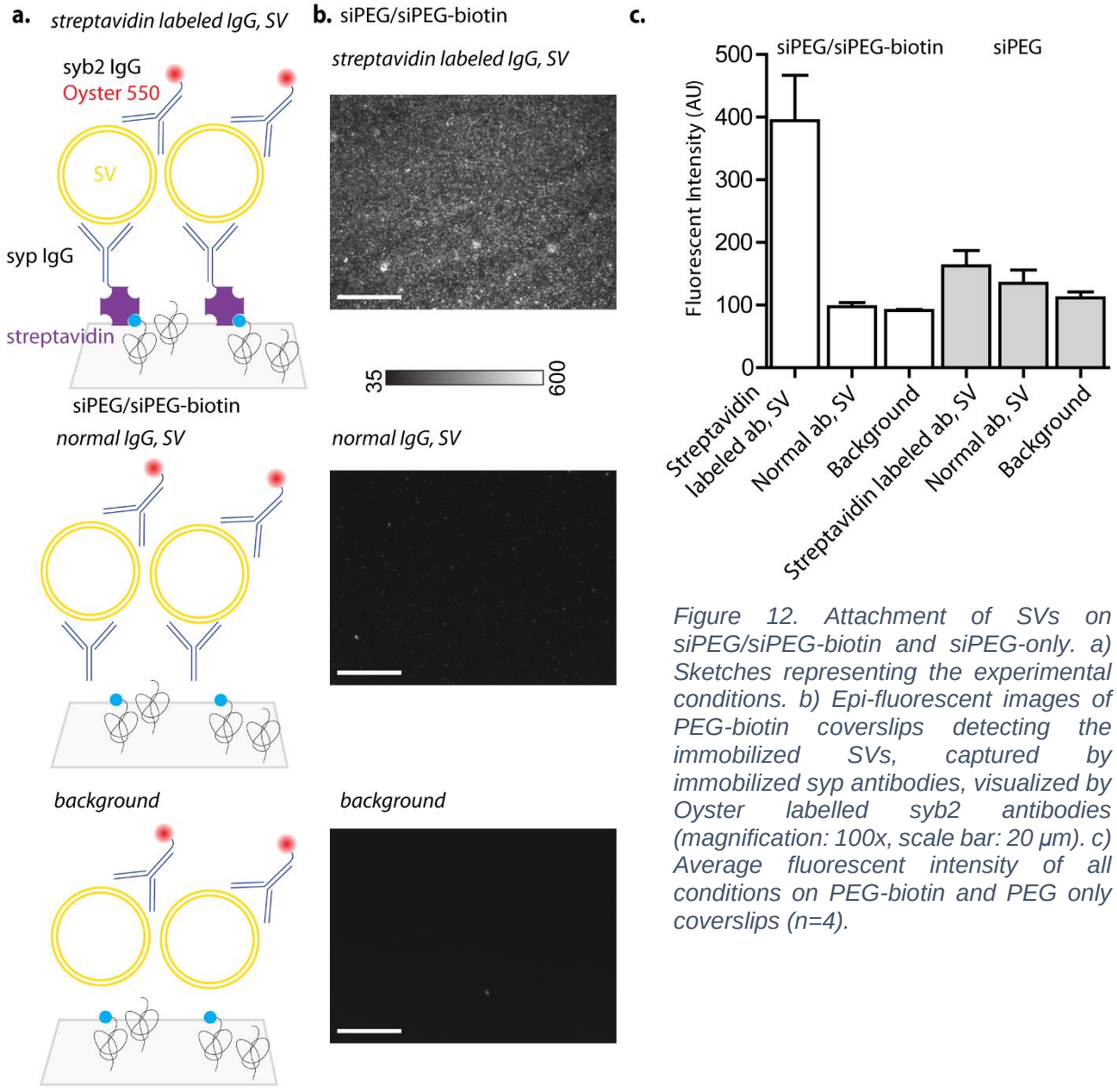

Figure 12. Attachment of SVs on siPEG/siPEG-biotin and siPEG-only. a) Sketches representing the experimental conditions. b) Epi-fluorescent images of PEG-biotin coverslips detecting the immobilized SVs, captured by immobilized syp antibodies, visualized by Oyster labelled syb2 antibodies (magnification: 100x, scale bar: 20 µm). c) Average fluorescent intensity of all conditions on PEG-biotin and PEG only coverslips (n=4).

3.3.3 Copoly(DMA-NAS-MAPS) coverslip

After binding syp antibodies to the copoly(DMA-NAS-MAPS) coverslip and blocking the unused chemical groups, the coverslips were treated the same as the 2D epoxy and siPEG/siPEG-biotin coverslips. I observed homogenously fluorescent dots when labeling the SVs with Oyster 550 syb2 antibodies, with minimal background in the absence of immobilized syp antibodies (Figure 13). Therefore, I concluded that the syp antibodies on the copoly(DMA-NAS-MAPS) coverslips retained their activity despite their binding to the glass surface, and SV binding was specific to these immobilized antibodies. SV capture using rabbit polyclonal syp antibodies was briefly tested too and actually resulted in higher fluorescent signals (data now shown). However, I chose to continue using the mouse monoclonal syp antibody to eliminate the possible impact of variability between different polyclonal antibody preparations.

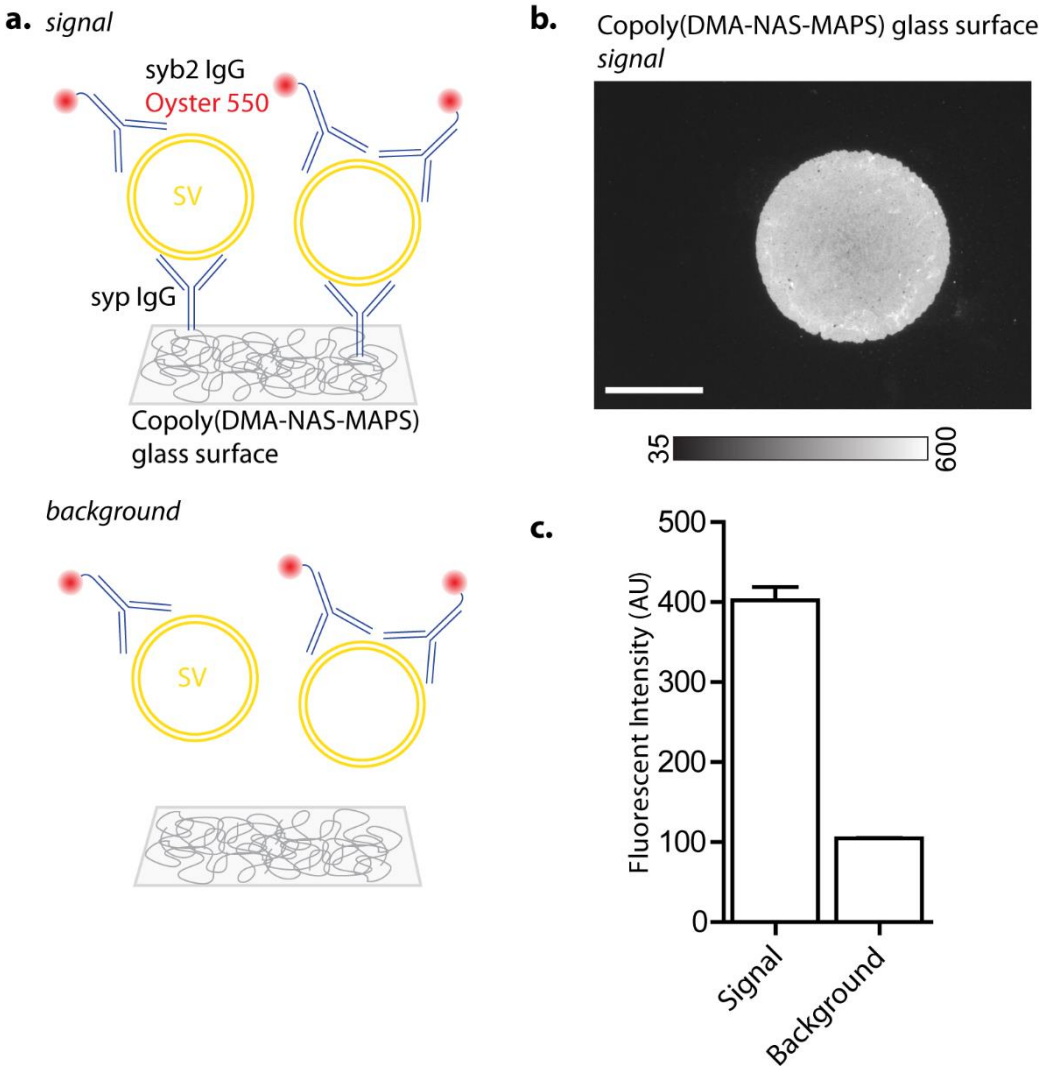

Figure 13. Capture of SVs by syp antibodies on the copoly(DMA-NAS-MAPS) coverslip. a) Sketch of experimental conditions. b) Representative epi-fluorescent image of captured SVs from LS1 by immobilized syp antibodies, visualized by Oyster 550 syb2 antibodies (magnification: 20x, scale bar: 100 µm). c) Average intensity in the presence and absence SVs (n=3).

3.4 Design and assembly of the microfluidic system

Successfully capturing SVs in static conditions for all three surfaces requires a microfluidic system to test them under flow conditions further. The microfluidic device employed here was developed in collaboration with Dr. Eleonora Perego in the Sarah Köster group (Perego, 2019), more details in Methods 2.3.2. It is a three-inlet and one outlet PDMS device with a channel width of 1000 µm width and 100 µm height, resulting in a plug flow profile with a constant velocity across the width of the channel (Figure 14).

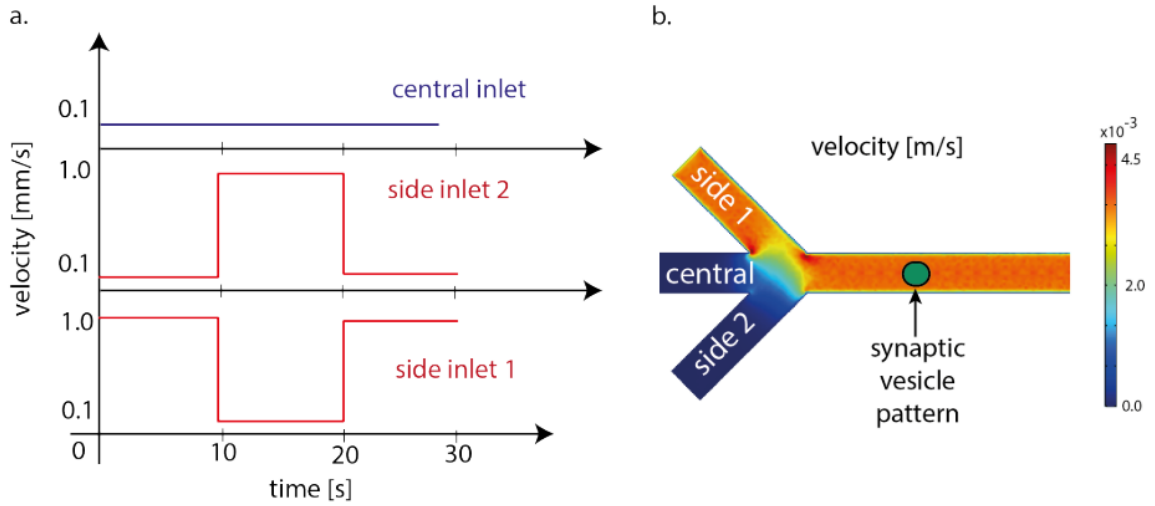

Figure 14. Input velocity profile applied to the inlets of the microfluidic device (1000 µm width and 100 µm height for switchable buffer on SVs. a) Input velocity patterns for each inlet of the microfluidic device. The side inlets periodically switch from maximum to minimum velocity in an asynchronous pattern. b) FEM simulation of flow velocity. FEM simulations and illustration from Dr. Eleonora Perego (Perego, 2019), an experimental comparison of the simulations by Sebastian Smyk in their bachelor thesis.

The microfluidic device was designed to resolve the uptake kinetics of transporters on the SVs. We know from a previous study that time-wise these kinetics fall into the second range (Farsi et al., 2016), requiring a microfluidic device that can switch solutions fast enough to resolve these kinetics. Finite element method (FEM) simulations were used to determine the response time of the microfluidic device. The response time is the time required to change the solution that the SVs are exposed to by switching from one inlet to another. Epi-fluorescent images of a region of interest in the main channel were analyzed to detect the changes in fluorescent intensity over time using fluorescein solution and water. The response time in simulations with 3 mm/s total velocity was 0.34 ± 0.01 s (Perego, 2019), in line with the experimental findings; 0.462 ± 0.008 s (Sebastian Smyk, 2017). These response times <1s fulfill our requirement for fast solution changes to resolve the uptake kinetics.

3.4.1 Attachment of the microfluidic device

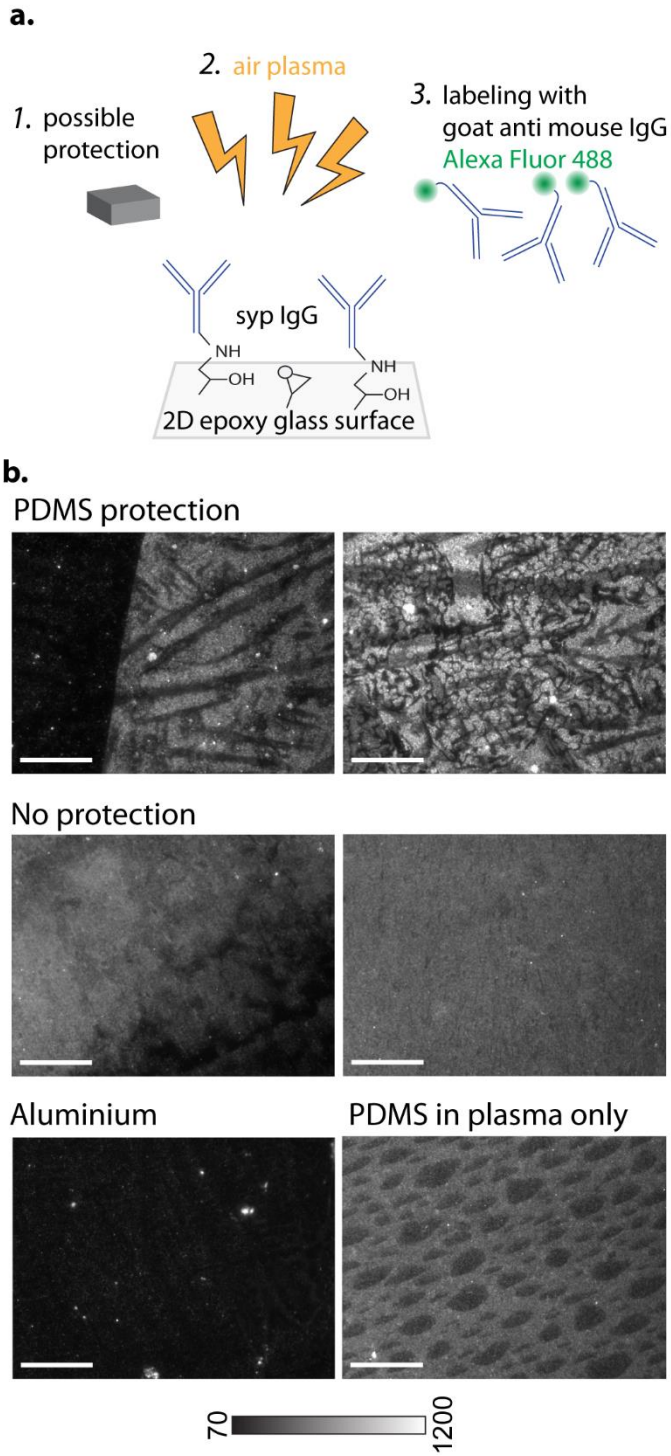

Figure 15. Effect of plasma treatment on syp antibodies immobilized on 2D epoxy coverslips. a) Schematic representation of procedure. b) Epi-fluorescent images of the syp antibody layer after plasma-treatment (magnification:100x, scale bar: 20 µm).

Usually, microfluidic devices made from PDMS are attached to glass by plasma-treating each surface functionalizing them to bind to each other (Duffy et al., 1998). Unfortunately, biological materials do not survive the aggressive plasma treatment (Huang et al., 2013). Multiple ways have been suggested to protect the biological material from exposure to plasma while exposing the surroundings to plasma for attachment (Hattori et al., 2013; Huang et al., 2013). Therefore, I immobilized syp antibodies on 2D epoxy coverslips and exposed the coverslip with unprotected or protected antibodies (by PDMS or aluminium) to plasma treatment. Unfortunately, none of these methods protected the antibodies on the surface sufficiently (Figure 15). Additionally, only the microfluidic PDMS part was treated with plasma as this can result in binding with glass too (based on experience from Dr. Eleonora Perego). However, this requires the glass (with the immobilized antibodies) and the device to be dried in an oven for three hours, effectively damaging the antibodies. An alternative method of attachment is pressure-clamping. In this approach, the microfluidic PDMS device and the glass coverslip are held together by a small device that applies pressure on both parts to keep them together. We designed our own version of this device (Figure 6) based on a device described in (Chen et al., 2014). This approach does not require any harsh treatment of the antibodies or SVs. This device was successfully used in all experiments concerning the microfluidic system and flow in this thesis.

3.5 Immunocapture stability under flow conditions

Successful capturing of SVs on all three surfaces and a functioning pressure clamping microfluidic device allowed me to continue with all three surfaces to analyze their ability to withstand the shear stress in the microfluidic device. Superfusion of solutions in a microfluidic chamber puts additional constraints on the binding requirements of SVs. Not only should the antibodies and organelles be bound in static conditions, but the binding also has to be retained under flow conditions. The required response time of the device is within the second range to observe the dynamics of the ionic mechanisms of the SVs, which is achieved using 3 mm/s as total velocity. For fluids in a pipe, the shear rate is defined as the gradient of the velocity measured across the height of the microfluidic device. The shear rate can be calculated for the FEM simulations, with 3 mm/s in a 1000 µm x 100 µm device, the shear rate in the center of the channel is 170 s^{-1}, the shear stress is 0.4 Pa (Perego, 2019). Every surface was tested whether the binding of antibodies and synaptic vesicles could withstand this rate for the maximum required length of future experiments (30 min).

3.5.1 2D epoxy coverslip

Syp antibodies and SVs were bound as described above on a 2D epoxy coverslip. I then attached the microfluidic PDMS device in the pressure clamping holder and either exposed the immobilized antibodies (and SVs) to 30 minutes of 3mm/s flow or no flow at all, capturing the fluorescent signal either after 30 minutes of no flow, or after 30 minutes of flow. At first glance, the binding of the syp antibodies to the 2D epoxy surface alone, without SVs attached to them, appears to be maintained even under flow (Figure 16a), as no reduction in fluorescent signal can be detected after 30 minutes of buffer flow. However, in the presence of SVs bound to the syp antibodies, a significant reduction in fluorescent signal is observed after 30 minutes (Figure 16b). The remaining fluorescent signal is significantly reduced and unfortunately no longer homogenous and thereby rendered useless for future experiments.

The detachment of SVs from 2D epoxy surface was unexpected based on the promising results in static conditions. The loss of fluorescent signal observed could come from four different ‘breaking points’; 1. labeled syb2 antibodies detach, 2. syp antibody-SV attachment breaks, 3. syp antibody attachment to surface breaks/detaches, 4. the surface chemistry layer is affected. Antibodies have been shown to be able to bind their target even under a shear stress of 0.5-0.8 Pa (Bavli et al., 2016), above the shear stress in our microfluidic device (0.4 Pa). Additionally, SVs captured by antibodies bound to epoxy group coated Eupergit C1Y methacrylate microbeads (Burger et al., 1989; Takamori et al., 2000b) can survive the shear stress applied through centrifugation. Therefore, the detachment of SVs from syp or syb2 antibodies is an unlikely breaking point in this scenario. 2D epoxy coverslips were commercially prepared, and therefore, I could not influence the surface chemistry layer, leaving the most likely candidate option 3; syp antibody attachment to the surface is affected.

One possibility to explain the detachment of the antibody from the surface is that the antibody is not covalently bound to the surface as intended, however instead adsorbed to the surface. When antibodies adsorb to the glass surface instead of binding covalently through the intended chemistry, the initial results of static conditions can look promising. However, when exposed to extended flow and the corresponding shear stress, they will not remain attached as the adsorptive attachment would not be sufficient to withstand the shear stress. Therefore I investigated the 2D epoxy surface for their adsorptive ability to evaluate whether the antibodies observed on the surface (Figure 11), were attached through the epoxy amine chemistry or adsorption.

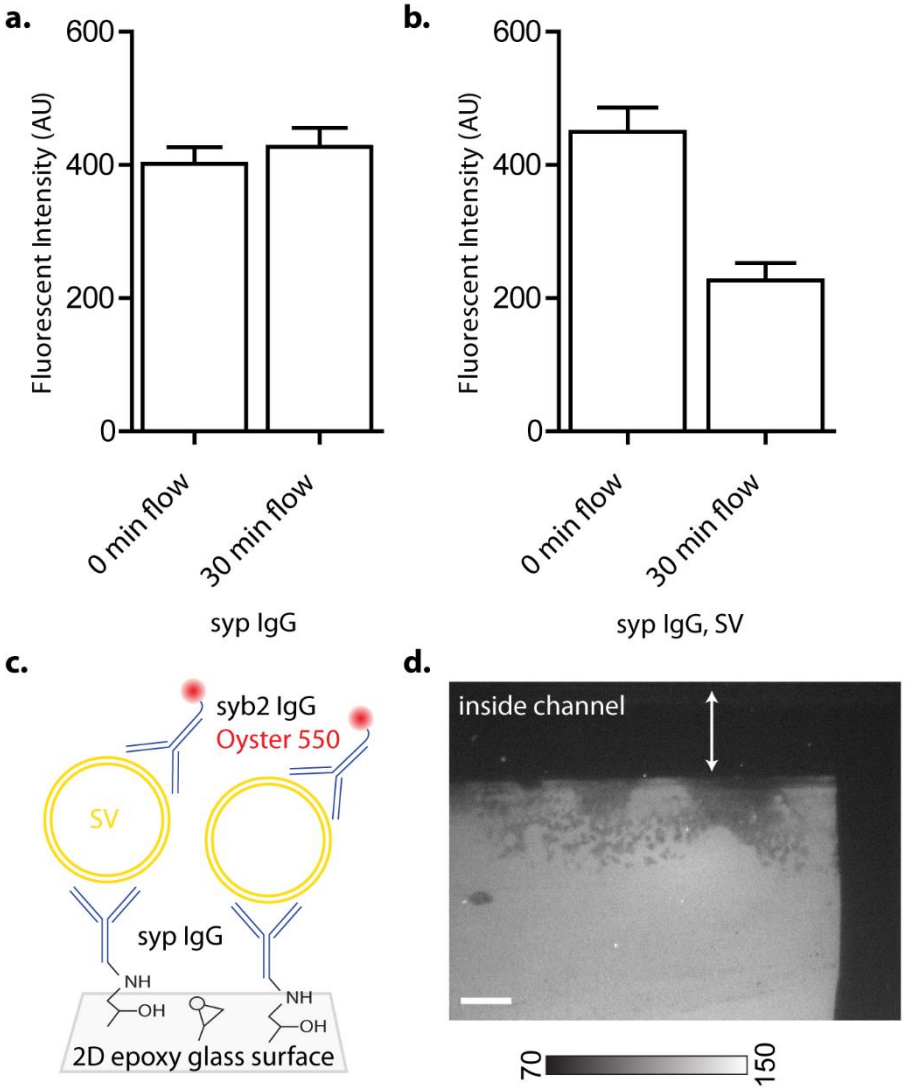

Figure 16. Effect of 3 mm/s 30 min flow on the binding of antibodies and SVs on 2D epoxy coverslips. a) Average fluorescent signal of syp antibody detected on the coverslip with and without flow (0 min flow; n=4, 30 min flow; n=2). b) Average fluorescent signal of SVs detected by Oyster 550 labeled syb2 antibody on the coverslip with and without flow (n=3). c) sketch of experimental conditions. d) Epi-fluorescent image of SVs detected through Oyster 550 syb2 after 30 min of 3 mm/s flow. A clear reduction in signal can be observed inside the channel (white arrow depicts width of channel in image) (magnification: 10x, scalebar: 20 µm).

I performed the same experiment as described for Figure 11, with an additional modification in which the epoxy groups on the glass surface are deactivated before the antibodies were added. A similar fluorescent signal can be observed in the presence and absence of active epoxy groups on the surface (Figure 17a), indicating that the antibodies find a way to attach themselves to the glass surfaces even without active epoxy groups available. Additionally, the commercially available 2D NeutrAvidin[6] coverslip from PolyAn was tested, and it revealed that normal, non-biotinylated antibodies resulted in an equally strong fluorescent signal as biotinylated antibodies (Figure 17b). These test cases indicate that the commercially available coverslips lack the ability to prevent the adsorption of antibodies on their glass surfaces, resulting in the binding of the antibodies in a non-sustainable way for the microfluidic device. A variety of blocking agents can reduce adsorption, for example, pre-blocking with BSA, beta-casein, and unspecific antibodies/proteins. These approaches, however, were unfortunately unsuccessful in preventing the adsorption of antibodies (data now shown).

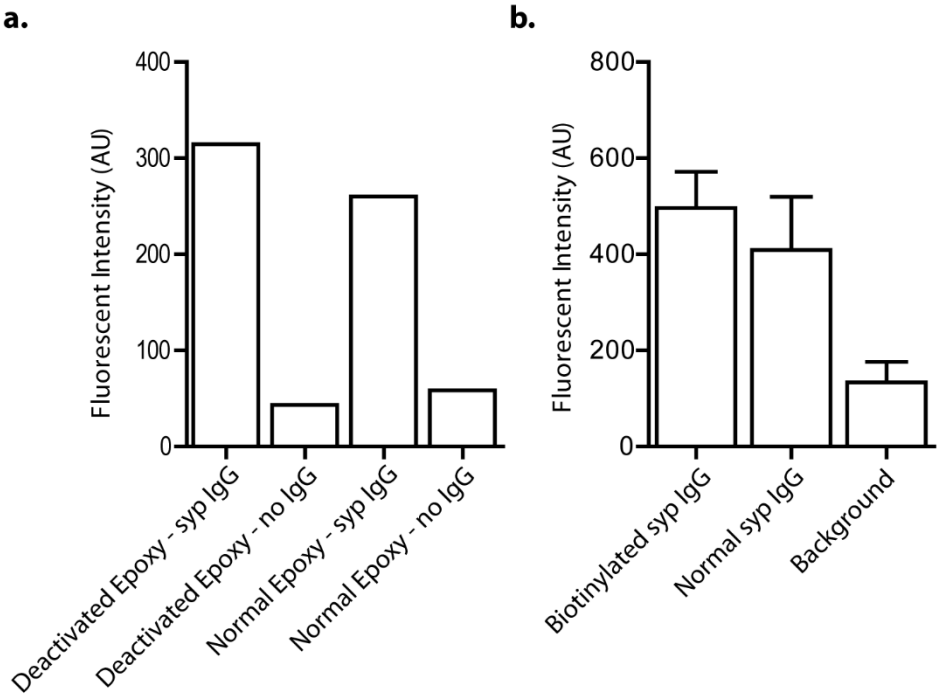

Figure 17. Immobilization of syp antibodies on 2D epoxy and neutravidin coverslips from PolyAn happens through adsorption. Fluorescent intensity measured using 10x magnification on epi-fluorescent microscope. a) Comparison of syp antibody immobilization on 2D epoxy coverslips with and without active epoxy groups for covalent binding (n=1). b) Comparison of immobilization of biotinylated vs not-biotinylated syp antibody on 2D neutravidin coverslips (n=2).

[6] NeutrAvidin is an avidin analogue. It is deglycosylated and is only slightly acidic, which should reduce nonspecific binding to proteins (Vermette et al., 2003).

3.5.2 siPEG/siPEG-biotin coverslip

The siPEG/siPEG-biotin surface was directly tested for the antibody-SVs combination because the 2D epoxy surface modification already showed that even though the syp antibodies might survive 30 minutes of flow exposure immunocapture of SVs to these antibodies can change their stability in flow conditions. The previously mentioned experiment was repeated with the siPEG/siPEG-biotin coverslips. 30 minutes of flow exposure resulted in a significant reduction of the fluorescent signal as also observed for the 2D epoxy coverslips. The remaining surface was unusable for future acidification measurements due to the limited remaining fluorescent signal and the heterogeneous signal distribution (Figure 18).

The siPEG/siPEG-biotin coverslip addresses the problem of adsorption already through the characteristics of the polyethelyne chains, which form a matrix to prevent adsorption. This prevention is confirmed by the antibody immobilization experiments (Figure 9b). The antibody that is not labeled with streptavidin does not immobilize on the siPEG/siPEG-biotin coverslip, and the streptavidin labeled antibody does not immobilize on the siPEG-only coverslips. Nonetheless, a significant reduction of fluorescent signal was observed after 30 minutes of 3 mm/s flow. As for siPEG/siPEG-biotin coverslips, the adsorption of the antibody cannot explain the loss of fluorescence. Either the surface chemistry layer is affected by the flow, the binding affinity of the antibody to SVs is affected by the modification with streptavidin, or the binding affinity of streptavidin to biotin is affected by the modification with the antibody.

3.5.3 Copoly(DMA-NAS-MAPS) coverslip

As the first two surfaces that were tested showed a significant reduction of signal, I wanted to have a little more insight into whether this reduction of signal happened immediately at the start of the flow, or reduced slowly over time. Therefore, the same experiment was executed for the copoly(DMA-NAS-MAPS) coverslips with one small change; instead of measuring the beginning and endpoint only, images were taken every minute to follow the fluorescent signal over time. The copolymer surface modification did not show a significant reduction in fluorescent signal over time. In the first minute, a minimal reduction in signal could be observed, and the following 30 minutes, the signal remained stable, and the resulting fluorescent signal was homogenous across the surface even after 30 minutes of flow (Figure 19).

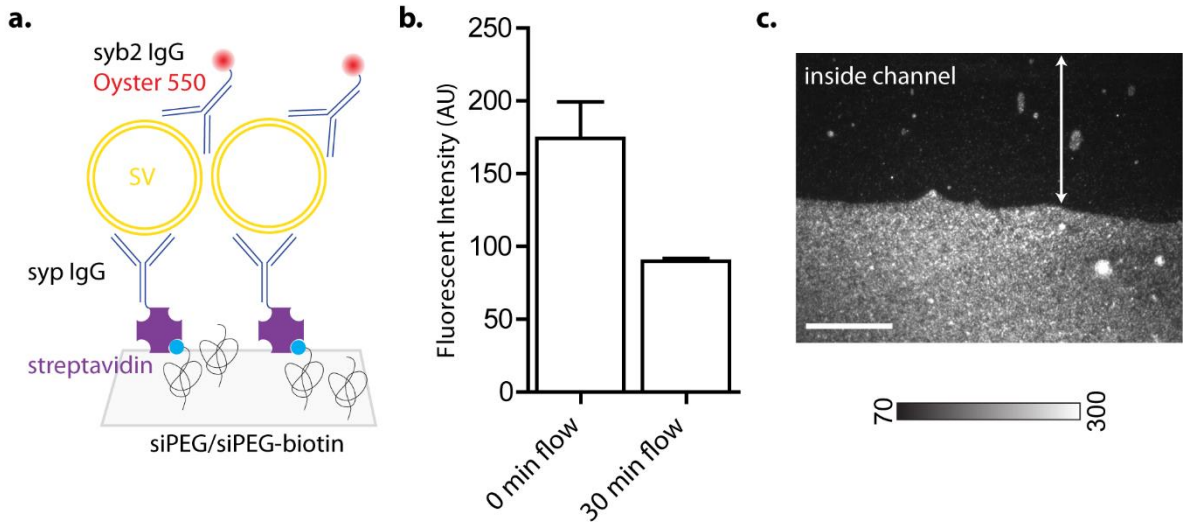

Figure 18. Effect of 3 mm/s 30 minute flow on the binding of antibodies-SVs on siPEG/siPEG-biotin coverslips. a) Sketch of experimental conditions. b) Average fluorescent intensity of SVs (immobilized through syp antibodies, detected by Oyster 550 syb2 antibodies) with and without flow (0 min flow; n=4, 30 min flow; n=3). c) Epi-fluorescent image depicting the loss of fluorescent signal in the channel after 30 minutes of flow (magnification: 100x, scalebar = 20 µm).

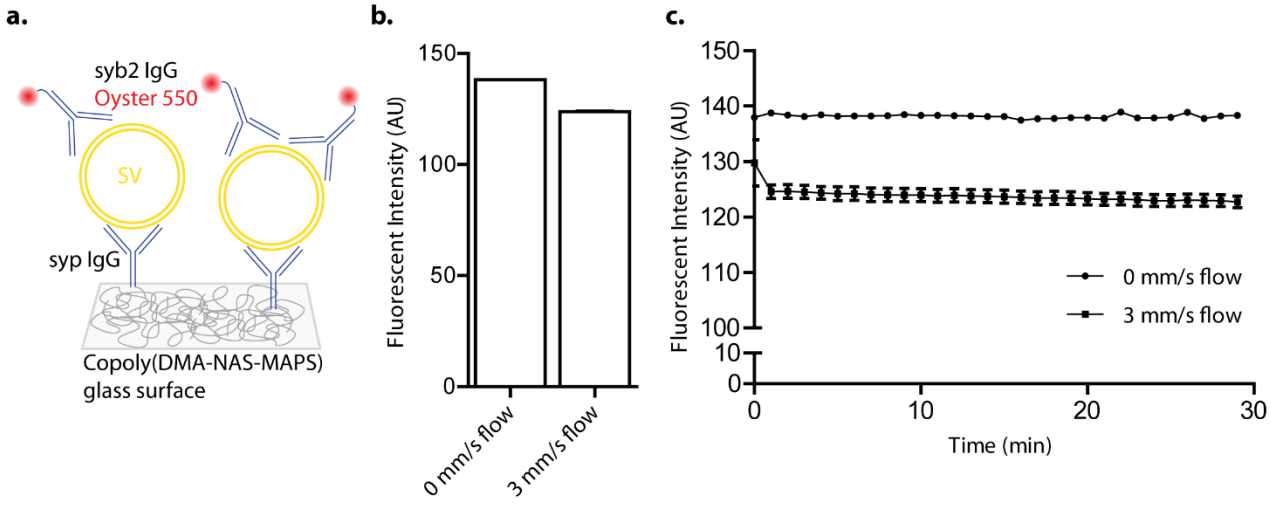

Figure 19. Fluorescent signal on copoly(DMA-NAS-MAPS) coverslips in the presence and absence of 3mm/s flow for 30 minutes. Imaged using epi-fluorescent microscope at 10x magnification. a) Sketch of experimental conditions. b) Average fluorescent intensity of SVs after 30 minutes (immobilized by syp antibodies, detected by labelled syb2 antibodies) with and without flow (0 mm/s flow; n=1, 30 mm/s flow; n=4). c) Time progression of fluorescent signal (exposure time 1 sec, imaging interval 1 min).

3.6 Preliminary characterization of SVs

The copoly(DMA-NAS-MAPS) coverslips exhibit strong binding of antibodies and SVs, and therefore I chose to continue with that approach. Extremely important for the assay is that the SVs bound in the device retain their activity. Vesicle acidification is a good indicator of the health of immobilized SVs. The acidification inside SVs can be measured using pH-sensitive dyes. In this case, SVs were isolated from transgenic mice expressing the genetically encoded fluorescent indicator synaptopHluorin (Li et al., 2005). These SVs contain the pH-sensitive probe pHluorin attached to syb2 in their lumen (spH-SVs). I first confirmed that using LS1 from synaptopHluorin mice resulted in sufficient fluorescent signal. The fluorescent signal inside the SVs could be detected clearly (Figure 20a) without losing fluorescence due to washing away or bleaching (Figure 20b).

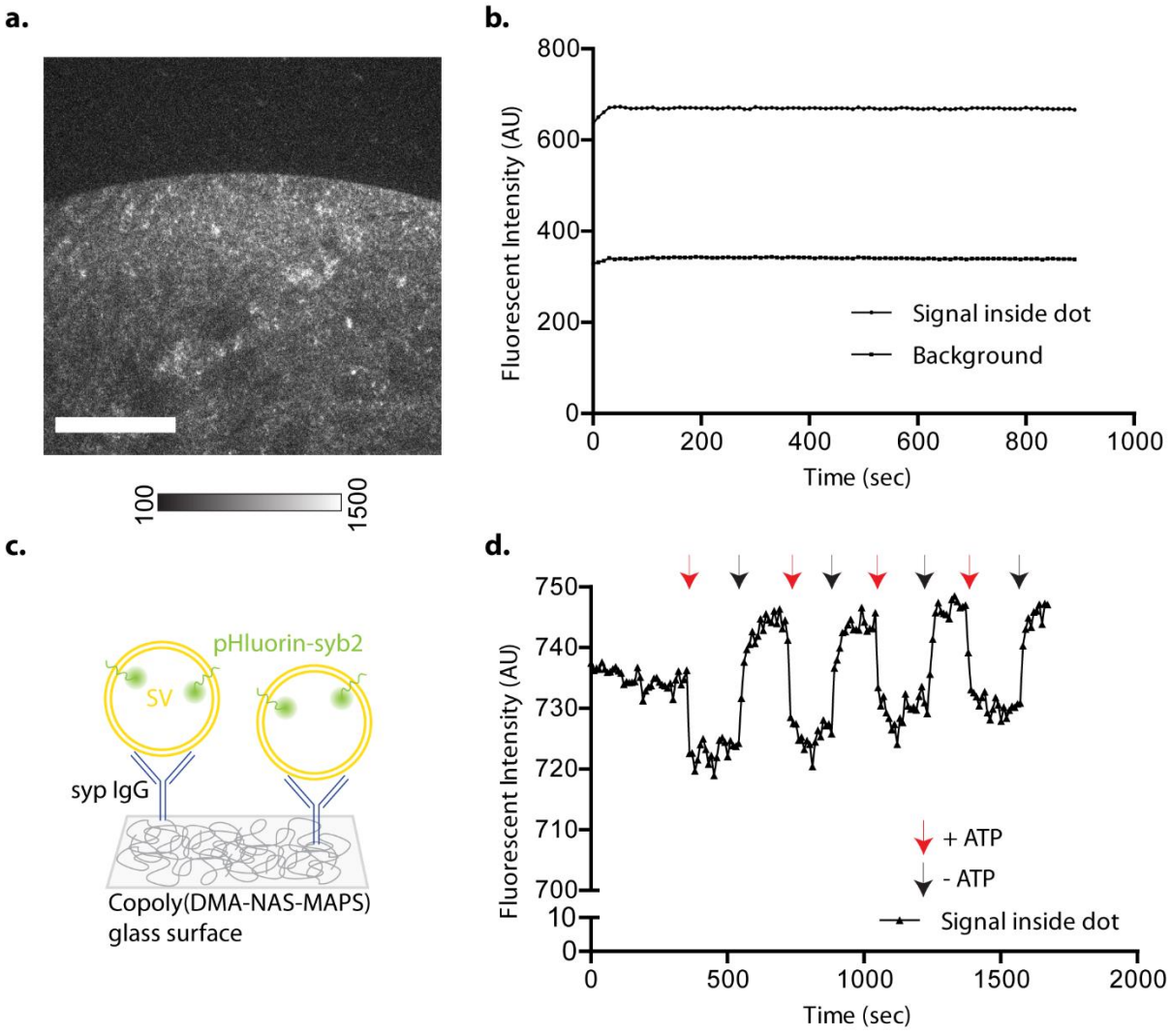

Figure 20. Immobilization and activity of synaptopHluorin mice SVs on copoly(DMA-NAS-MAPS) coverslips. a) TIRF microscopy image of immobilized spH-SVs (magnification: 100x, 5 mW laser power, EM gain 250, scalebar: 10 µm). b) Fluorescent signal during 30 minutes of 3 mm/s flow (exposure time: 200 ms, time interval: 10 seconds). c) Sketch of experimental conditions. d) Fluorescent signal changes during 30 minutes of 3 mm/s flow, switching between buffer with and without 2 mM MgATP (exposure time: 200 ms, time interval: 10 seconds).

Acidification in SVs requires MgATP in the solution for the V-ATPase to pump protons in the lumen of the vesicles. Without MgATP, no acidification is expected. Using the solution exchange system, immobilized SVs were alternatingly exposed to buffer with and without MgATP. An apparent decrease in fluorescent signal and therefore a decrease in pH is observed when buffer containing MgATP superfuses the SVs. When switched back to buffer not containing MgATP, the fluorescent signal quickly increases again (Figure 20d). The results show that the changes in fluorescence are MgATP dependent and reversible.

The changes in pH and, therefore, in fluorescence occur within seconds (Farsi et al., 2016). When images are taken only every 10 seconds the kinetics of acidification cannot be observed. I, therefore, reduced the time interval of the images. Images were taken every 200 ms to reveal the acidification dynamics over time until it plateaus (Figure 21a). Solution changes in the absence of ATP did not cause these dynamics, indicating that the changes are ATP-dependent. Additionally, as previously described in other work (Farsi et al., 2016), maximum acidification is increased in the presence of higher amounts of ATP (Figure 21b).

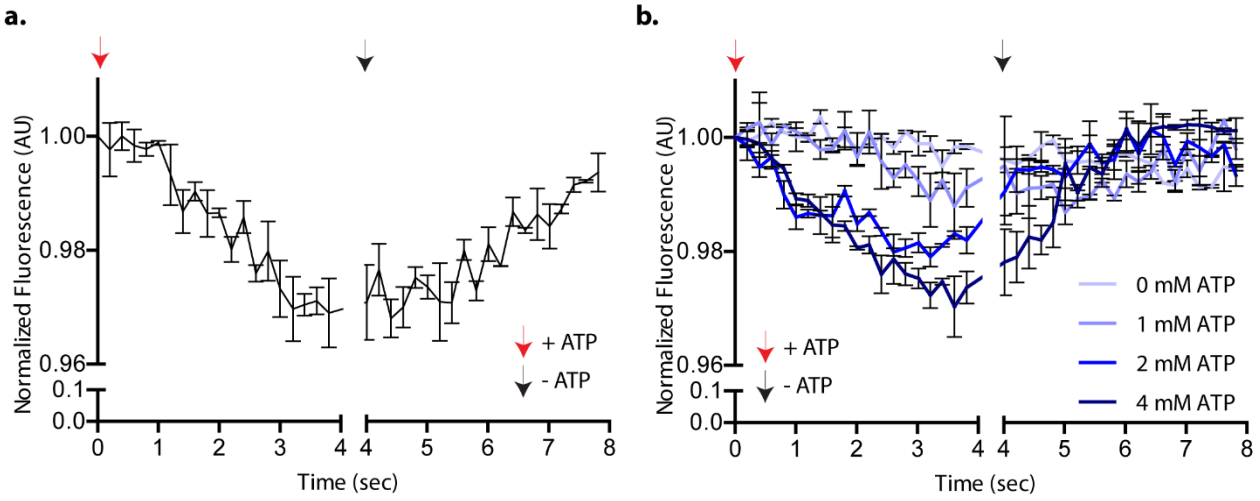

Figure 21. Acidification kinetics in immobilized mice spH-SVs on copoly (DMA-NAS-MAPS) coverslips. Images taking using TIRF microscope, 100x magnification, 50 ms exposure time, 200 ms time interval, laser power 5 mW, EM gain 250. a) Acidification and efflux by addition and removal of 2 mM MgATP, respectively. b) Changes in maximum acidification plateau by varying amounts of MgATP (0-4 mM).

3.6.1 The required concentration of immobilizing antibody and target SVs

In all previous experiments, immobilization of SVs was ascertained by immobilizing 1 mg/ml of antibody on the surface (as determined as optimal concentration by (Cretich et al., 2004), and at least 600 µg/ml of LS1. However, to make the system more versatile for other applications, either because of the limited availability of specific antibodies or the reduced concentration of samples obtained from cell culture, I tested how reduced concentration of antibodies and SVs would impact the fluorescent intensity (Figure 22).

It revealed that even though a higher concentration of antibodies increased the overall signal, 0.25 mg/ml of antibody is sufficient to capture SVs and visualize them. In that case, 50 µg/ml of LS1 is sufficient to saturate the available antibodies on the surface. A higher concentration of antibodies (>0.5 mg/ml and up) revealed a difference in fluorescent intensity between the different concentrations of LS1.

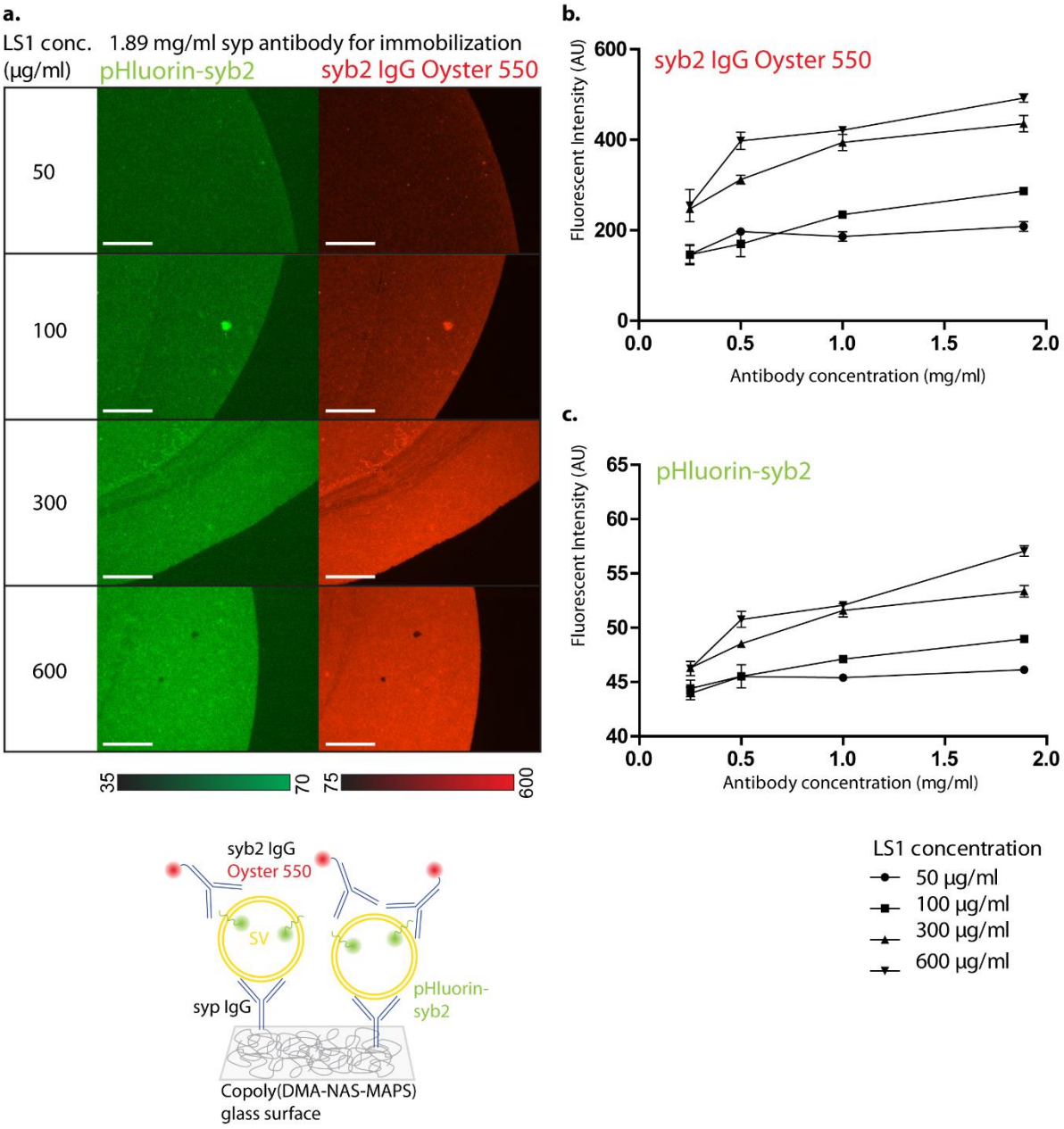

Figure 22. Immobilization ability for varying concentrations of syp antibody and spH-LS1. a) Epi-fluorescent images of immobilized spH-SVs by 1.89 mg/ml syp antibodies (magnification: 100x, scale bar: 20 µm). b) Fluorescent intensity of immobilized SVs by Oyster 550 labelled syb2 antibodies. Error bars represent intra-sample variation. c) Fluorescent intensity of immobilized SVs by luminal pHluorin-syb2. Error bars represent intra-sample variation.

3.6.2 Immobilization of specific immunoisolated subpopulation of SVs

SVs isolated from rodent brains roughly consist of approximately 85% glutamatergic SVs and 15% GABAergic SVs. Specifically looking at a subpopulation of SVs is important to obtain kinetic information relevant to that population and the storage of that specific neurotransmitter, especially if this population is not the dominant population, as is the case with GABAergic SVs. Even though it should be possible to capture subpopulations directly on the microfluidic platform using VGAT specific antibodies, studying the function of the transporter might be affected as the binding of antibodies to the proteins might affect its function. It has been shown that some VGLUT1 nanobodies (Schenck et al., 2017) and some antibodies (Eriksen et al., 2021) inhibit glutamate uptake. Therefore, a Master student in our group developed an immunoisolation approach in which subpopulations of SVs can be isolated using ProteinG Dynabeads and eluted at the end (Zhuleku, 2020). Although this method was initially developed for GABAergic SVs for this microfluidic platform, it has now also been successfully applied for Zn^{2+} SVs (Upmanyu et al., 2021). The immunoisolated GABAergic SVs were successfully immobilized on this microfluidic platform (Figure 23). The signal of immunoisolated SVs is lower than SVs directly immobilized from spH-LS1. This reduction is most likely due to the reduced concentration of SVs in the immunoisolated sample, which we have seen to result in reduced fluorescent intensity (Figure 22). This approach enables the microfluidic platform to study subpopulations of SVs, such as GABAergic SVs, without affecting the function of the transporters.

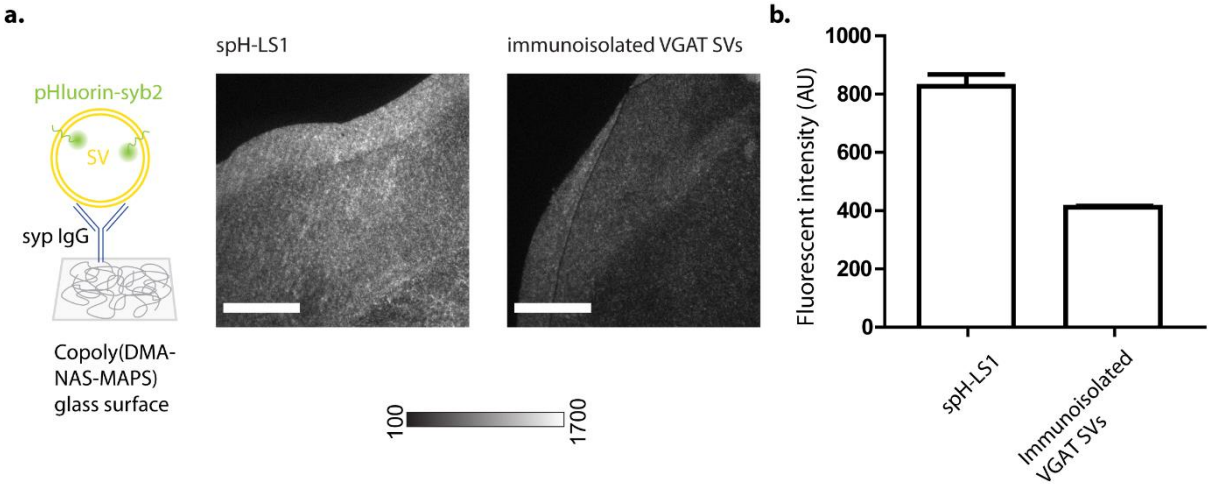

Figure 23. Immobilization of GABAergic SVs specifically. SVs were immunoisolated using ProteinG dynabeads in combination with a VGAT antibody as optimized by Evi Zhuleku in her Master thesis. a) TIRF images of SVs immobilized from spH-LS1 or from the immunoisolated VGAT SVs (magnification: 100x, laser power, EM gain 250, scalebar: 10 µm). b) Comparison of fluorescent intensity from SVs immobilized from spH-LS1 vs immunisolated VGAT SVs.

4 Discussion

During my PhD, I developed a novel microfluidic antibody microarray device to enable us to answer remaining questions in the neurotransmitter transporter field requiring high temporal resolution in switching kinetics. For example, how the glutamate uptake in SVs is coupled to the energy gradient by studying how the on- and off-kinetics of ΔΨ and ΔpH are affected by the presence of increasing glutamate concentration at different ATP-concentrations and different Cl^- concentrations. By testing three different surfaces, the system developed here now overcomes the challenges of protein immobilization and capture of nanometer-sized-organelles on glass. This system enables the stable immunocapture of SVs and a high temporal resolution in switching kinetics of the solutions that the SVs are exposed to. These data provide valuable information about the practical considerations when choosing a surface modification method, further discussed here. Furthermore, the developed assay was shown to be functional, and its potential will be discussed here.

4.1 Challenges of stable antibody and SV immobilization

4.1.1 Antibody stability during flow

For the SVs to remain in place during fast solution changes, high stability of the antibody binding to the glass surface is required. Therefore, the antibodies needed to be covalently bound to the surface to prevent antibody detachment during flow. The copoly(DMA-NAS-MAPS) coverslips fulfilled this requirement and achieved stable antibody binding and immunocapture of SVs under flow conditions (Figure 19). However, siPEG/siPEG-biotin coverslips and 2D epoxy coverslips did not (Figure 18 and 16, respectively).

One possible explanation for this result in the 2D epoxy coverslips is the non-covalent binding of the antibodies to the surface. As previous experience in our lab revealed that adsorptive forces are not sufficient to survive strong flow (Farsi et al., 2016). Deactivation of the epoxy groups before ‘binding’ of syp antibodies revealed that on 2D epoxy coverslips the syp antibodies actually can be attached to the surface through adsorption (Figure 17). This non-specific background is one of the most commonly seen problems in antibody microarrays caused by physical adsorption. They adsorb to the surface quickly and form a layer of about 4nm (following antibody sizing). Despite rapid adsorption to the surface, the secondary structure of the antibodies remain intact (Bee et al., 2006; Hoehne et al., 2011), allowing for full functionality as long as the antibody binding sites remain available. This is also observed by the ability of the adsorbed immobilized antibodies on the 2D epoxy coverslips to capture SVs (Figure 11). The ability of the primary antibodies to remain active does not allow a distinction between adsorbed and covalently immobilized antibodies based on their activity, complicating the interpretation of experiments with immobilized antibodies in static conditions. This complication resulted in the late discovery of insufficient stability of antibody binding to the 2D epoxy coverslips.

With this evidence that at least part of the primary antibodies was immobilized on the surface through adsorption, the question arises why this does not happen for the secondary detection antibody (Figure 8 and 11). The explanation is relatively simple; in the primary antibody's binding process, all factors are optimized to maximize the covalent binding of the antibody to the surface. Unfortunately, the long binding time and high antibody concentration also increase the ability of the antibody to adsorb to the surface firmly. Time allows these initial weak adsorptive forces to increase their interactions and result in relatively strong binding. These findings for 2D epoxy coverslips are in line with previously found behavior of antibodies and their ability to adsorb to surfaces with negative, positive, and neutral charges (Bee et al., 2006) and that preventing non-specific protein adsorption by physically blocking these surfaces with BSA is not always successful (Kusnezow et al., 2003).

siPEG/siPEG-biotin successfully prevented unspecific binding of the primary antibody (Figure9d-f). Therefore, the loss of signal during flow cannot be explained by washed-off adsorbed primary antibodies. However, the stability of the antibody during flow is affected by the stability of the surface modification layer, in this case, the siPEG/siPEG-biotin layer. In an ideal situation, the silanization and thereby PEGylation of the surface would form a monolayer (Van Der Voort and Vansant, 1996). Theoretically, the silanes can bind to the surface through each alkoxysilane group, allowing for multiple binding sites on the surface. However, polymerization of the silanol can occur either while attached on the surface or earlier while in solution still. This can lead to a heterogeneous surface often observed in silanization experiments. Additionally, the exact mechanism of the reactivity of trialkoxysilanes with surfaces is debated (Schlecht and Maurer, 2011). Unfortunately, the chemical complexity and the dependency of the silanization process on many variables (type of silane used, temperature, hydration conditions, reaction time and surface cleaning) make obtaining a uniform and reproducible surface difficult (Cras et al., 1999). Consequently, a heterogeneous multilayer could have been formed, of which patches may not have attached properly to the glass surface, allowing these patches, the antibodies, and SVs bound to them to be disturbed in the microfluidic device. Another possibility is that the streptavidin-biotin bridge does not hold under flow conditions. Typically streptavidin-biotin binding is one of the strongest non-covalent pairing present in nature (Green, 1966; Hyre et al., 2006). However, the binding affinity of the streptavidin may be reduced by the modifications of the covalent attachment to the antibody. A reduced binding affinity of the streptavidin-biotin bridge could result in reduced stability of antibody attachment to the surface.

4.1.2 Stable immunocapture of SVs

Stable antibody binding does not automatically guarantee stable immunocapture of SVs. The wash-off observed on 2D epoxy and siPEG/siPEG-biotin coverslips can also be an indicator of instability of the immunocapture of the SVs besides the instability of the immobilization of the antibody. When the immobilized antibodies without immunocapturing SVs were tested for their stability during flow, they did not wash off (Figure 16a), in contrast to the wash-off observed when the antibodies had captured SVs. The differential effect of shear stress depending on particle size could explain this difference (Tokárová et al., 2013). The bigger particle size of the antibody-SV complex results in increased impact of the shear stress and can therefore lead to easier wash-off.

Additionally, stable immunocapture relies heavily on the binding strength of the antibody-antigen bond. The surface chemistries of the 2D epoxy and the copoly(DMA-NAS-MAPS) coverslips rely on covalent binding with the amines present on the antibodies, just as the chemistry for covalently binding streptavidin to the antibody used for siPEG/siPEG-biotin coverslips. Amines from lysines and arginines on the antibody are present throughout the protein, also on the variable fragment (Fv) of the antibody, which contains the antigen-binding site. Therefore, chemistries based on binding with amines result in randomly oriented antibodies on the surface, affecting binding affinity when amines in the antigen-binding site happen to react with the functional groups used for immobilization. Additionally, random orientation of the antibodies and their antigen-binding sites possibly results in steric blockage of the antigen-binding sites due to their orientation to the surface. This heterogeneity in immobilized antibodies can result in less stable immunocapture resulting in the wash-off of SVs observed for the 2D epoxy and siPEG/siPEG-biotin coverslips. A way to circumvent this would be oriented immobilization (Trilling et al., 2013). For example, using thiol-groups, or a secondary approach for immobilization using Protein A/G (Kusnezow and Hoheisel, 2003) results in less variation in antibody affinities and thereby improved target binding (Vijayendran and Leckband, 2001). However, oriented immobilization also frequently leads to a lower density of bound antibodies, as random immobilization usually relies on heavily available coupling groups (such as amines). In contrast, oriented immobilization relies on only a few available groups impacting the immobilization efficiency (Oates et al., 1998).

The stable immunocapture on the copoly(DMA-NAS-MAPS) coverslips compared to the other surfaces might be explained by their difference in antibody binding density. The density of antibodies a surface can bind depends on the density and availability of reactive groups on the surface. Classical 2D coatings involving silanization approaches have been reported to mainly have an attachment density in the low 10^{12} orders of magnitude of molecules/cm^2 (Pirrung, 2002). For the copoly(DMA-NAS-MAPS) a density of $8.9*10^{13}$ active esters/cm^2 has been calculated, of which about half react with molecules (attachment density of $4*10^{13}$ molecules/cm^2) (Pirri et al., 2004).

Considering that probably not all the bound antibodies are still capable of capturing SVs or their binding affinity can be decreased, the density of antibodies a surface can immobilize becomes increasingly important. The density is especially important considering that increasing the number of IgG molecules results in higher critical shear rates (Gao and Jin, 2005; Kuo and Lauffenburger, 1993). Critical shear rate is the shear rate at which, in this case antibody-antigen, bonds begin to break. A higher reactive group density can result in a higher antibody density which results in a higher shear rate necessary to break the antibody-antigen bonds. Calculations of the strength of biological bonds support the notion that more than one antibody binding to a target increases the necessary force to break the bond. Additionally, these calculations reveal that to pull an integral membrane protein out of a lipid bilayer requires approximately the same force as rapidly breaking an antigen-antibody bond (Bell, 1978). The surface coverage required to have at least one antibody bind to each SVs can be roughly calculated with a simple 'back of the envelope calculation'; an SV has a diameter of 40 nm. Therefore, at least one antibody per 40 nm^2 is required, which is equivalent to $2.5*10^{12}$ antibodies/cm^2. The density reported for copoly(DMA-NAS-MAPS) surfaces is one order of magnitude higher than found in most silanization procedures and would therefore actually produce a surface where more than one antibody can bind to each SV, as where most silanization procedures report densities in the 10^{12} range, limiting the antibody to SV ratio to 1. This difference in antibody density and the resulting antibody to SV ratio may explain the observed difference in SV wash-off.

Stable immunocapture also depends on the used antibody. On 2D epoxy coverslips, it was observed that immobilization of syb2 antibodies has a higher variability than syp antibodies, even though both are mouse monoclonal antibodies. Variability of immobilization quality between antibodies has been observed before by comparing 11 different coatings and 5 different antibodies (Angenendt et al., 2002). Theoretically, it is hard to predict the behavior of different antibodies and each coating-antibody pairing has to be tested and optimized for the specific goal of the experiment. Additionally, on copoly(DMA-NAS-MAPS) coverslips, preliminary tests revealed increased fluorescence when syp polyclonal antibodies were used compared to syp monoclonal antibodies. This difference can be explained by the variability of antigen-binding sites in polyclonal antibodies. If another antibody already occupies the binding site of a monoclonal antibody, or the binding site is unavailable due to steric hindrance, that monoclonal antibody cannot bind an SV. However, polyclonal antibodies can bind various antigen binding sites, increasing the change of their binding site still being accessible, resulting in more and potentially stronger binding. Nonetheless, I chose to continue using the mouse monoclonal syp antibody to eliminate the possible impact of variability between different polyclonal antibody preparations.

4.1.3 Functional microfluidic system with active SVs

The copoly(DMA-NAS-MAPS) surface was the only approach that resulted in stable antibody binding and stable immunocapture of the SVs. As discussed above, this may be explained due to its high density of reactive groups allowing for a high density of antibodies, to successful passivation of the glass surface preventing non-specific adsorption, and to a homogenous formed surface layer, all characteristics of this specific copolymer (Cretich et al., 2004; Pirri et al., 2004). Therefore, this surface was combined with the specifically designed three-inlet PDMS microfluidic device and the successfully developed pressure clamping holder to form the final developed microfluidic system. This system was successfully tested using SVs containing the pH-sensitive probe pHluorin (Figure 20). The observed on-kinetics of the ΔpH in the spH-SVs occurred within seconds as expected based on previous data (Farsi et al., 2016). For the first time, it was possible to observed the off-kinetics of the ΔpH by the removal of ATP, also occurring within seconds. Using this new assay, I was able to obtain preliminary data concerning the on- and off-kinetics at varying ATP concentrations with high temporal resolution (Figure 21). Additionally, it was shown that this system can be used to effectively capture SVs from low concentration samples (Figure 22) and therefore can be used to study less abundant SV subpopulations, as shown by the immobilization of immunoisolated GABAergic SVs (Figure 23).

4.2 Outlook

The development of this assay now allows us to obtain highly resolved kinetic measurements of the ionic mechanisms of the vesicular glutamate transporters. The coupling of glutamate uptake in the SVs with the electrochemical gradient requires clarification. For example, is the glutamate uptake coupled to Cl^- transport or H^+ antiport, and if so, under which conditions? Detailed study of the on- and off-kinetics ΔΨ and ΔpH is required to find answers to these questions. Studying the on-kinetics is made possible by this platform due to the ability to precisely time the addition of components such as varying concentrations of ATP, Cl^-, and glutamate. Studying the off-kinetics of these components is made available by the ability of the system to remove components from the environment of the SVs with a high temporal resolution. Moreover, the ability of the platform to timely introduce components that can reversibly arrest the V-ATPase, provides a second new approach to studying the off-kinetics of the ΔpH. For VGAT, similar questions remain and especially the role of Cl^- concentrations in VGAT uptake mechanism remains debated. Studying the on- and off-kinetics ΔΨ and ΔpH of immunoisolated VGAT SVs by precisely timing the addition and removal of Cl^- can help to elucidate this debate.

Additionally, we will be able to address how glutamate levels are maintained in SVs by (pre)loading them with glutamate followed by monitoring of efflux. The flexibility of the developed system allows for precise timing on when to remove external glutamate, or influence ΔΨ and ΔpH by the addition or removal of components such as ATP. One of the open questions is whether glutamate efflux is mediated by VGLUT (as we would expect (Hartinger and Jahn, 1993)). This system allows the timely addition and removal of VGLUT-inhibitors or glutamate itself while simultaneously measuring the changes in the electrochemical gradient of these components. The removal of glutamate allows us to study the kinetics of glutamate efflux, while the addition and removal of inhibitors will help answer the question whether the efflux is VGLUT-mediated. This flexibility to remove glutamate or inhibitors from the solution is a novel feature of this platform.

4.2.1 Advantages of the microfluidic platform

The assay developed in this thesis has the following advantages compared to already existing methods:

i. *There is no need for highly pure SV preparations.* Using immunocapture as a mechanism to immobilize SVs allows for vesicle capture from crude extracts, as shown with this assay, and that is in line with previous research (Burger et al., 1989; Takamori et al., 2000b). Therefore, there is no need for highly enriched SV preparations from rodent brains and from other crude samples, for which an SV purification method is not available. SVs can be immobilized without further processing steps. Using crude samples decreases the time needed to prepare a sample, an advantage in itself, as well as the expectation of less protein degradation and increased activity due to reduced time spend on isolating the sample. Immunocapture also allows for direct immobilization of subpopulations of SVs with specific proteins. However, the potential of the antibodies to inhibit the functioning of this protein has to be considered (Eriksen et al., 2021; Schenck et al., 2017). Therefore, in conjunction with this method, a subpopulations purification method based on affinity isolation was developed.
ii. *Immobilized antibodies can capture a wide range of targets.* This system is not limited to SVs from rodent brains but can capture other native vesicles and (proteo)liposomes (for example, by incorporating biotinylated lipids in the preparation) or hybrid vesicles.
iii. *Micrometer-sized spots containing concentrated vesicles yield better signal-to-noise ratios than the single vesicle assay*. Strong fluorescent signals simplify the analysis and allow for the analysis of many concentrated SVs simultaneously.
iv. *Only small amounts of SVs are needed.* The small amounts needed allows analysis of SVs (or other targets) derived from small brain regions or primary cultured neurons. This flexibility in the source of SVs provides access to SVs labeled with genetically encoded sensors, SVs with altered protein composition (overexpression, CRISPR-CAS, KO, mutants), or SVs containing chemical sensors that are loaded by endocytosis.

v. *Microfluidics allow for fast and repetitive exchange of solutions by superfusion*. Repetitively changing the solutions finally allows for monitoring on-off kinetics, which until now was not possible. The fast changes in solutions allow for a high temporal resolution, with changes happening in less than 1 second (as shown in Figure 21).

vi. *The system allows for a high degree of experimental flexibility.* All parameters can be easily changed (flow profile, geometry, the immobilized protein, and the target), resulting in a high level of flexibility. For example, increasing the number of inlets allows for an increase in the number of conditions the immobilized target can be exposed to.

Overall, the microfluidic platform developed during my PhD allows the study of SV loading at a temporal resolution and flexibility of factors that was previously not possible. This set-up in combination with the constant improvement of fluorescent probes has the potential to answer major open questions that have been discussed in the field for almost 30 years.

Bibliography

Abbas, Y.M., Wu, D., Bueler, S.A., Robinson, C.V., and Rubinstein, J.L. (2020). Structure of V-ATPase from the mammalian brain. Science (80-.). *367*, 1240–1246.

Ahmed, S., Holt, M., Riedel, D., and Jahn, R. (2013). Small-scale isolation of synaptic vesicles from mammalian brain. Nat. Protoc. *8*, 998–1009.

Ahnert-Hilger, G., and Jahn, R. (2011). CLC-3 spices up GABAergic synaptic vesicles. Nat. Neurosci. *14*, 405–407.

Aihara, Y., Mashima, H., Onda, H., Hisano, S., Kasuya, H., Hori, T., Yamada, S., Tomura, H., Yamada, Y., Inoue, I., et al. (2000). Molecular cloning of a novel brain-type Na+-dependent inorganic phosphate cotransporter. J. Neurochem. *74*, 2622–2625.

Alfonso, A., Grundahl, K., Duerr, J.S., Han, H.P., and Rand, J.B. (1993). The Caenorhabditis elegans unc-17 gene: A putative vesicular acetylcholine transporter. Science (80-.). *261*, 617–619.

Angenendt, P., Glökler, J., Murphy, D., Lehrach, H., and Cahill, D.J. (2002). Toward optimized antibody microarrays: A comparison of current microarray support materials. Anal. Biochem. *309*, 253–260.

Aravanis, A.M., Pyle, J.L., and Tsien, R.W. (2003). Single synaptic vesicles fusing transiently and successively without loss of identity. Nature *423*, 643–647.

Aubrey, K.R. (2016). Presynaptic control of inhibitory neurotransmitter content in VIAAT containing synaptic vesicles. Neurochem. Int. *98*, 94–102.

Barberis, A., Petrini, E.M., and Cherubini, E. (2004). Presynaptic source of quantal size variability at GABAergic synapses in rat hippocampal neurons in culture. Eur. J. Neurosci. *20*, 1803–1810.

Bavli, D., Ezra, E., Kitsberg, D., and Vosk-artzi, M. (2016). One step antibody-mediated isolation and patterning of multiple cell types in microfluidic devices. Biomicrofluidics *024112*, 1–10.

Bee, J.S., Chiu, D., Sawicki, S., Stevenson, J.L., Chatterjee, K., Freund, E., Carpenter, J.F., and Randolph, T.W. (2006). Monoclonal Antibody Interactions with Micro- and Nanoparticles: Adsorption, Aggregation and Accelerated Stress Studies. J Pharm Sci. *98*, 3218–3238.

Bell, G.I. (1978). Models for the specific adhesion of cells to cells. Science (80-.). *200*, 618–627.

Bellocchio, E.E., Hu, H., Pohorille, A., Chan, J., Pickel, V.M., and Edwards, R.H. (1998). The localization of the brain-specific inorganic phosphate transporter suggests a specific presynaptic role in glutamatergic transmission. J. Neurosci. *18*, 8648–8659.

Bellocchio, E.E., Reimer, R.J., Fremeau, J., and Edwards, R.H. (2000). Uptake of glutamate into synaptic vesicles by an inorganic phosphate transporter. Science (80-.). *289*, 957–960.

Bevensee, M.O. (2014). Vesicular Neurotransmitter Transporters: mechanistic aspects. In Exchangers, p. 438.

Bianchini, L., and Pouyssegur, J. (1994). Molecular structure and regulation of vertebrate Na+/H+ exchangers. J. Exp. Biol. *196*, 337–345.

Blakely, R.D., and Edwards, R.H. (2012). Vesicular and Plasma Membrane Transporters for Neurotransmitters. Cold Spring Harb Perspect Biol *4*.

Bole, D.G., Hirata, K., and Ueda, T. (2002). Prolonged depolarization of rat cerebral

synaptosomes leads to an increase in vesicular glutamate content. Neurosci. Lett. *322*, 17–20.

Brose, N., Petrenko, A.G., Sudhof, T.C., and Jahn, R. (1992). Synaptotagmin: A calcium sensor on the synaptic vesicle surface. Science (80-.). *256*, 1021–1025.

Buddhala, C., Hsu, C.C., and Wu, J.Y. (2009). A novel mechanism for GABA synthesis and packaging into synaptic vesicles. Neurochem. Int. *55*, 9–12.

Burger, P.M., Mehl, E., Cameron, P.L., Maycox, P.R., Baumert, M., Lottspeich, F., De Camilli, P., and Jahn, R. (1989). Synaptic vesicles immunoisolated from rat cerebral cortex contain high levels of glutamate. Neuron *3*, 715–720.

Burger, P.M., Hell, J., Mehl, E., Krasel, C., Lottspeich, F., and Jahn, R. (1991). GABA and glycine in synaptic vesicles: storage and transport characteristics. Neuron *7*, 287–293.

Carlson, M.D., and Ueda, T. (1990). Accumulated glutamate levels in the synaptic vesicle are not maintained in the absence of active transport. Neurosci. Lett. *110*, 325–330.

del Castillo, Y., and Katz, B. (1954). Quantal components of the end-plate potential. J. Physiol. 560–573.

Chang, R., Eriksen, J., and Edwards, R.H. (2018). The dual role of chloride in synaptic vesicle glutamate transport. Elife *7*, 1–16.

Chaudhry, F. a., Reimer, R.J., Bellocchio, E.E., Danbolt, N.C., Osen, K.K., Edwards, R.H., and Storm-Mathisen, J. (1998). The vesicular GABA transporter, VGAT, localizes to synaptic vesicles in sets of glycinergic as well as GABAergic neurons. J. Neurosci. *18*, 9733–9750.

Chaudhry, F. a, Edwards, R.H., and Fonnum, F. (2008). Vesicular neurotransmitter transporters as targets for endogenous and exogenous toxic substances. Annu. Rev. Pharmacol. Toxicol. *48*, 277–301.

Chen, Q., Li, G., Nie, Y., Yao, S., and Zhao, J. (2014). Investigation and improvement of reversible microfluidic devices based on glass-PDMS-glass sandwich configuration. Microfluid. Nanofluidics *16*, 83–90.

Cheret, C., Ganzella, M., Preobraschenski, J., Jahn, R., and Ahnert-Hilger, G. (2021). Vesicular Glutamate Transporters (SLCA17 A6, 7, 8) Control Synaptic Phosphate Levels. Cell Rep. *34*.

Cras, J.J., Rowe-Taitt, C.A., Nivens, D.A., and Ligler, F.S. (1999). Comparison of chemical cleaning methods of glass in preparation for silanization. Biosens. Bioelectron. *14*, 683–688.

Cretich, M., Pirri, G., Damin, F., Solinas, I., and Chiari, M. (2004). A new polymeric coating for protein microarrays. Anal. Biochem. *332*, 67–74.

Daniels, R.W., Collins, C.A., Chen, K., Gelfand, M. V., Featherstone, D.E., and DiAntonio, A. (2006). A single vesicular glutamate transporter is sufficient to fill a synaptic vesicle. Neuron *49*, 11–16.

Duffy, D.C., McDonald, J.C., Schueller, O.J.A., and Whitesides, G.M. (1998). Rapid prototyping of microfluidic systems in poly(dimethylsiloxane). Anal. Chem. *70*, 4974–4984.

Edwards, R.H. (2007). The Neurotransmitter Cycle and Quantal Size. Neuron *55*, 835–858.

Egashira, Y., Takase, M., and Takamori, S. (2015). Monitoring of Vacuolar-Type H+ ATPase-Mediated Proton Influx into Synaptic Vesicles. J. Neurosci. *35*, 3701–3710.

Egashira, Y., Takase, M., Watanabe, S., Ishida, J., Fukamizu, A., Kaneko, R., Yanagawa, Y., and Takamori, S. (2016). Unique pH dynamics in GABAergic synaptic vesicles

illuminates the mechanism and kinetics of GABA loading. Proc. Natl. Acad. Sci. U. S. A. *113*, 10702–10707.

Erickson, J.D., Eiden, L.E., and Hoffman, B.J. (1992). Expression cloning of a reserpine-sensitive vesicular monoamine transporter. Proc. Natl. Acad. Sci. U. S. A. *89*, 10993–10997.

Erickson, J.D., Varoqui, H., Schafer, M.K.H., Modi, W., Diebler, M.F., Weihe, E., Rand, J., Eiden, L.E., Bonner, T.I., and Usdin, T.B. (1994). Functional identification of a vesicular acetylcholine transporter and its expression from a “cholinergic” gene locus. J. Biol. Chem. *269*, 21929–21932.

Erickson, J.D., Eiden, L.E., Schäfer, M.K.H., and Weihe, E. (1995). Reserpine- and tetrabenazine-sensitive transport of3H-histamine by the neuronal isoform of the vesicular monoamine transporter. J. Mol. Neurosci. *6*, 277–287.

Erickson, J.D., Schäfer, M.K.H., Bonner, T.I., Eiden, L.E., and Weihe, E. (1996). Distinct pharmacological properties and distribution in neurons and endocrine cells of two isoforms of the human vesicular monoamine transporter. Proc. Natl. Acad. Sci. U. S. A. *93*, 5166–5171.

Eriksen, J., Chang, R., McGregor, M., Silm, K., Suzuki, T., and Edwards, R.H. (2016). Protons Regulate Vesicular Glutamate Transporters through an Allosteric Mechanism. Neuron *90*, 768–780.

Eriksen, J., Li, F., Stroud, R.M., and Edwards, R.H. (2021). Allosteric Inhibition of a Vesicular Glutamate Transporter by an Isoform-Specific Antibody. Biochemistry.

Farsi, Z. (2015). A Single Vesicle Assay to Study the Electrochemical Gradient Regulation in Glutamatergic and GABAergic Synaptic Vesicles.

Farsi, Z., Preobraschenski, J., Riedel, D., Jahn, R., and Woehler, A. (2016). Single-vesicle imaging reveals different transport mechanisms between glutamatergic and GABAergic vesicles. Science (80-.). *351*, 981–984.

Farsi, Z., Jahn, R., and Woehler, A. (2017). Proton electrochemical gradient: Driving and regulating neurotransmitter uptake. BioEssays *39*, 1–9.

Fatt, P., and Katz, B. (1952). Spontaneous subthreshold activity at motor nerve endings. J. Physiol. *117*, 109–128.

Fon, E.A., Pothos, E.N., Sun, B.C., Killeen, N., Sulzer, D., and Edwards, R.H. (1997). Vesicular transport regulates monoamine storage and release but is not essential for amphetamine action. Neuron *19*, 1271–1283.

Forgac, M. (2007). Vacuolar ATPases: Rotary proton pumps in physiology and pathophysiology. Nat. Rev. Mol. Cell Biol. *8*, 917–929.

Fremeau, R.T., Burman, J., Qureshi, T., Tran, C.H., Proctor, J., Johnson, J., Zhang, H., Sulzer, D., Copenhagen, D.R., Storm-Mathisen, J., et al. (2002). The identification of vesicular glutamate transporter 3 suggests novel modes of signaling by glutamate. Proc. Natl. Acad. Sci. U. S. A. *99*, 14488–14493.

Fremeau, R.T., Kam, K., Qureshi, Y., Johnson, J., Copenhagen, D.R., Storm-Mathisen, J., Chaudhry, F.A., Nicoll, R.A., and Edwards, R.H. (2004). Vesicular glutamate transporters 1 and 2 target to functionally distinct synaptic release sites. Science (80-.). *304*, 1815–1819.

Ganzella, M., Ninov, M., Riedel, D., and Jahn, R. (2021). Isolation of synaptic vesicles from mammalian brain. In Synaptic Vesicles, J. Dahlmanns, and M. Dahlmanns, eds. (Springer New York), p.

Gao, B., and Jin, G. (2005). Study of Interaction Force between Antigen and Antibody

using Flow Chamber Method (IEEE).

Gasnier, B. (2004). The SLC32 transporter, a key protein for the synaptic release of inhibitory amino acids. Pflugers Arch. Eur. J. Physiol. *447*, 756–759.

Gidi, Y., Bayram, S., Ablenas, C.J., Blum, A.S., and Cosa, G. (2018). Efficient One-Step PEG-Silane Passivation of Glass Surfaces for Single-Molecule Fluorescence Studies. ACS Appl. Mater. Interfaces *10*, 39505–39511.

Goh, G.Y., Huang, H., Ullman, J., Borre, L., Hnasko, T.S., Trussell, L.O., and Edwards, R.H. (2011). Presynaptic regulation of quantal size: K+/H+ exchange stimulates glutamate storage by increasing membrane potential. Nat. Neurosci. *14*, 1285–1292.

Granseth, B., Odermatt, B., Royle, S.J.J., and Lagnado, L. (2006). Clathrin-Mediated Endocytosis Is the Dominant Mechanism of Vesicle Retrieval at Hippocampal Synapses. Neuron *51*, 773–786.

Gras, C., Herzog, E., Bellenchi, G.C., Bernard, V., Ravassard, P., Pohl, M., Gasnier, B., Giros, B., and El Mestikawy, S. (2002). A third vesicular glutamate transporter expressed by cholinergic and serotoninergic neurons. J. Neurosci. *22*, 5442–5451.

Graves, A.R., Curran, P.K., Smith, C.L., and Mindell, J.A. (2008). The Cl-/H+ antiporter ClC-7 is the primary chloride permeation pathway in lysosomes. Nature *453*, 788–792.

Green, N. (1966). Thermodynamics of the binding of biotin and some analogues by avidin. Biochem. J. *101*, 774–780.

Grønborg, M., Pavlos, N.J., Brunk, I., Chua, J.J.E., Münster-Wandowski, A., Riedel, D., Ahnert-Hilger, G., Urlaub, H., and Jahn, R. (2010). Quantitative comparison of glutamatergic and GABAergic synaptic vesicles unveils selectivity for few proteins including MAL2, a novel synaptic vesicle protein. J. Neurosci. *30*, 2–12.

Gualix, J., Pintor, J., and Miras-Portugal, M.T. (1999). Characterization of nucleotide transport into rat brain synaptic vesicles. J. Neurochem. *73*, 1098–1104.

Halliwell, C.M., and Cass, A.E.G. (2001). A factorial analysis of silanization conditions for the immobilization of oligonucleotides on glass surfaces. Anal. Chem. *73*, 2476–2483.

Hartinger, J., and Jahn, R. (1993). An anion binding site that regulates the glutamate transporter of synaptic vesicles. J. Biol. Chem. *268*, 23122–23127.

Hattori, K., Yoshimitsu, R., Sugiura, S., Maruyama, A., Ohnuma, K., and Kanamori, T. (2013). Masked plasma oxidation: Simple micropatterning of extracellular matrix in a closed microchamber array. RSC Adv. *3*, 17749–17754.

Haucke, V., Neher, E., and Sigrist, S.J. (2011). Protein scaffolds in the coupling of synaptic exocytosis and endocytosis. Nat. Rev. Neurosci. *12*, 127–138.

Hell, J.W., Maycox, P.R.R., and Jahn, R. (1990). Energy dependence and functional reconstitution of the gamma-aminobutyric acid carrier from synaptic vesicles. J. Biol. Chem. *265*, 2111–2117.

Heuser, J.E., and Reese, T.S. (1973). Evidence for recycling of synaptic vesicle membrane during transmitter release at the frog neuromuscular junction. J. Cell Biol. *57*, 315–344.

Hiasa, M., Miyaji, T., Haruna, Y., Takeuchi, T., Harada, Y., Moriyama, S., Yamamoto, A., Omote, H., and Moriyama, Y. (2014). Identification of a mammalian vesicular polyamine transporter. Sci. Rep. *4*.

Hires, S.A., Zhu, Y., and Tsien, R.Y. (2008). Optical measurement of synaptic glutamate spillover and reuptake by linker optimized glutamate-sensitive fluorescent reporters. Proc. Natl. Acad. Sci. U. S. A. *105*, 4411–4416.

Hoehne, M., Samuel, F., Dong, A., Wurth, C., Mahler, H., Carpenter, J.F., and Randolph, T.W. (2011). Adsorption of Monoclonal Antibodies to Glass Microparticles. J. Pharm. Sci. *100*, 123–132.

Huang, J., Lee, I., Luo, X., Cui, X.T., and Yun, M. (2013). Shadow Masking for Nanomaterial-Based Biosensors Incorporated with Microfluidic Device. Biomed Microdevices *15*, 531–537.

Huttner, W.B., Schiebler, W., Greengard, P., and De Camilli, P. (1983). Synapsin I (protein I), a nerve terminal-specific phosphoprotein. III. Its association with synaptic vesicles studied in a highly purified synaptic vesicle preparation. J. Cell Biol. *96*, 1374–1388.

Hyre, D.E., Trong, I.L., Merritt, E.A., Eccleston, J.F., Green, N.M., Stenkamp, R.E., and Stayton, P.S. (2006). Cooperative hydrogen bond interactions in the streptavidin-biotin system. Protein Sci. *15*, 459–467.

Ishikawa, T., Sahara, Y., and Takahashi, T. (2002). A single packet of transmitter does not saturate postsynaptic glutamate receptors. Neuron *34*, 613–621.

Jahn, R., and Boyken, J. (2013). Molecular Regulation of Synaptic Release. In Neuroscience in the 21st Century, (Springer Science + Business Media), pp. 351–401.

Jahn, R., and Südhof, T.C. (1993). Synaptic Vesicle Traffic: Rush Hour in the Nerve Terminal. J. Neurochem. *61*, 12–21.

Jahn, R., and Südhof, T.C. (1994). Synaptic vesicles and exocytosis. Annu. Rev. Neurosci. *17*, 219–246.

Jentsch, T.J. (2007). Chloride and the endosomal-lysosomal pathway: emerging roles of CLC chloride transporters. J. Physiol. *578*, 633–640.

Juge, N., Yoshida, Y., Yatsushiro, S., Omote, H., and Moriyama, Y. (2006). Vesicular glutamate transporter contains two independent transport machineries. J. Biol. Chem. *281*, 39499–39506.

Juge, N., Muroyama, A., Hiasa, M., Omote, H., and Moriyama, Y. (2009). Vesicular inhibitory amino acid transporter is a Cl-/ ??-aminobutyrate co-transporter. J. Biol. Chem. *284*, 35073–35078.

Juge, N., Gray, J.A., Omote, H., Miyaji, T., Inoue, T., Hara, C., Uneyama, H., Edwards, R.H., Nicoll, R.A., and Moriyama, Y. (2010). Metabolic Control of Vesicular Glutamate Transport and Release. Neuron *68*, 99–112.

Juge, N., Omote, H., and Moriyama, Y. (2013). Vesicular GABA transporter (VGAT) transports beta-alanine. J. Neurochem. *127*, 482–486.

Kandel, E.., Schwartz, J.H., Jessell, T.M., Siegelbaum, S.A., and Hudspeth, A.J. (2012). Principles of Neural science (McGraw-Hill Education Ltd).

Katz, B. (1971). Quantal mechanism of transmitter release. Science *173*, 123–126.

Katz, B., and Miledi, R. (1969). Spontaneous and evoked activity of motor nerve endings in calcium Ringer. J. Physiol. *203*, 689–706.

Klein, A.-K., and Dietzel, A. (2020). A Primer on Microfluidics: From Basic Principles to Microfabrication. In Adv Biochem Eng Biotechnol, (Berlin, Heidelberg: Springer Berlin Heidelberg), pp. 1–19.

Kuo, S.C., and Lauffenburger, D.A. (1993). Relationship between receptor/ligand binding affinity and adhesion strength. Biophys. J. *65*, 2191–2200.

Kusnezow, W., and Hoheisel, J.D. (2003). Solid supports for microarray immunoassays. J. Mol. Recognit. *16*, 165–176.

Kusnezow, W., Jacob, A., Walijew, A., Diehl, F., and Hoheisel, J.D. (2003). Antibody microarrays: An evaluation of production parameters. Proteomics *3*, 254–264.

Law, C.J., Maloney, P.C., and Wang, D.N. (2008). Ins and outs of major facilitator superfamily antiporters. Annu. Rev. Microbiol. *62*, 289–305.

Lee, R.Y.N., Sawin, E.R., Chalfie, M., Horvitz, H.R., and Avery, L. (1999). EAT-4, a Homolog of a Mammalian Sodium-Dependent Inorganic Phosphate Cotransporter, Is Necessary for Glutamatergic Neurotransmission in Caenorhabditis elegans. J. Neurosci. *19*, 159–167.

Li, F., Eriksen, J., Finer-Moore, J., Chang, R., Nguyen, P., Bowen, A., Myasnikov, A., Yu, Z., Bulkley, D., Cheng, Y., et al. (2020). Ion transport and regulation in a synaptic vesicle glutamate transporter. Science (80-.). *368*, 893–897.

Li, Z., Burrone, J., Tyler, W.J., Hartman, K.N., Albeanu, D.F., and Murthy, V.N. (2005). Synaptic vesicle recycling studied in transgenic mice expressing synaptopHluorin. Proc. Natl. Acad. Sci. *102*, 6131–6136.

Lichtenberg, J.Y., Ling, Y., and Kim, S. (2019). Non-specific adsorption reduction methods in biosensing. Sensors (Switzerland) *19*, 1–17.

Liu, Y., Peter, D., Roghani, A., Schuldiner, S., Prive, G.G., Eisenberg, D., Brecha, N., and Edwards, R.H. (1992). A cDNA that suppresses MPP+ toxicity encodes a vesicular amine transporter. Cell *70*, 539–551.

Luqmani, Y.A. (1981). Nucleotide uptake by isolated cholinergic synaptic vesicles: Evidence for a carrier of adenosine 5'-triphosphate. Neuroscience *6*, 1011–1021.

Martens, H., Weston, M.C., Boulland, J., Grønborg, M., Grosche, J., Kacza, J., Hoffmann, A., Matteoli, M., Takamori, S., Harkany, T., et al. (2008). Unique Luminal Localization of VGAT-C Terminus Allows for Selective Labeling of Active Cortical GABAergic Synapses. J. Neurosci. *28*, 13125–13131.

Marvin, J.S., Borghuis, B.G., Tian, L., Cichon, J., Harnett, M.T., Akerboom, J., Gordus, A., Renninger, S.L., Chen, T., Bargmann, C.I., et al. (2013). An optimized fluorescent probe for visualizing glutamate neurotransmission. Nat. Methods *10*, 162–170.

Masharina, A., Reymond, L., Maurel, D., Umezawa, K., and Johnsson, K. (2012). A fluorescent sensor for GABA and synthetic GABAB receptor ligands. J. Am. Chem. Soc. *134*, 19026–19034.

Masson, J., Sagné, C., Hamon, M., and El Mestikawy, S. (1999). Neurotransmitter transporters in the central nervous system. Pharmacol. Rev. *51*, 439–464.

Maycox, P.R., Deckwerth, T., Hell, J.W., and Jahn, R. (1988). Glutamate uptake by brain synaptic vesicles. Energy dependence of transport and functional reconstitution in proteoliposomes. J. Biol. Chem. *263*, 15423–15428.

Mazhab-Jafari, M.T., Rohou, A., Schmidt, C., Bueler, S.A., Benlekbir, S., Robinson, C. V., and Rubinstein, J.L. (2016). Atomic model for the membrane-embedded VO motor of a eukaryotic V-ATPase. Nature *539*, 118–122.

McDonald, J.C., and Whitesides, G.M. (2002). Poly (dimethylsiloxane) as a Material for Fabricating Microfluidic Devices. Acc. Chem. Res. *35*, 491–499.

McIntire, S.L., Jorgensen, E., and Horvitz, H.R. (1993). Genes required for GABA function i Caenorhabditis elegans. Nature *364*, 334–337.

McIntire, S.L., Reimer, R.J., Schuske, K., Edwards, R.H., and Jorgensen, E.M. (1997). Identification and characterization of the vesicular GABA transporter. Nature *389*, 870–876.

Miller, E.W., Lin, J.Y., Frady, E.P., Steinbach, P.A., Kristan, W.B., and Tsien, R.Y. (2012).

Optically monitoring voltage in neurons by photoinduced electron transfer through molecular wires. Proc. Natl. Acad. Sci. U. S. A. *109*, 2114–2119.

Milosavljevic, N., Monet, M., Léna, I., Brau, F., Lacas-Gervais, S., Feliciangeli, S., Counillon, L., and Poët, M. (2014). The Intracellular Na+/H+ Exchanger NHE7 Effects a Na+-Coupled, but Not K+-Coupled Proton-Loading Mechanism in Endocytosis. Cell Rep. *7*, 689–696.

Miyazaki, T., Fukaya, M., Shimizu, H., and Watanabe, M. (2003). Subtype switching of vesicular glutamate transporters at parallel fibre-Purkinje cell synapses in developing mouse cerebellum. Eur. J. Neurosci. *17*, 2563–2572.

Moriyama, Y., and Yamamoto, A. (1995). Vesicular L-glutamate transporter in microvesicles from bovine pineal glands: Driving force, mechanism of chloride anion activation, and substrate specificity. J. Biol. Chem. *270*, 22314–22320.

Mutch, S.A., Kensel-Hammes, P., Gadd, J.C., Fujimoto, B.S., Allen, R.W., Schiro, P.G., Lorenz, R.M., Kuyper, C.L., Kuo, J.S., Bajjalieh, S.M., et al. (2011). Protein quantification at the single vesicle level reveals a subset of synaptic vesicle proteins are trafficked with high precision. J. Neurosci. *31*, 1461–1470.

Nagy, A., Baker, R.R.R., Morris, S.J.J., and Whittaker, V.P.P. (1976). The preparation and characterization of synaptic vesicles of high purity. Brain Res. *109*, 285–309.

Naito, S., and Ueda, T. (1985). Characterization of Glutamate Uptake into Synaptic Vesicles. J. Neurochem. *44*, 99–109.

Nakamura, N., Tanaka, S., Teko, Y., Mitsui, K., and Kanazawa, H. (2005). Four Na+/H+ exchanger isoforms are distributed to Golgi and post-Golgi compartments and are involved in organelle pH regulation. J. Biol. Chem. *280*, 1561–1572.

Naves, L.A., and Van Der Kloot, W. (2001). Repetitive nerve stimulation decreases the acetylcholine content of quanta at the frog neuromuscular junction. J. Physiol. *532*, 637–647.

Ni, B., Rosteck, P.R., Nadi, N.S., and Paul, S.M. (1994). Cloning and expression of a cDNA encoding a brain-specific Na+-dependent inorganic phosphate cotransporter. Proc. Natl. Acad. Sci. U. S. A. *91*, 5607–5611.

Norde, W. (2008). My voyage of discovery to proteins in flatland ...and beyond. Colloids Surfaces B Biointerfaces *61*, 1–9.

Oates, M.R., Clarke, W., Marsh, E.M., and Hage, D.S. (1998). Kinetic studies on the immobilization of antibodies to high-performance liquid chromatographic supports. Bioconjug. Chem. *9*, 459–465.

Oberstrass, L. (2018). Development of New Techniques for Measuring Neurotransmitter Transport by Synaptic Vesicles.

Olsthoorn, H.M. (2017). Reconstitution and Functional Characterization of the Vesicular GABA Transporter.

Omote, H., and Moriyama, Y. (2013). Vesicular Neurotransmitter Transporters : An Approach for Studying Transporters With Purified Proteins. Physiology *28*, 39–50.

Palay, S.L. (1956). Synapses in the central nervous system. J. Biophys. Biochem. Cytol. *2*, 193–202.

Perego, E. (2019). Studying Molecular Interactions under Flow with Fluorescence Fluctuation Spectroscopy.

Pietrancosta, N., Djibo, M., Daumas, S., El Mestikawy, S., and Erickson, J.D. (2020). Molecular, Structural, Functional, and Pharmacological Sites for Vesicular Glutamate Transporter Regulation. Mol. Neurobiol. *57*, 3118–3142.

Pirri, G., Damin, F., Chiari, M., Bontempi, E., Depero, L.E., Molecolare, R., and Chimica, S. (2004). Characterization of A Polymeric Adsorbed Coating for DNA Microarray Glass Slides. Anal. Chem. *76*, 1352–1358.

Pirrung, M.C. (2002). How to make a DNA chip. Angew. Chemie - Int. Ed. *41*, 1276–1289.

Pothos, E.N., Lersen, K.E., Krantz, D.E., Liu, Y.J., Haycock, J.W., Setlik, W., Gershon, M.D., Edwards, R.H., and Sulzer, D. (2000). Synaptic vesicle transporter expression regulates vesicle phenotype and quantal size. J. Neurosci. *20*, 7297–7306.

Preobraschenski, J., Zander, J.F., Suzuki, T., Ahnert-Hilger, G., and Jahn, R. (2014). Vesicular glutamate transporters use flexible anion and cation binding sites for efficient accumulation of neurotransmitter. Neuron *84*, 1287–1301.

Preobraschenski, J., Cheret, C., Ganzella, M., Zander, J.F., Richter, K., Schenck, S., Jahn, R., and Ahnert-Hilger, G. (2018). Dual and Direction-Selective Mechanisms of Phosphate Transport by the Vesicular Glutamate Transporter. Cell Rep. *23*, 535–545.

Riazanski, V., Deriy, L. V, Shevchenko, P.D., Le, B., Gomez, E.A., and Nelson, D.J. (2011). Presynaptic CLC-3 Determines Quantal Size of Inhibitory Transmission in the Hippocampus. Nat Neurosci *14*, 487–494.

Riveros, N., Fiedler, J., Lagos, N., Munoz, C., and Orrego, F. (1986). Glutamate in rat brain cortex synaptic vesicles: influence of the vesicle isolation procedure. Brain Res. *386*, 405–408.

Rizzoli, S.O. (2014). Synaptic vesicle recycling. *33*, 2014.

De Robertis, E.D., and Bennett, H.S. (1955). Some features of the submicroscopic morphology of synapses in frog and earthworm. J. Biophys. Biochem. Cytol. *1*, 47–58.

Rossano, A.J., Kato, A., Minard, K.I., Romero, M.F., and Macleod, G.T. (2017). Na+/H+ exchange via the Drosophila vesicular glutamate transporter mediates activity-induced acid efflux from presynaptic terminals. J. Physiol. *595*, 805–824.

Rottenberg, H., and Moreno-Sanchez, R. (1993). The proton pumping activity of H+-ATPases: An improved fluorescence assay. BBA - Bioenerg. *1183*, 161–170.

Sackmann, E.K., Fulton, A.L., and Beebe, D.J. (2014). The present and future role of microfluidics in biomedical research. Nature *507*, 181–189.

Sagné, C., El Mestikawy, S., Isambert, M.F., Hamon, M., Henry, J.P., Giros, B., and Gasnier, B. (1997). Cloning of a functional vesicular GABA and glycine transporter by screening of genome databases. FEBS Lett. *417*, 177–183.

Sawada, K., Echigo, N., Juge, N., Miyaji, T., Otsuka, M., Omote, H., Yamamoto, A., and Moriyama, Y. (2008). Identification of a vesicular nucleotide transporter. Proc. Natl. Acad. Sci. U. S. A. *105*, 5683–5686.

Schaedel, L., Triclin, S., Chrétien, D., Abrieu, A., Aumeier, C., Gaillard, J., Blanchoin, L., Théry, M., and John, K. (2019). Lattice defects induce microtubule self-renewal. Nat. Phys. *15*, 830–838.

Schäfer, M.K.H., Varoqui, H., Defamie, N., Weihe, E., and Erickson, J.D. (2002). Molecular cloning and functional identification of mouse vesicular glutamate transporter 3 and its expression in subsets of novel excitatory neurons. J. Biol. Chem. *277*, 50734–50748.

Scheel, O., Zdebik, A.A., Lourdel, S., and Jentsch, T.J. (2005). Voltage-dependent electrogenic chloride/proton exchange by endosomal CLC proteins. Nature *436*, 424–427.

Schenck, S., Wojcik, S.M., Brose, N., and Takamori, S. (2009). A chloride conductance in VGLUT1 underlies maximal glutamate loading into synaptic vesicles. Nat. Neurosci. *12*, 156–162.

Schenck, S., Kunz, L., Sahlender, D., Pardon, E., Geertsma, E.R., Savtchouk, I., Suzuki, T., Neldner, Y., Štefanić, S., Steyaert, J., et al. (2017). Generation and Characterization of Anti-VGLUT Nanobodies Acting as Inhibitors of Transport. Biochemistry *56*, 3962–3971.

Schlecht, C.A., and Maurer, J.A. (2011). Functionalization of glass substrates: Mechanistic insights into the surface reaction of trialkoxysilanes. RSC Adv. *1*, 1446–1448.

Sebastian Smyk (2017). Design and fabrication of microfluidic devices for neurosciences.

Shapiro, H.M. (2000). Membrane potential estimation by flow cytometry. Methods *21*, 271–279.

Song, Y., Cheng, D., and L, Z. (2018). Microfluidics. Fundamentals, devices and applications. Wiley-VCH, Weinheim.

Stobrawa, S.M., Breiderhoff, T., Takamori, S., Engel, D., Schweizer, M., Zdebik, A.A., Bösl, M.R., Ruether, K., Jahn, H., Draguhn, A., et al. (2001). Disruption of ClC-3, a chloride channel expressed on synaptic vesicles, leads to a loss of the hippocampus. Neuron *29*, 185–196.

Südhof, T.C. (2004). The synaptic vesicle cycle. Annu. Rev. Neurosci. *27*, 509–547.

Sun-Wada, G.H., Wada, Y., and Futai, M. (2003). Vacuolar H+ Pumping ATPases in Luminal Acidic Organelles and Extracellular Compartments: Common Rotational Mechanism and Diverse Physiological Roles. J. Bioenerg. Biomembr. *35*, 347–358.

Tabb, J.S., Kish, P.E., Van Dyke, R., and Ueda, T. (1992). Glutamate transport into synaptic vesicles: Roles of membrane potential, pH gradient, and intravesicular pH. J. Biol. Chem. *267*, 15412–15418.

Takahashi, N., Miner, L.L., Sora, I., Ujike, H., Revay, R.S., Kostic, V., Jackson-Lewis, V., Przedborski, S., and Uhl, G.R. (1997). VMAT2 knockout mice: Heterozygotes display reduced amphetamine-conditioned reward, enhanced amphetamine locomotion, and enhanced MPTP toxicity. Proc. Natl. Acad. Sci. U. S. A. *94*, 9938–9943.

Takami, C., Eguchi, K., Hori, T., and Takahashi, T. (2017). Impact of vesicular glutamate leakage on synaptic transmission at the calyx of Held. J. Physiol. *595*, 1263–1271.

Takamori, S., Riedel, D., and Jahn, R. (2000a). Immunoisolation of GABA-specific synaptic vesicles defines a functionally distinct subset of synaptic vesicles. J. Neurosci. *20*, 4904–4911.

Takamori, S., Rhee, J.S., Rosenmund, C., and Jahn, R. (2000b). Identification of a vesicular glutamate transporter that defines a glutamatergic phenotype in neurons. Nature *407*, 189–194.

Takamori, S., Rhee, J.S., Rosenmund, C., and Jahn, R. (2001). Identification of differentiation-associated brain-specific phosphate transporter as a second vesicular glutamate transporter (VGLUT2). J. Neurosci. *21*, 1–6.

Takamori, S., Holt, M., Stenius, K., Lemke, E.A., Gronborg, M., Riedel, D., Urlaub, H., Schenck, S., Brügger, B., Ringler, P., et al. (2006). Molecular Anatomy of a Trafficking Organelle. Cell *127*, 831–846.

Taoufiq, Z., Ninov, M., Villar-Briones, A., Wang, H.Y., Sasaki, T., Roy, M.C., Beauchain, F., Mori, Y., Yoshida, T., Takamori, S., et al. (2021). Hidden proteome of synaptic vesicles in the mammalian brain. Proc. Natl. Acad. Sci. U. S. A. *117*, 33586–33596.

Tokárová, V., Pittermannová, A., Král, V., Řezáčová, P., and Štěpánek, F. (2013). Feasibility and constraints of particle targeting using the antigen– antibody interaction. Nanoscale *5*, 11490–11498.

Trilling, A.K., Beekwilder, J., and Zuilhof, H. (2013). Antibody orientation on biosensor surfaces: A minireview. Analyst *138*, 1619–1627.

Upmanyu, N., Jin, J., Ganzella, M., Bösche, L., Malviya, V.N., Zhuleku, E., Politi, A., Ninov, M., Silbern, I., Urlaub, H., et al. (2021). Co-localization of different Neurotransmitter Transporters on the same Synaptic Vesicle is Bona-fide yet Sparse. BioRxiv Prepr. 1–29.

Vermette, P., Gengenbach, T., Divisekera, U., Kambouris, P.A., Griesser, H.J., and Meagher, L. (2003). Immobilization and surface characterization of NeutrAvidin biotin-binding protein on different hydrogel interlayers. J. Colloid Interface Sci. *259*, 13–26.

Voglmaier, S.M., Kam, K., Yang, H., Fortin, D.L., Hua, Z., Nicoll, R.A., and Edwards, R.H. (2006). Distinct Endocytic Pathways Control the Rate and Extent of Synaptic Vesicle Protein Recycling. Neuron *51*, 71–84.

Van Der Voort, P., and Vansant, E.F. (1996). Silylation of the silica surface. A review.

Wang, R., Long, T., Hassan, A., Wang, J., Sun, Y., Xie, X.S., and Li, X. (2020). Cryo-EM structures of intact V-ATPase from bovine brain. Nat. Commun. *11*, 1–9.

Watanabe, S., Rost, B.R., Camacho-Pérez, M., Davis, M.W., Söhl-Kielczynski, B., Rosenmund, C., and Jorgensen, E.M. (2013). Ultrafast endocytosis at mouse hippocampal synapses. Nature *504*, 242–247.

Watanabe, S., Trimbuch, T., Camacho-Pérez, M., Rost, B.R., Brokowski, B., Söhl-Kielczynski, B., Felies, A., Davis, M.W., Rosenmund, C., and Jorgensen, E.M. (2014). Clathrin regenerates synaptic vesicles from endosomes. Nature *515*, 228–233.

Weinert, S., Gimber, N., Deuschel, D., Stuhlmann, T., Puchkov, D., Farsi, Z., Ludwig, C.F., Novarino, G., López-cayuqueo, K.I., Planells-cases, R., et al. (2020). Uncoupling endosomal CLC chloride / proton exchange causes severe neurodegeneration. EMBO J. *39*, 1–19.

Whitesides, G.M. (2006). The origins and the future of microfluidics. Nature *442*, 368–373.

Wilhelm, B.G., Mandad, S., Truckenbrodt, S., Kröhnert, K., Schäfer, C., Rammner, B., Koo, S.J., Claßen, G. a, Krauss, M., Haucke, V., et al. (2014). Composition of isolated synaptic boutons reveals the amounts of vesicle trafficking proteins. Science (80-.). *344*, 1023–1028.

Williams, J. (1997). How does a vesicle know it is full? Neuron *18*, 683–686.

Wojcik, S.M., Rhee, J.S., Herzog, E., Sigler, a, Jahn, R., Takamori, S., Brose, N., and Rosenmund, C. (2004). An essential role for vesicular glutamate transporter 1 (VGLUT1) in postnatal development and control of quantal size. Proc. Natl. Acad. Sci. U. S. A. *101*, 7158–7163.

Wojcik, S.M., Katsurabayashi, S., Guillemin, I., Friauf, E., Rosenmund, C., Brose, N., and Rhee, J.S. (2006). A Shared Vesicular Carrier Allows Synaptic Corelease of GABA and Glycine. Neuron *50*, 575–587.

Wolosker, H., De Souza, D.O., and De Meis, L. (1996). Regulation of glutamate transport into synaptic vesicles by chloride and proton gradient. J. Biol. Chem. *271*, 11726–11731.

Wu, X.S., Xue, L., Mohan, R., Paradiso, K., Gillis, K.D., and Wu, L.G. (2007). The origin of quantal size variation: Vesicular glutamate concentration plays a significant role. J. Neurosci. *27*, 3046–3052.

Yaffe, D., Vergara-Jaque, A., Shuster, Y., Listov, D., Meena, S., Singh, S.K., Forrest, L.R., and Schuldiner, S. (2014). Functionally important carboxyls in a bacterial homologue of the vesicular monoamine transporter (VMAT). J. Biol. Chem. *289*, 34229–34240.

Yang, P.-C., and Mahmood, T. (2012). Western blot: Technique, theory, and trouble shooting. N. Am. J. Med. Sci. *4*, 429.

Zhuleku, E. (2020). A method for the immunoisolation of functional VGAT-specific synaptic vesicles.

List of figures

List of abbreviations

ADP	Adenosine diphosphate
APC	Acid/polyamine/organocation
ATP	Adenosine triphosphate
BSA	Bovine serum albumin
CHO	Chinese hamster ovary
CLC	Chloride channel
CNS	Central nervous system
DIDS	4,4'-Diisothiocyanatostilbene-2,2'-disulfonate
DMA	N,N-dimethylacrylamide
EIPA	ethyl-isopropyl amiloride
EM	Electron microscopy
(m)EPSC	(miniature) excitatory postsynaptic current
GABA	γ-amino butyric acid
GTP	Guanosine-5'-triphosphate
MAPS	[3-(methacryloyl-oxy)propyl]trimethoxysilyl
MFS	Major facilitator superfamily
MS	mass spectrometry
MWCO	Molecular weight cut-off
NAS	N,N-acryloyloxysuccinimide
NHE	Na^+/H^+ exchanger
NMWL	Nominal molecular weight limit
NSF	N-ethylmaleimide-sensitive fusion protein
PCR	Polymeric chain reaction
PDMS	Polydimethylsiloxane
PEG	Poly(ethylene glycol)
PNS	Peripheral nervous system
SDS-PAGE	sodium dodecyl sulphate–polyacrylamide gel electrophoresis
SLC	Solute carrier
SNARE	SNAP receptor
SNAP	Soluble NSF attachment protein
SV	Synaptic vesicle
TIRF	Total internal reflection
VAChT	Vesicular acetylcholine transporter
V-ATPase	Vacuolar ATPase
VEAT	Vesicular excitatory amino acid transporter
VGAT/VIAAT	Vesicular GABA transporter/Vesicular inhibitory amino acid transporter
VGLUT	Vesicular glutamate transporter
VMAT	Vesicular monoamine transporter
VNUT	Vesicular nucleotide transporter
VPAT	Vesicular polyamine transporter
WB	Western blotting
FEM	Finite element method